

# **Arrested Coalescence in Food Emulsions**



**UNSW**  
A U S T R A L I A

A thesis in fulfilment of the requirements for the degree of

**DOCTOR OF PHILOSOPHY**

By

**Prerna Dahiya**

School of Chemical Engineering

Faculty of Engineering

August 2017

THE UNIVERSITY OF NEW SOUTH WALES  
Thesis/Dissertation Sheet

**Surname or Family name:** Dahiya

**First name:** Prerna

**Other name/s:**

**Abbreviation for degree as given in the University calendar:**

**School:** Chemical Engineering

**Faculty:** Engineering

**Title:** Arrested Coalescence in Food Emulsions.

### Abstract

Arrested coalescence is an unique instability observed in oil-in-water emulsions. It occurs when droplets begin the coalescence process but then stop at an intermediate state because of some resistance, usually rheological, in origin. Emulsions with arrested structures can either aid or harm product quality depending on whether the resultant structures enhance or disrupt product aesthetics. Past work has examined doublets, two same-sized droplets forming a stable arrested structure, but this thesis extends that work to consider differences in size, the behaviour of greater numbers of droplets in arrested structures, and the effects of edible fat crystallization on arrest. The first part of this project evaluates the effect of droplet size on the final deformation of the resulting doublet. An increase in size of droplets caused less deformation, and a decrease in size caused high deformation, because of the resulting curvature differences. When doublets form from two different sized-droplets they form a less compact structure than equivalent mono-disperse droplets because of differences in surface area. Addition of a third droplet to doublets can cause rearrangement of the newly-added droplet if the liquid meniscus bridge overlaps with one of the existing droplets. Restructuring is shown to produce more compact shapes but only occurs for systems with sufficiently low internal elasticity and when the approach angle is low. In the second part, microstructures formed by larger numbers of arrested droplets in a bulk emulsion were studied, to evaluate whether the mechanisms of structure formation by doublets and triplets is broadly valid. Important differences occur when flow dominates, as rotation and restructuring can occur, as can larger droplet deformation because of inertial effects, resulting in more compact structures. The final part applies the current model to more complex edible fat systems: coconut oil, goose fat and duck fat. In these systems heterogeneity of the crystallization causes coalescence and arrest to be much more variable and irregular than in the model systems previously studied. Different locations of the crystals in droplets can trigger or prevent coalescence.

Declaration relating to disposition of project thesis/dissertation

I hereby grant to the University of New South Wales or its agents the right to archive and to make available my thesis or dissertation in whole or in part in the University libraries in all forms of media, now or here after known, subject to the provisions of the Copyright Act 1968. I retain all property rights, such as patent rights. I also retain the right to use in future works (such as articles or books) all or part of this thesis or dissertation.

I also authorize University Microfilms to use the 350 word abstract of my thesis in Dissertation Abstracts International (this is applicable to doctoral theses only).

.....  
**Signature**

.....  
**Witness Signature**

.....**01/08/2017**.....  
**Date**

The University recognizes that there may be exceptional circumstances requiring restrictions on copying or conditions on use. Requests for restriction for a period of up to 2 years must be made in writing. Requests for a longer period of restriction may be considered in exceptional circumstances and require the approval of the Dean of Graduate Research.

FOR OFFICE USE ONLY

**Date of completion of requirements for Award:**

### **ORIGINALITY STATEMENT**

'I hereby declare that this submission is my own work and to the best of my knowledge it contains no materials previously published or written by another person, or substantial proportions of material which have been accepted for the award of any other degree or diploma at UNSW or any other educational institution, except where due acknowledgement is made in the thesis. Any contribution made to the research by others, with whom I have worked at UNSW or elsewhere, is explicitly acknowledged in the thesis. I also declare that the intellectual content of this thesis is the product of my own work, except to the extent that assistance from others in the project's design and conception or in style, presentation and linguistic expression is acknowledged.'

Signed .....

Date .....01/08/2017.....

### **COPYRIGHT STATEMENT**

'I hereby grant the University of New South Wales or its agents the right to archive and to make available my thesis or dissertation in whole or part in the University libraries in all forms of media, now or here after known, subject to the provisions of the Copyright Act 1968. I retain all proprietary rights, such as patent rights. I also retain the right to use in future works (such as articles or books) all or part of this thesis or dissertation. I also authorise University Microfilms to use the 350 word abstract of my thesis in Dissertation Abstract International (this is applicable to doctoral theses only).

I have either used no substantial portions of copyright material in my thesis or I have obtained permission to use copyright material; where permission has not been granted I have applied/will apply for a partial restriction of the digital copy of my thesis or dissertation.'

Signed .....

Date .....01/08/2017.....

### **AUTHENTICITY STATEMENT**

'I certify that the Library deposit digital copy is a direct equivalent of the final officially approved version of my thesis. No emendation of content has occurred and if there are any minor variations in formatting, they are the result of the conversion to digital format.'

Signed .....

Date .....01/08/2017.....

## **ACKNOWLEDGEMENT**

I would like to extend my sincere gratitude to my supervisor Associate Professor Patrick Spicer for his valuable time, ceaseless encouragement, professional advices, and endless help, in refining my writing and calculations, throughout by doctoral studies. His immense knowledge helped me to gain a lot of research methods and experimental skills. I am privileged to get a fortuity to be one of his students.

I would also like to thank my co-supervisor Dr Stuart Prescott for his beneficial discussions and suggestions. My gratitude is also extended to Assistant Professor Timothy J Atherton and Andrew DeBenedictis from Tufts University for sharing their knowledge and expertise in simulation and calculations in reference to Chapter 4 of this work. I am very grateful to my committee members Dr Robert Driscoll (Chair), Dr Francisco Trujillo and Dr. PJ Cullen for their time, encouragement and perspective comments.

I would like to thank UNSW Complex Fluid group for the inspiring conversations and friendly environment in the laboratory. I also thank Dr. Vincent Pouliche and Matthew Terkel for their help in designing microfluidic device for the latter part of my work.

I am beholden to my family for their constant moral, financial support and encouragement for all these years. And I cannot sufficiently express in words how obliged I am to my husband Aman Bisla for his patience and never-ending support. They all kept me going, and this degree would have not been possible without them.

## LIST OF PUBLICATIONS AND PRESENTATIONS

- DAHIYA P., CAGGIONI M. AND SPICER P. T. 2017. Arrested coalescence of viscoelastic droplets: Bulk monodisperse emulsions, *Journal of the American Oil Chemists' Society*, (in preparation).
- DAHIYA P., WANG X., HARTEL R. W. AND SPICER P. T. 2017. Arrested coalescence in edible fats: Crystal heterogeneity effects, *Food Structure*, (in preparation).
- DAHIYA P., DEBENEDICTS A., ATHERTON T. J., CAGGIONI M., PRESCOTT S. W., HARTEL R. W. AND SPICER P. T. 2016. Arrested coalescence of viscoelastic droplets: Triplet shape and restructuring, *Soft Matter*, 13, 2686-2697.
- DAHIYA P., CAGGIONI M. AND SPICER P. T. 2016. Arrested coalescence of viscoelastic droplets: polydisperse doublets, *Philosophical Transactions of The Royal Society A*, 374, 20150132.
- DAHIYA P. AND SPICER P. T. 2016. Arrested coalescence of viscoelastic droplets: Connectivity and restructuring. Presented at: *90th ACS colloid and Surface Science Symposium*, Harvard University, USA, June 5-8 - oral presentation.
- DAHIYA P. AND SPICER P. T. 2016. Arrested coalescence of viscoelastic droplets: Mono and poly-disperse droplets. Presented at: *30th Australian Colloid and Surface Science Student Conference (ACIS)*, NSW, Australia, February 1-4 - oral presentation.
- DAHIYA P. AND SPICER P. T. 2015. Connectivity and deformation of microstructured droplet emulsions. Presented at: *Sydney Surfaces And Soft Stuff (SASSY) meeting*, Sydney, Australia, June 10-11 - poster presentation.

## **TABLE OF CONTENTS**

|                                     |    |
|-------------------------------------|----|
| <b>Table Of Contents</b>            | 1  |
| <b>List Of Figures</b>              | 5  |
| <b>List Of Tables</b>               | 12 |
| <b>ABSTRACT</b>                     | 13 |
| <b>CHAPTER 1 Introduction</b>       | 14 |
| <b>CHAPTER 2 Literature Review</b>  | 17 |
| 2.1. Basics of emulsion             | 17 |
| 2.1.1. Definition and types         | 17 |
| 2.1.2. Emulsion Composition         | 18 |
| 2.1.3. Emulsion Formation           | 22 |
| 2.1.4. Emulsion Forces              | 23 |
| 2.1.4.1. Van der waals Forces       | 23 |
| 2.1.4.2. Electrostatic repulsion    | 24 |
| 2.1.5. Instability                  | 25 |
| 2.1.5.1. Sedimentation and Creaming | 26 |
| 2.1.5.2. Flocculation               | 27 |
| 2.1.5.3. Ostwald Ripening           | 28 |
| 2.1.5.4. Coalescence                | 28 |
| 2.2. Solid fat content - Crystals   | 30 |
| 2.2.1. Crystallization Theory       | 32 |
| 2.2.1.1. Nucleation                 | 32 |
| 2.2.1.2. Crystal growth             | 32 |

|   |    |
|---|----|
| 2.2.2. Crystals' arrangement in emulsion  | 32 |
| 2.2.3. Crystal size and polymorphism  | 33 |
| 2.2.4. Crystallization of fat in an emulsion  | 34 |
| 2.3. Pickering emulsion   | 36 |
| 2.3.1. Stability of Pickering emulsion  | 37 |
| 2.4. Adsorption of particles  | 38 |
| 2.5. Arrested coalescence   | 40 |
| 2.5.1. Theories on arrested coalescence   | 40 |
| 2.5.2. Dispersed phase  | 41 |
| 2.6. Colloidal particles  | 42 |
| 2.6.1. Multiple connections of droplets   | 45 |
| 2.7. Droplet size distribution  | 47 |
| 2.7.1. Instruments for determination of particle size distribution                    | 50 |
| 2.8. Emulsion Rheology  | 51 |
| 2.9. Conclusion   | 53 |
| <b>CHAPTER 3 Arrested coalescence of viscoelastic droplets: polydisperse doublets</b> |    |
|   | 54 |
| 3.1. Introduction   | 54 |
| 3.2 Experiment  | 56 |
| 3.2.1. Emulsion preparation   | 56 |
| 3.2.2. Microscopy   | 57 |
| 3.3. Theory   | 58 |
| 3.4. Results and discussion   | 59 |

|  |    |
|--|----|
| 3.5. Conclusion  | 71 |
| <b>CHAPTER 4 Arrested coalescence of viscoelastic droplets: Triplet shape and Restructuring</b>      | 73 |
| 4.1. Introduction  | 73 |
| 4.2 Experiment   | 75 |
| 4.2.1. Materials and methods   | 75 |
| 4.2.2. Microscopy  | 75 |
| 4.3. Results and discussion  | 76 |
| 4.3.1. Elasticity-dominated structures   | 77 |
| 4.3.2. Interface-dominated structures  | 79 |
| 4.3.3. Approach angle effects  | 83 |
| 4.3.4. Triplet restructuring theory  | 85 |
| 4.4. Conclusions   | 93 |
| <b>CHAPTER 5 Arrested coalescence of viscoelastic droplets: Monodisperse multidroplet aggregates</b> | 95 |
| 5.1. Introduction  | 95 |
| 5.2. Experiment  | 96 |
| 5.2.1. Materials   | 96 |
| 5.2.2. Formation of monodisperse droplets  | 96 |
| 5.2.3. Fabrication of capillary to induce flow   | 97 |
| 5.2.4. Microscopy  | 97 |
| 5.3. Results and discussion  | 98 |
| 5.3.1. Structure formation   | 98 |

|  |     |
|--|-----|
| 5.3.2. Flow directions and mechanisms during the formation of multidroplet networks                            | 100 |
| 5.3.3. Image analysis of the structure deformation and packing   | 102 |
| 5.4. Conclusion  | 105 |
| <b>CHAPTER 6 Arrested coalescence of viscoelastic edible fat droplets: Effects of fat crystal partitioning</b> | 107 |
| 6.1. Introduction  | 107 |
| 6.2. Materials and methods   | 108 |
| 6.2.1. Emulsion preparation  | 108 |
| 6.2.2. Microscopic study   | 109 |
| 6.2.3. Differential Scanning Calorimetry (DSC) experiments   | 109 |
| 6.3. Results and discussion  | 109 |
| 6.3.1. Thermal stability   | 109 |
| 6.3.2. Crystal structure   | 110 |
| 6.3.3. Crystals' distribution or location: Internal vs External  | 111 |
| 6.3.4. Structure of droplets: dense or hollow  | 112 |
| 6.3.5. Wettability of crystals   | 115 |
| 6.3.6. Heterogeneity in edible fats: distribution of fat crystals  | 116 |
| 6.3.7. Deformation of droplets as a result of coalescence  | 119 |
| 6.4. Conclusion  | 121 |
| <b>CHAPTER 7 Conclusions &amp; Recommendations</b>   | 123 |
| <b>REFERENCES</b>  | 126 |

## LIST OF FIGURES

|   |    |
|---|----|
| <b>Figure 1.</b> Molecular structure of triglycerides (simple and mixed)  | 19 |
| <b>Figure 2.</b> Various types of association colloids formed by surfactants in water   | 21 |
| <b>Figure 3.</b> Intermolecular forces between two spherical emulsion droplets  | 24 |
| <b>Figure 4.</b> Various breakdown mechanisms in emulsions  | 26 |
| <b>Figure 5.</b> Coalescence due to quiescent and turbulent flow  | 29 |
| <b>Figure 6.</b> Arrangement of the movable crystals at the interface   | 32 |
| <b>Figure 7.</b> Subcell structure of tree polymorphs   | 34 |
| <b>Figure 8.</b> Arrangement of the semi-crystalline globules in O/W emulsion   | 35 |
| <b>Figure 9.</b> Fat crystallization in oil-in-water emulsions: a) without hydrophobic additives, b) with hydrophobic additives   | 35 |
| <b>Figure 10.</b> Types of nucleation in oil-water emulsions  | 36 |
| <b>Figure 11.</b> The 2-Dimensional confocal slice showing a typical Pickering emulsion droplet. The large saltwater droplet is dyed in green and coated by the small PMMA particles which are dyed in red. The particles have the diameter $d = 3\mu\text{m}$ for this particular sample. The magnified image in the inset shows the contact angle of particles at the interface: $\alpha = 133 \pm 5^\circ$ | 37 |
| <b>Figure 12.</b> (a) Nonspherical supracolloidal structure formed by the arrested coalescence of droplets, (b) highlighting the jammed particles in the neck region between partially coalesced droplets   | 38 |
| <b>Figure 13.</b> Mechanism of arrested coalescence   | 40 |
| <b>Figure 14.</b> Variation in the energies during the different coalescence stage. The minimum strain is represented in the graph at zero for the highest arrest (arrest at high level of solid content) while maximum strain is observed to be at 0.37 for total coalescence of the droplets  | 41 |

|   |    |
|---|----|
| <b>Figure 15.</b> Coalescence arrest at different level of solid fat content (SFC). Right column represents the strain associated with each situation   | 42 |
| <b>Figure 16.</b> Different arrangements of various number of primary particles   | 46 |
| <b>Figure 17.</b> Structural changes in aggregates of 256 monodisperse primary particles with the passage of time. Blue and red color represents: large and small aggregate curvature, respectively   | 48 |
| <b>Figure 18.</b> Polydisperse oil-in-water emulsion containing oil droplets dispersed in continuous phase  | 50 |
| <b>Figure 19.</b> Droplets exhibiting shear thinning behaviour in an emulsion   | 52 |
| <b>Figure 20.</b> Conceptual model of droplet coalescence arrest, where the driving force bringing droplets together to reduce surface energy is offset by the resistance to deformation of the elastic energy storage capacity of the structure. The predictions of equation (3.1) are also shown for monodisperse droplets at different strain levels consistent with different stages of the coalescence process                       | 55 |
| <b>Figure 21.</b> Comparison of analytical and empirical fit results for monodisperse droplet area change during coalescence  | 61 |
| <b>Figure 22.</b> The total energy of the doublet is the sum of its interfacial and elastic contributions. The minimum in the total energy curve determines the doublet's ultimate stable arrested state  | 61 |
| <b>Figure 23.</b> Arrested doublets have larger strains at smaller droplet radii as a result of the increased interfacial curvature and Laplace pressure that drives the droplets together. Higher pressures further compress the internal elastic structure, resisting complete coalescence. The line is a plot of the prediction of the physical model showing the strong effect of drop radius on the ultimate doublet arrested strain | 63 |
| <b>Figure 24.</b> Coalescence of two different-sized droplets. The analytical model describes the shapes of Polydisperse doublets at all stages of coalescence  | 64 |
| <b>Figure 25.</b> Decay of area, normalized by its initial value, for doublets with increasing radius ratio, N, as their strain increases and coalescence is approached. Higher   |    |

Polydispersity within a doublet reduces the amount that area can decrease during the coalescence process 65

**Figure 26.** Changes in doublet polydispersity and solids level alter the resulting doublet arrest strain by changing the amount of area reduction that can occur and the droplet elasticity, respectively 66

**Figure 27.** Increasing the overall doublet size decreases the strain of the structure for all solids levels 67

**Figure 28.** Examples of polydisperse doublets arrested by different solids levels for different values of the radius ratio, N. 69

**Figure 29.** A comparison of the predicted level of strain and the experimentally observed value shows reasonable agreement at low strains but poorer agreement at high strains. The droplets may deform following more nonlinear elastic dynamics at high strains, causing disagreement with the simple model used here 70

**Figure 30.** Microscopy images of a doublet changing its strain, and thus shape, in response to a dilution-induced increase in the local interfacial tension. As surfactant diffuses back in to re-equilibrate the local concentration, the strain increases but the droplet does not return to its original strain, probably because of structural rearrangements that cause hysteresis in the droplet's rheological response 71

**Figure 31.** An emulsion exhibiting arrested coalescence of a number of droplets, with the connections mapped by white lines. A wide range of angles between droplets is visible. Some droplets are quite closely packed while others have a surprising amount of space between them 77

**Figure 32.** (a) Successive images of arrested coalescence of droplets at 40% solids level, showing changes in area and compactness of the shape. Scale bar is 200  $\mu\text{m}$ . (b) Close-up study of the changes occurring during triplet formation in (a), showing neck width growth and two separate meniscus regions 78

**Figure 33.** Arrested coalescence of droplets at 30% solids level, where changes in the meniscus between droplets can occur but are not strong enough to significantly restructure the triplet 80

**Figure 34.** (a) Images of restructuring of droplets (25% solids) as a result of meniscus dynamics, the driving force to make the droplet relocate to a denser packing state (b) Close-up study of triplet formation in (a), showing neck width growth and the merging of the two separate meniscus regions, resulting in a significant amount of restructuring.... 80

**Figure 35.** Restructuring of droplets (20% solids level), showing more extreme changes in area and compactness of the triplet shape 82

**Figure 36.** . Images showing the effect of different approach angles on the restructuring of droplets containing 25% and 30% solid concentrations 84

**Figure 37.** Results plotted for numerous triplet formation processes, mapping the initial and final angle between the third droplet added and the initial doublet. The diagonal line of equality indicates the cases when no restructuring occurs and deviation from the line maps the boundaries of the specific cases of restructuring 86

**Figure 38.** Panel (a) shows diagrams of our analytical model for angles less than, equal to, and greater than the critical angle  $\theta_c$  given equally sized droplets with a strain of 10%. Panel (b) shows a series of simulation visualizations at  $\theta = 60, 129, 130$ , and  $180^\circ$  for the series  $\epsilon = 10\%$ . Panel (c) overlays the results of simulations (red outline) with experimental images for 25% solid triplets with angles of  $75^\circ$  (left) and  $115^\circ$  (right) 89

**Figure 39.** Panel (a) shows surface area, normalized by the surface area of three unconnected spheres, of several simulations runs for  $r_0 = r_1 = r_2$ . Panel (b) plots the critical angle  $\theta_c$  as a function of strain based on analytical results (dashed line) which do not conserve droplet volume and simulation results (solid line) which do conserve droplet volume 91

**Figure 40.** A design map of the possible shapes formed following the initiation of coalescence in an aggregate of three viscoelastic droplets. The shapes are a result of the balance between interfacial pressures and elastic deformation of droplet microstructure and indicate where shape complexity, stability, and dynamic behaviour is found 92

**Figure 41.** Schematic diagram of microfluidic made of borosilicate glass for the droplet production. Inset: images showing monodisperse droplets formed in square capillary 97

|   |     |
|---|-----|
| <b>Figure 42.</b> Schematic diagram showing arrangement of flat capillary for salt diffusion into the emulsion  | 98  |
| <b>Figure 43.</b> Microscopic images showing sequence of formation of structures for 50% solids   | 99  |
| <b>Figure 44.</b> Microscopic images showing sequence of formation of structures for 40% solids   | 99  |
| <b>Figure 45.</b> Microscopic images showing sequence of formation of structures for 30% solids   | 99  |
| <b>Figure 46.</b> Microscopic images showing various rotations during network formation at 50% solids   | 101 |
| <b>Figure 47.</b> Microscopic images indicating individual rotation and restructuring events at 40% solids  | 101 |
| <b>Figure 48.</b> Microscopic images showing formation of a compact aggregate of droplets at 30% solids   | 102 |
| <b>Figure 49.</b> Microscopic images and graph showing strain of doublets varying throughout the network for A) 40% solids [ Green: $\varepsilon > 0.15$ , Yellow: $0.15 < \varepsilon > 0.1$ , Red: $\varepsilon < 0.1$ ], B) 50% solids, [Green: $\varepsilon > 0.05$ , Yellow: $0.05 < \varepsilon > 0.02$ , Red: $\varepsilon < 0.02$ ] | 103 |
| <b>Figure 50.</b> Microscopic images and graph showing the distribution of angles of triplets varying throughout the network for A) 40% solids, B) 50% solids, Green: angle below $100^\circ$ , Yellow: angle between $100^\circ - 150^\circ$ , Red: angle above $150^\circ$  | 104 |
| <b>Figure 51.</b> Final shapes exhibiting total volume, of all the droplets undergone coalescence to make final structures, for 50%, 40% and 30% solids   | 105 |
| <b>Figure 52.</b> Microscopic images showing multidroplet network for: polydisperse droplets having 25% solids and monodisperse droplets having 50% solids concentration..  | 106 |
| <b>Figure 53.</b> Melting point of coconut oil, goose fat and duck fat  | 110 |

|  |     |
|--|-----|
| <b>Figure 54.</b> Pure fats: solid fraction dispersion in liquid fraction: a) coconut oil, b) goose fat and c) duck fat  | 110 |
| <b>Figure 55.</b> Microscopic images and schematic diagrams showing crystals' distribution in a) coconut oil, b) goose fat and c) duck fat droplet, having 20% solids concentration, stored at room temperature for 3 days   | 112 |
| <b>Figure 56.</b> Microscopic images showing droplets of coconut oil, goose fat and duck fat, having different solids concentration, stored at room temperature for at least 3 days  | 113 |
| <b>Figure 57.</b> Deformation of droplets and the internal crystal network (having 20% solids concentration) during suction of oil: a) coconut oil, b) goose fat and c) duck fat d) vaseline-hexadecane; and size of neck width formed by suction of oil with the help of a pulled capillary   | 114 |
| <b>Figure 58.</b> Microscopic images showing interparticle spacing between crystals in goose fat   | 115 |
| <b>Figure 59.</b> Wettability of a) coconut oil, b) goose fat and, c) duck fat crystals: contact angle at oil-water interface when a dispersed droplet (having liquid and solid fraction, left side) is touched to a liquid oil (having liquid fraction only, right side) droplet, having 20% solids concentration, stored for at least 3 days | 116 |
| <b>Figure 60.</b> Microscopic images showing different distribution of fat crystals in coconut oil (20% solids, prepared and stored at room temperature for 3 days)  | 117 |
| <b>Figure 61.</b> Microscopic images and schematic diagram showing effect of availability of liquid oil during coalescence in coconut oil (15% solids)   | 118 |
| <b>Figure 62.</b> Microscopic images showing higher pressure required for breaking the drops' interface to begin coalescence in goose fat (20% solids)   | 118 |
| <b>Figure 63.</b> Effect of location of crystals on arrested coalescence of coconut oil droplets (20% solids): large and small deformation, respectively   | 118 |
| <b>Figure 64.</b> Effect of location of crystals on arrested coalescence of goose fat droplets (20% solids): large and small deformation, respectively   | 119 |
| <b>Figure 65.</b> Effect of location of crystals on arrested coalescence of duck fat droplets (20% solids): large and small deformation, respectively  | 119 |

|  |     |
|--|-----|
| <b>Figure 66.</b> Strain of various doublet shapes obtained by coalescence of two droplets in coconut oil  | 120 |
| <b>Figure 67.</b> Strain of various doublets shapes obtained from coalescence of two droplets in goose fat | 121 |
| <b>Figure 68.</b> Strain of various doublets shapes obtained from coalescence of two droplets in duck fat  | 122 |

## **LIST OF TABLES**

**Table 1.** The colloidal dispersions types

44

## ABSTRACT

Arrested coalescence is an unique instability observed in oil-in-water emulsions. It occurs when droplets begin the coalescence process but then stop at an intermediate state because of some resistance, usually rheological, in origin. Emulsions with arrested structures can either aid or harm product quality depending on whether the resultant structures enhance or disrupt product aesthetics. Past work has examined doublets, two same-sized droplets forming a stable arrested structure, but this thesis extends that work to consider differences in size, the behaviour of greater numbers of droplets in arrested structures, and the effects of edible fat crystallization on arrest. The first part of this project evaluates the effect of droplet size on the final deformation of the resulting doublet. An increase in size of droplets caused less deformation, and a decrease in size caused high deformation, because of the resulting curvature differences. When doublets form from two different sized-droplets they form a less compact structure than equivalent mono-disperse droplets because of differences in surface area. Addition of a third droplet to doublets can cause rearrangement of the newly-added droplet if the liquid meniscus bridge overlaps with one of the existing droplets. Restructuring is shown to produce more compact shapes but only occurs for systems with sufficiently low internal elasticity and when the approach angle is low. In the second part, microstructures formed by larger numbers of arrested droplets in a bulk emulsion were studied, to evaluate whether the mechanisms of structure formation by doublets and triplets is broadly valid. Important differences occur when flow dominates, as rotation and restructuring can occur, as can larger droplet deformation because of inertial effects, resulting in more compact structures. The final part applies the current model to more complex edible fat systems: coconut oil, goose fat and duck fat. In these systems heterogeneity of the crystallization causes coalescence and arrest to be much more variable and irregular than in the model systems previously studied. Different locations of the crystals in droplets can trigger or prevent coalescence.

## **CHAPTER 1 : Introduction**

Emulsions, metastable dispersions of one liquid in another, are of significant importance in a wide range of food, pharmaceutical, cosmetic and coating products. When mixtures of high- and low-melting-point materials are emulsified into water, as with dairy emulsions and petroleum emulsions, oil-in-water emulsions form containing droplets with fat or wax crystals inside them. Since such emulsions play a vital role in providing structure and texture to many products, study of their microscopic properties and flow behaviour has greatly increased. Although the droplet size, shape, and surface properties are always of interest, a key phenomenon is arrested, or partial, coalescence.

Arrested coalescence occurs when the fusing or coalescence process of two droplets is halted at an intermediate stage before it forms a large spherical droplet. The arrest of the shapes can be because of elasticity of an internal crystal network or the presence of particles at the interface of the droplets, providing rheological resistance to total coalescence (Pawar et al., 2011, Pawar et al., 2012). The anisotropic arrested shapes that result have a common liquid bridge that holds the two drops together, distinguishing them from simply aggregated or flocculated drops studied earlier (Torza and Mason, 1969, Elimelech et al., 1997). Arrested coalescence might be undesirable, like in milk or cream, as it might cause an unstable product (Petrut et al., 2016). On the other hand, it might be desirable, as in margarine and ice cream, where it can enhance mechanical strength, improving viscosity and resisting phase separation (Van Boekel and Walstra, 1981, Vanapalli et al., 2002a, Boode et al., 1991). In either case, the aim of research in this area is to understand and control arrest in emulsions, so as to later implement it in various products and allow commercial-scale production. In recent years, a number of scientific studies have examined droplet arrest at an individual droplet level but have not extended their insights to more realistic emulsions with numerous, polydisperse droplets undergoing flow and rearrangement.

Earlier research in this area has been directed towards indentifying the cause of instability in emulsions, and this was observed to be because of the presence of crystals at an interface (Van Boekel and Walstra, 1981). Previous work showed droplets contained crystals that can vary widely in position within a droplet, affecting coalescence, but never directly observed the coalescence process (Boode and Walstra, 1993, Boode et al., 1993). Pawar et al. (2012) recently developed an energetic model

that predicts arrest for doublets, arrested shapes containing two droplets. The work also showed that arrest could occur when crystals remained completely inside of droplets, as opposed to the mechanisms previously proposed (Van Boekel and Walstra, 1981). Pawar et al. (2012) used calculated interfacial and elastic energy terms to describe arrest of droplet shapes at certain coalescence stages as a local equilibrium. The interfacial energy drives the coalescence, while elastic energy from an internal crystal network opposes the coalescence. The model predicts a wide range of shape formation as a function of solids concentration, used to vary the elasticity of the droplets. The model, developed for petrochemical materials, was compared with milk fat, glyceryl tristearate and glyceryl trioleate by Thiel et al. (2016). They found the structure formed by coalesced milk fat droplets can sometimes be distinct from the structure predicted for petrochemical emulsions.

In summary, although there has been steady research into droplet coalescence, its arrest, and the shapes formed at the individual droplet level, much is still not known. Significant gaps of knowledge exist in how the mechanisms observed for small numbers of droplets will scale to larger systems with varying size and number of droplets. Better understanding of bulk emulsion connectivity would enable prediction of network strength, product rheology, and ultimate stability.

This PhD research is thus aimed at improving the understanding of behaviour of droplets, at small and large scale, through study of emulsions' microstructure formation. The overall goal of this project is to expand the knowledge about arrested coalescence in emulsions and to do so in order to improve and expand the applications of the phenomenon. The specific objectives are:

1. Study the binary arrest of mono-disperse and poly-disperse emulsions by investigating the behaviour of different-sized droplets containing a wide range of solids concentration.
2. Investigate the effects of multiple droplet connections on individual droplet deformation, and to probe microstructural changes due to interfacial effects on relocation or restructuring of droplets in a network.
3. Apply and enhance the current model of arrest for more complex edible fats like coconut oil, goose fat, and duck fat.

4. Study the microstructure resulting from multiple arrested connections of droplets in a bulk emulsion and evaluate the accuracy of the current model and determine additional effects that require study.

The thesis compiles a general introduction, followed by a literature review in this area, focusing on arrested coalescence of droplets, emulsion microstructure, and bulk properties. Chapter 3 examines the effects of different-sized droplets on droplet deformation, for various solids levels. Chapter 4 studies the impact of multiple droplet connections by observing addition of a new droplet to an existing arrested structure and its ability to rearrange the microstructure. Chapter 5 describes the full emulsion microstructure formed by the connections of mono-disperse and poly-disperse droplets. Chapter 6 compares the long-used petrochemical emulsion model arrest behaviour with edible plant and animal fat systems. Finally, Chapter 7 summarises the major conclusions of the research and provides recommendations for future study in this area.

## **CHAPTER 2 Literature Review**

Arrested coalescence is one of the factors which determine the stability in an emulsion (Walstra, 2003a). The droplets are the structural components of various food emulsions which form numerous shapes by undergoing arrested coalescence and hence define the shelf-life and quality of the end product (McClements, 2004). Droplet characteristics, like size, charge, concentration, interactions and interfacial properties govern the physicochemical properties of the emulsion (McClements, 2007a). A detailed knowledge of basic physicochemical and sensory properties of a food emulsion may therefore provide sufficient information to enhance their formulation.

The aim of this review is to provide some of the underlying principles of food emulsions as relevant to arrested coalescence. The first half of this study begins with the discussion of overall concepts and properties of emulsions while the second half will summarize the phenomena behind arrested coalescence and their effect on fluid rheological properties.

### **2.1. Basics of Emulsion**

Arrested coalescence is one of the leading causes of instability in emulsions. The following sections briefly explain what breakdown mechanisms are most likely to happen and how they cause instability.

#### **2.1.1. Definition and types**

A mixture of two immiscible liquids, one liquid (dispersed phase) dispersed in other liquid (aqueous phase), is known as an emulsion (McClements, 2007a, Cosgrove, 2010, Vanapalli et al., 2002b). Emulsion can be classified into oil-in-water (O/W), water-in-oil (W/O) and multiple (O/W/O or W/O/W) emulsion based on the distribution of water and oil phases. O/W refers to an emulsion in which oil is dispersed into an aqueous phase, e.g. milk, creams, beverages, sauces, mayonnaise and dressings. While W/O refers to the dispersion of an aqueous phase in oil, e.g. margarine, butter and spreads. Multiple emulsions are a dispersion of two immiscible liquids with multiple levels of structure. Originally the emulsions were distinguished as molecular (particle size < 0.001 $\mu\text{m}$ ), colloidal (particle size 0.001 $\mu\text{m}$  to 0.1 $\mu\text{m}$ ) and coarse (particle size > 0.1 $\mu\text{m}$ ) (Ostwald, 1919). The recent classification of emulsions has divided it into (1) micro-

emulsions (<100nm), (2) mini-emulsions (100nm to 1 $\mu$ m) (3) macro-emulsions (>1 $\mu$ m), based on the size. Emulsions are homogeneous at a macroscopic scale and heterogeneous at a microscopic scale (Pichot, 2010). This is significantly important in a wide range of industries like food (Coupland and McClements, 2001, Home, 1996, Kalnin et al., 2002), pharmaceuticals (Itho et al., 1995, Okochi and Nakano, 2000, Rogers et al., 2003, Muguet et al., 2001), cosmetics (Dahms and Zombeck, 1995, Miller et al., 1999, Miller et al., 2001, Eccleston, 1997), petroleum (Fang et al., 2001, Eow and Ghadiri, 2002, Lee, 1999) and paints (Watson and Mackley, 2002, Huybrechts et al., 2000). The present research is concerned with the properties of O/W emulsions.

### 2.1.2. Emulsion Composition

There is a wide range of food products which are partly or wholly emulsions or have gone through an emulsified stage during their processing (Ghosh, 2007, McClements, 2004). Food emulsions having various chemical constituents are complex in nature. Along with water and oil, food emulsions consist of emulsifiers, preservatives, chelating agents, buffering systems, sweeteners, antioxidants, salts, flavours and colorants (McClements, 2004, Dickinson, 1992). The type and amount of these constituents strongly influence the physicochemical and organoleptic properties of the emulsion.

The O/W food emulsion mostly consists of triglycerides dispersed in the aqueous phase. The triglycerides are formed mainly of fatty acids which are present in the form of esters of glycerol. The chemical structure of triglycerides has three fatty acids grouped with one glycerol molecule, which forms 'simple' or 'mixed' triglycerides depending on the similarity of the fatty acids (**Figure 1**). If all the three fatty acids are similar, it forms a simple triglyceride. The presence of two or three non-identical fatty acids forms a mixed triglyceride. The types and proportions of fatty acids strongly influence the characteristics (both physical and chemical) of fats. And the degree of saturation helps in classifying the fatty acids; they may be: saturated, unsaturated or polyunsaturated (Campbell et al., 2006).

Fats and oils play a vital role in nutritional and physicochemical properties of the emulsion in various ways. The scattering of light by oil droplets results in an opaque emulsion (McClements, 2002). It is also found that flavour of emulsions (Buttery et al., 1973, Relkin et al., 2004, van Ruth et al., 2002) and texture of the emulsions get

influenced by the lipids as they crystallize and form fat crystal networks which ultimately increases mechanical strength to overcome any external force (Ghosh, 2007, Narine and Marangoni, 2002).

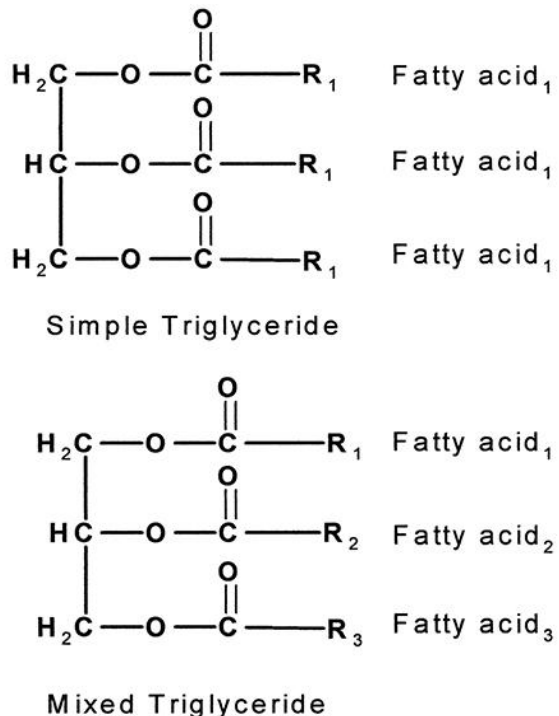


**Figure 1.** Molecular structure of triglycerides (simple and mixed) (Campbell et al., 2006).

The aqueous phase of O/W emulsion contains many water soluble constituents and their interaction with water determines the solubility and chemical reactivity (McClements, 2004). Crystallization and freezing of water strongly affects the stability and physicochemical properties (Cramp et al., 2004, Thanasukarn et al., 2004a). Some foods are modified using additives to alter their formulation to withstand freeze-thaw (e.g. frozen sauces) (Ghosh et al., 2006, Thanasukarn et al., 2004b).

The single boundary at the surface shared with two phases either liquid/liquid; gas/liquid or solid/liquid is known as an interface. It is of great interest since it leads to further interactions between the molecules. The term ‘interfacial tension’ represents the force which is required to deform the interface (Walstra, 2003a).

For emulsion stabilization, emulsifiers are the most important components. Various constituents like solid particles, biopolymers, and low molecular weight surfactants may

be found at an oil-water interface, which may help in reducing the interfacial tension and hence enable the emulsion to remain stable. However, there are chances that small molecule surfactants will form micelles in aqueous phase and interact with biopolymers, which will ultimately affect the emulsion properties (Courthaudon et al., 1991, Holmberg et al., 2002). The stabilization of the food emulsions by solid particles can be achieved when they get adsorbed at droplet interface. The stabilization resulting from the adsorption of the solid particle is referred as Pickering stabilization (Binks et al., 2005, Garti, 2002, Rousseau, 2000).

Surfactants, also known as surface-active-agents, are one of main components of an emulsion. It is the substance which gets adsorbed on the interface of the droplets and keeps them apart. These structures consist of a lyophobic group (no solvent attraction) and lyophilic group (strong solvent attraction). Hydrophilic and hydrophobic groups of surfactant are generally known as head and tail respectively and provide variety of structure (Eastoe and Cosgrove, 2005). Surfactant can be classified (based on hydrophilic group) as:

- (1) Anionic: head negatively charged
- (2) Cationic: head positively charged
- (3) Nonionic: head has no charge
- (4) Zwitterionic: head positively and negatively charged

Out of these surfactants, anionic and cationic are not compatible while nonionic and zwitterionic are compatible with all types (Pichot, 2010). When surfactants are added into water they form a variety of thermodynamically stable structures known as ‘association colloids’. **Figure 2** shows a schematic representation of various association colloids. These structures are formed due to their tendency to minimize the unfavourable contact between water molecules and the non-polar tail parts of surfactant molecules. The type of association colloid is governed by the polarity and geometry of the surfactant molecules (Dickinson and McClements, 1995).

Surfactants form micelles in water when their concentration exceeds a level referred to as the ‘critical micelle concentration’ or cmc (Myers, 1988). Below the cmc value, surfactants are dispersed mostly in the form of monomers, however, at concentrations higher than the cmc, surfactants form micelles and the concentrations of monomers

remain constant. Interestingly, despite the dynamic nature of micelles, their size and shape are well-defined under the given environmental conditions and addition of more surfactants mainly results in an increase in the number of micelles. Due to the fact that monomers and micelles have different properties, an abrupt change in some physicochemical properties is observed in surfactant solutions once the cmc value is exceeded (Myers, 1988). For example, surfactant monomers are highly surface active, whereas surfactant micelles have little surface activity due to their coverage by the hydrophilic head groups. Therefore, the surface tension of aqueous solutions (or, equivalently, the interfacial tension between oil and their solutions) decreases with an increase in surfactant concentration below cmc, but remains largely the same at concentrations higher than cmc.

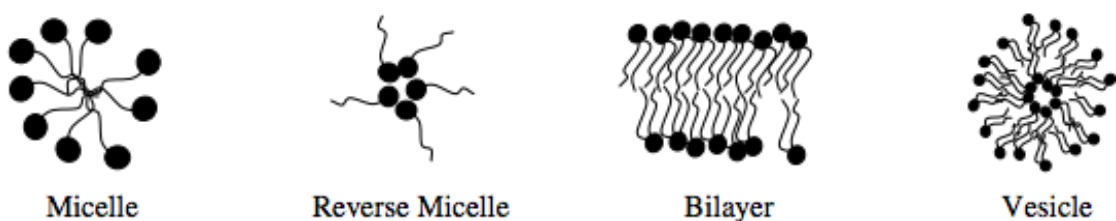


**Figure 2.** Various types of association colloids formed by surfactants in water.

In general, surfactants should possess three characteristics to be effective on emulsion production and long-term stability. Firstly, they should rapidly adsorb on the oil and water interface with relative high desorption activation energy (Hsu et al., 2000). This results in strong adsorption on the interface and, consequently, the surfactants ‘sit’ firmly on the interface. Secondly, when the surfactants are adsorbed, they should have the ability to reduce the interfacial tension. This can facilitate droplet break-up since less energy is required for droplet disruption, resulting in smaller droplets. Finally, the surfactants should form a layer at the droplet interface to suppress droplet coalescence when droplets collide. Not only should this property be able to stabilize droplets during the shelf-life of a product, but also during emulsification. Depending on the type of the surfactants, they induce coalescence stability by various mechanisms. Nonionic surfactants, such as those employed in this work, generate such stability by a number of short-range repulsive forces such as steric overlap repulsion, thermal fluctuation interactions and hydration (McClements, 2005). Additionally, surfactants are able to stabilize droplets against coalescence by the so-called “Gibbs-Marangoni” effect

(Boode et al., 1993, Walstra and Smulders, 1998). This stability mechanism is based on the movement of the surfactant along the droplets interfaces. When two droplets collide the planar continuous phase squeezes out between droplets, dragging some of the surfactants. This action generates a concentration gradient along the interface. This results in a tendency of surfactants to move to the regions of low surfactant concentration, dragging some of the continuous phase along with them. This motion of the continuous phase causes an increase in the planar film thickness, hence stabilizing the droplets. The combination of these factors results in the overall effectiveness of nonionic surfactants for emulsification.

### **2.1.3. Emulsion Formation**

Emulsion formation is known as emulsification. The dispersed and continuous phase is mixed together by means of energy incorporated by some mechanical devices (e.g. homogenizer). Sufficient energy leads to the breakdown of the big droplets to smaller droplets, which leads to phase separation over a certain period of time. To avoid this separation, it becomes necessary to use emulsifier in the system to keep the droplets apart for a desired period of time. The emulsifier helps in decreasing the interfacial tension (due to its surface activity) which ultimately minimizes the effects of interfacial forces. The emulsifier (in homogenization) helps:

- (1) to decrease the interfacial tension between oil-water to facilitate droplet break-up
- (2) to form a shield (layer) around the droplet to restrict coalescence

High speed mixers (McClements, 2004, Loncin, 2012), ultrasonic homogenizers (Abismail et al., 1999, Patist and Bates, 2008) and membrane emulsification (Joscelyne and Trägårdh, 2000) are the most commonly used mechanical devices in food industry to form the emulsions. Homogenization is usually categorized into two steps: primary homogenization and secondary homogenization. The first step produces larger droplets while the second step reduces the droplet size further to the smaller ones (Pichot, 2010). Nevertheless, in general, it is hard to distinguish between these steps and they may occur at the same time as well.

To control the homogenization process, the forces acting on the droplets are of great importance. The disruptive forces (which breaks down the larger droplets) generated by

the homogenizers are opposite to the interfacial forces (which makes the droplets minimize their free energy by reducing the interfacial area by undergoing coalescence). The interfacial forces, which make the drops spherical, are referred as the Laplace pressure,  $\Delta P_L$  (the difference in pressure of droplets: inside and outside, at the oil-water interface) which is expressed as the following equation (Walstra, 1983, Lucassen-Reynders and Kuijpers, 1992):

$$\Delta P_L = 2\gamma / r \quad 2.1$$

where,  $\gamma$  is interfacial tension between oil and water, and  $r$  is the droplet radius. Equation 2.1 clearly indicates that the radius of droplet is indirectly proportional to the pressure gradient, meaning that if the pressure is high the radius will be smaller and vice-versa.

#### **2.1.4. Emulsion Forces**

There are three types of interactions between droplets:

##### **2.1.4.1. Van der waals Forces**

The van der waals attractions can be of three types: dipole-dipole (Keesom), dipole-induced dipole (Debye) and dispersion interactions (London). The first two forces (even if they are large) are vectors, and tend to cancel each other as they have different dipole orientations. Hence the London dispersion interactions are considered the most important, which occurs because of fluctuations in charge (Tadros, 2013). The interaction between two molecules or droplets remains unaffected by the presence of other droplets, making the total potential equal to the sum of potentials between the pairing droplets (Friberg et al., 2003).

The interaction energy,  $G_a$ , is strongly dependent on the shape of the droplets and the separation distance between them. And it can be presented as:

$$G_a = -\beta / r^6$$

where,  $\beta$ , the London dispersion constant, is obtained from polarizability of the droplet (Tadros, 2013). If two droplets having  $R$  radius are close enough ( $h \ll R$ ), then they tend to behave as two flat surfaces, whose potential,  $V_v$ , can be determined as:

$$V_v = AR / 12h$$

where A stands for Hamaker constant. And this equation states that the van der Waals attraction is inversely proportional to the separation between the droplets and directly proportional to the radius of the droplet.

#### 2.1.4.2. Electrostatic repulsion

Electrostatic forces are the repulsive forces between negatively charged particles or droplets, which make the emulsion stable unlike Van der waals forces, which leads to emulsion destabilization (**Figure 3**). In a system, if the sum of total repulsive forces

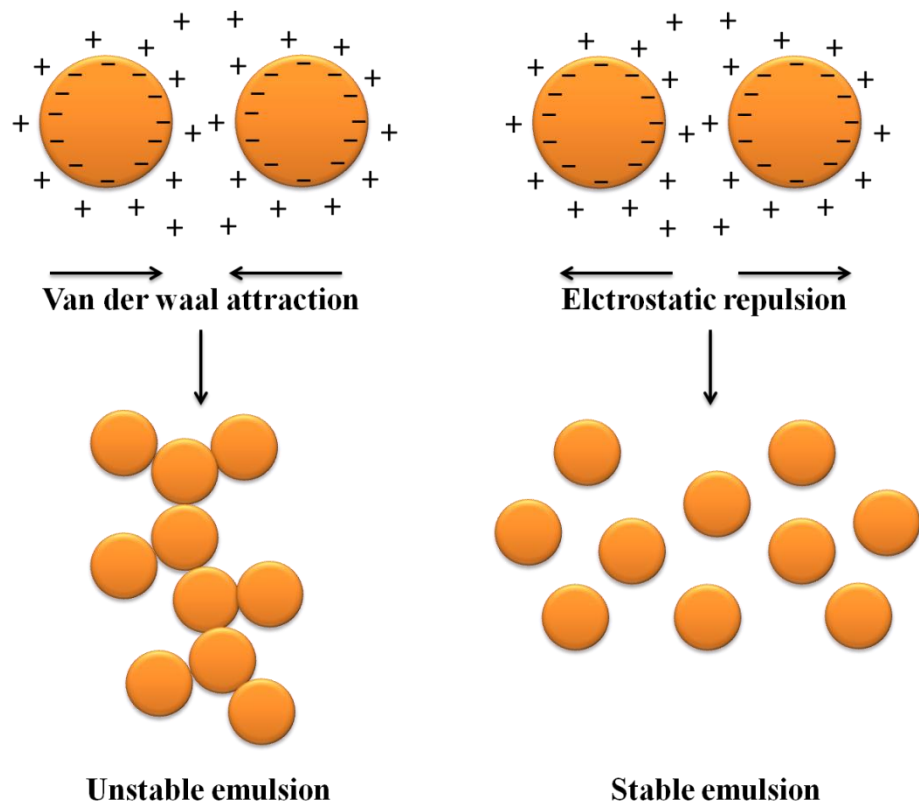


**Figure 3.** Intermolecular forces between two spherical emulsion droplets.

are greater than the sum of total attractive forces, then the emulsion would remain electrostatically stabilised (Dickinson, 2009). A DLVO (Derjaguin, Landau, Verwey, Overbeek) (Derjaguin and Churaev, 1989, Derjaguin, 1987, Hunter, 1986) theory states that the total potential energy of the particles can be used to determine the stability of the particles or droplets. Total potential energy is a sum of potential energies: of attractive interactions and repulsive interactions caused by van der waals and electrostatic forces, respectively. Van der waals forces being unresponsive to concentration of the charges get influenced by the distance between the particles.

Hence, it results into attraction of droplets if the distance between them is subsequently small. However, electrostatic forces are highly influenced by the charges rather than distance between the particles (Tadros, 2011).

### **2.1.5. Instability**

Emulsion stability is the ability of an emulsion to withstand the changes in its physicochemical properties over time (McClements, 2005). Thermodynamics provides the information of the processes occurring during emulsification or after homogenization while kinetics provides information about the rate of processes occurring. Being thermodynamically unstable, the emulsion undergoes some changes or breakdown due to the external forces like: gravitational, centrifugal, electrostatic or magnetic forces (Cosgrove, 2010, Borwankar et al., 1992). A variety of processes which may lead to the breakdown of the emulsion physically are creaming, sedimentation, flocculation, coalescence and Ostwald ripening (Dickinson, 1992, 1982) as illustrated here in **Figure 4** (Tadros, 2013). To understand the stabilization mechanism of emulsions, it is important to differentiate the thermodynamic and kinetic stability (McClements, 2004, Ivanov and Kralchevsky, 1997).

#### **2.1.5.1. Sedimentation and creaming**

Sedimentation and creaming result from the density difference between a discontinuous phase and continuous phase. If the density of the discontinuous phase is higher than the continuous phase, it will lead to sedimentation (the droplets will settle down at the bottom). And if the discontinuous phase has a lower density as compared to the continuous phase, it will cream (the droplets will move to the top) (Cosgrove, 2010). In general, the density difference in most O/W emulsions is negative which makes the droplets rise upwards while W/O emulsions tend to sediment (van Aken, 2003). A uniform mixing can re-disperse the droplets in case of creaming (Dickinson and Stainsby, 1988). Creaming usually occurs when the density difference of the two phases is higher than 0.1 and when the radius of the droplet is larger than few hundred nm. Nevertheless, it is a reversible process, which can be reversed with gentle mixing or shaking (Dickinson, 1992). The creaming velocity  $v$  (of a droplet), in a dilute emulsion, can be expressed by Stokes' Law (McClements, 2004):

$$v = 2gr^2(\rho_{\text{cont}} - \rho) / 9\mu_{\text{cont}}$$

2.2

where  $g$  is acceleration due to gravity,  $r$  and  $\rho$  are droplet radius and density respectively,  $\rho_{\text{cont}}$  and  $\mu_{\text{cont}}$  are density and Newtonian viscosity of the continuous phase. There are various methods to decrease the creaming (McClements, 2004, Phillips and Williams, 2009, Dickinson and Golding, 1998, Chanamai and McClements, 2000, Pichot, 2010):

- (1) minimizing the density difference between dispersed and continuous phase
- (2) reducing the size of droplets
- (3) increasing the viscosity of continuous phase
- (4) increasing the concentration of droplets

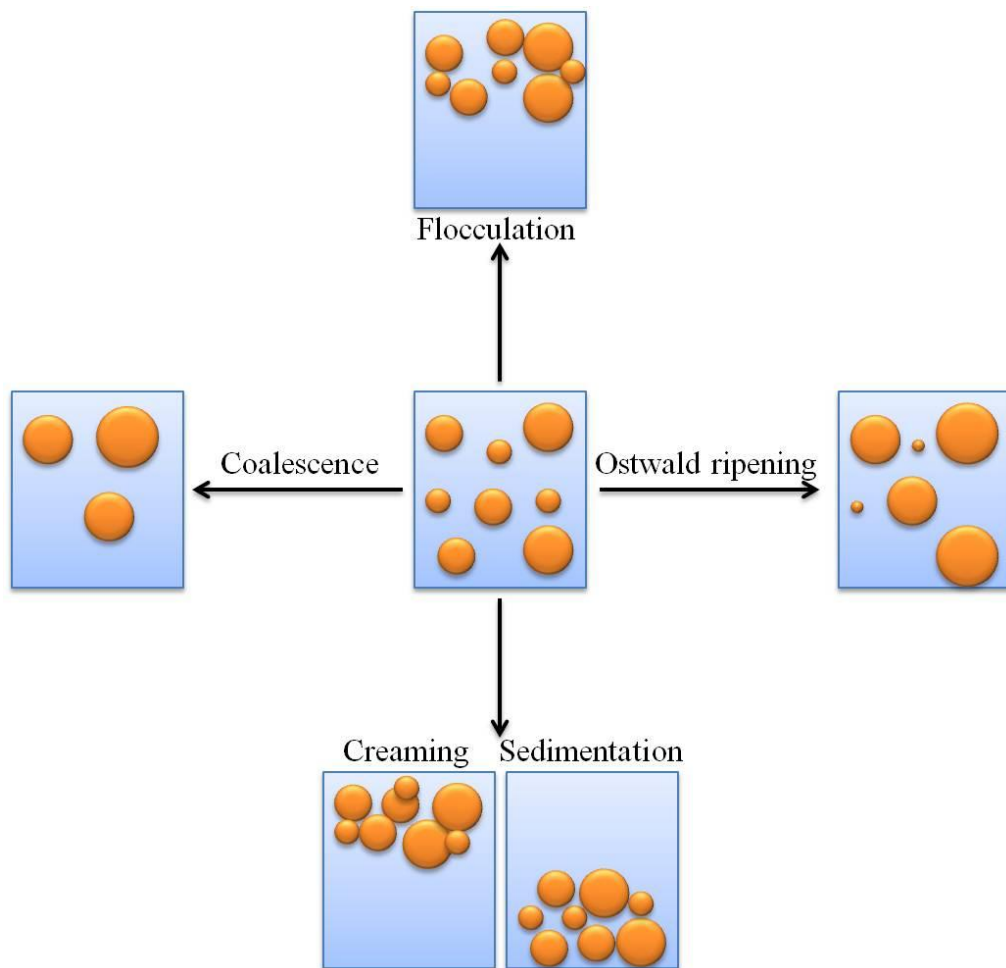


**Figure 4.** Various breakdown mechanisms in emulsions (Tadros, 2013).

### **2.1.5.2. Flocculation**

Formation of large units by the aggregation of droplets (without undergoing any change in size) is called flocculation (Cosgrove, 2010). In flocculation the particles retain their individual identity. Small force can be used to disrupt the droplets network formed and hence can re-disperse them in the system. It occurs when there is insufficient repulsion in the droplets due to the weak van der Waals forces. The magnitude of the attractive forces decides if the flocculation is weak or strong. The frequency and proportion of droplets' collision strongly influence the rate of flocculation (McClements, 2004). The collision can happen due to Brownian motion, gravitational flow or applied mechanical force.

The flocculation process is the most complicated of all instability processes as it depends on a number of factors like: emulsifier type, mean droplet size, oil volume fraction, pH, and ionic strength (Dickinson, 2010, Piorkowski and McClements, 2014). It can be categorized into bridging and depletion flocculation. Bridging flocculation occurs when adsorbed polymers bridge between droplets (Dickinson, 2009) while depletion flocculation occurs when the gap between two large droplets is smaller than hydrodynamic diameter of the non-absorbed polymers (when the droplets move towards each other). And the process of inversion of one phase to another phase due to any change in the conditions or time can, for example convert an O/W emulsion into a W/O emulsion.

### **2.1.5.3. Ostwald ripening**

The process of deposition of molecules of small droplets on the bigger droplets through diffusion in the continuous phase is called Ostwald ripening (Phillips and Williams, 2009, Kabalnov and Shchukin, 1992). Under this process, the small droplets get reduced in their size and finally disappear, which in turn makes the big droplets grow more and more. As the droplet size becomes smaller, the solubility of the oil phase gets increased. There are a few methods to control Ostwald ripening. The droplet size can be increased to slow down the rate of Ostwald ripening. The system with a narrow droplet size distribution also leads to reduction in the Ostwald ripening.

However, the occurrence of the listed processes may be seen at the same time and also one process can promote the other process to get started. For instance, the flocculation

may boost creaming and coalescence (Fredrick et al., 2010). The instability of emulsions has both positive and negative factors associated with it. For example, this may lead to the poor quality of mayonnaise as partial coalescence or total coalescence can cause phase separation while it can be noticed as important factor in achieving the desired properties in foods like ice cream, whipped cream.

#### **2.1.5.4. Coalescence**

Coalescence (total coalescence) refers to the fusion of two droplets, which were close enough at some point of time due to aggregation or creaming, to form a big droplet. Coalescence is desirable in butter and whipped cream as it gives good mouth feel. However, in most of the cases it is generally undesirable as it causes flocculation of oil droplets and reduces the shelf-life of the product. This process occurs when the thin film at the interface of the neighbouring droplet ruptures and initiates the coalescence. It results into a spherical shape because it gives the lowest value of Laplace pressure (Fredrick et al., 2010, Cosgrove, 2010). The processes of droplet deformation, droplet encounter, film thinning and film rupture are some of the initiators for coalescence (van Aken, 2003, Ghosh, 2007). The two neighbouring droplets get deformed when they approach each other with a very minor gap between them and forming a thin film due to the flattening of surfaces (**Figure 5**). The droplets get flattened when the external forces exceed the internal Laplace pressure (Walstra, 2002). In turbulent flow, the adsorbed layer at the interface gets dragged with an increase in the outflow of the aqueous phase (**Figure 5**), which forms a spot on the surface leading to high interfacial tension, film rupture and hence coalescence. The dimensionless Weber number is used to determine the tendency of the droplets to get deformed. The equation between Laplace pressure and external forces is expressed by Weber number:

$$We = \Delta\sigma_{exp} / PL = a^2\sigma_{exp} / 2\gamma h \quad 2.3$$

The droplets remain undeformed if  $We < 1$  but at  $We = 1$ , deformation of droplet eventually becomes stronger and leads to the formation of flat film. At  $We > 1$ , the flat film becomes larger and thus rate of coalescence gets increased (McClements, 2004, Sottmann and Strey, 2005).

Partial (arrested) coalescence is one of the stages of coalescence, where the merging process of two droplets is halted at an intermediate stage. This is undesirable in some

cases (like milk, cream) as it causes flocculation of droplets in emulsions (Petrut et al., 2016). However, in other cases, like butter, margarine and ice cream, this is important as it helps increase mechanical strength by improving viscosity (thickening) and phase separation (Boode et al., 1991, Vanapalli et al., 2002a, Van Boekel and Walstra, 1981). The chances of partial coalescence can be minimized by using appropriate emulsifiers or surfactants, as they can help in maintaining the distance between the droplets and resisting their coalescence. For example, SDS, an ionic surfactant, provides 10 - 30 nm distance between the droplets; whereas Na-caseinate can even provide 100 nm or more distance (Van Boekel and Walstra, 1981).

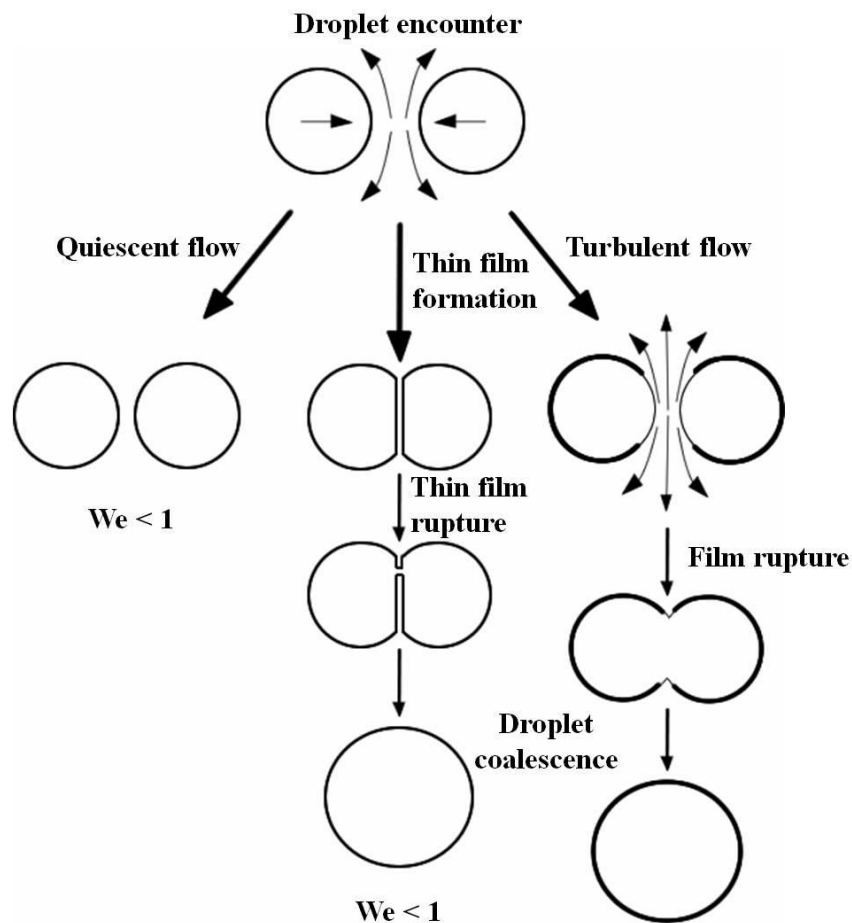


**Figure 5.** Coalescence due to quiescent and turbulent flow (McClements, 2004).

One of the remaining factors that can influence the stability of emulsion is the application of shear. At idle state, an emulsion might be stable, but once some force is applied it might result into instability. That is because applying shear to an emulsion decreases the space between the droplets and makes them approach each other (Van Boekel and Walstra, 1981, Darling, 1982, Mulder and Walstra, 1974). However, the

instability caused by shear also depends on the orientation of the fat crystals. It is observed that the interfaces having tangentially oriented crystals are more stable as compared to the ones which have radially oriented crystals (as they have tendency to pierce the thin film between the adjacent droplets when the shear is applied) (Darling, 1982, Boode and Walstra, 1993).

## **2.2. Solid fat content - Crystals**

The crystals present in an emulsion play a vital role in emulsion instability (particularly in arrested coalescence) and govern internal dynamics and mechanical properties which ultimately impacts the bulk behavior of the emulsions (from diluted to concentrated) (Giermanska et al., 2007). They can cause an emulsion to be stable or unstable, depending on their location. They may be present in dispersed phase or in continuous phase (Fredrick et al., 2010, Rousseau, 2000). Being in the continuous phase, the crystals can stick to the interface and hence can stabilize the emulsion. While being in the dispersed phase, the chances of solidification of crystals increase and they can protrude from the interface causing the droplets to coalesce. Surface tension keeps the warm droplets spherical and smooth, after cooling, which gets turned into rough shape due to the formation of irregular/un-oriented crystals which favours coalescence (Thivilliers et al., 2008).

From previous studies, it has been observed that the rate of coalescence is strongly influenced by the solid fat content (SFC). The crystals are considered as the connecting source between the approaching droplets, helping the oil to flow from one droplet to another and making them coalesce (Boode et al., 1993). The crystals cannot make the network by protruding very far but can only protrude through the interface when the droplets are very close to each other (Boode et al., 1993, Schuster, 1996, McClements, 1998).

For arrested coalescence, some specific amount of SFC is required to form the crystal network throughout the droplet. And if the crystallized fraction is high enough, the droplet will provide rigidity and won't result in to a spherical shape (caused by surface tension) during the coalescence (Thivilliers et al., 2006). The fractal aggregation theory can be used to evaluate the least SFC required to form a crystal network. According to fractal theory, the globule diameter should be higher than the fractal aggregate's critical

diameter which forms the crystal network (Fredrick et al., 2010). This can be expressed as (Boode et al., 1993, Schuster, 1996):

$$d > y\psi^{1/(D-3)} \quad 2.4$$

where, d is the globule diameter, y is the effective diameter of the aggregated crystals,  $\psi$  is the volume fraction of crystal and D is fractal dimensionality (< 3). This equation thus states that the size of globules and crystals formed affects the minimum SFC needed. The smaller globule will result in large crystals and hence will need more SFC to form a crystal network. Secondary nucleation enhances arrested coalescence since it forms small crystals which favour this process (Boode et al., 1993).

### **2.2.1. Crystallization Theory**

Crystallization occurs when molecules get arranged into a tightly-packed, ordered structure (Hendrickson, 2013). The difference in the chemical potential of solid and liquid phase can be used to determine the driving force (Himawan et al., 2006).

#### **2.2.1.1. Nucleation**

The nucleation, the very first stage, is the process of forming the localized structure, without which the formation of crystals is not possible. Homogenous and heterogeneous are the two main types of nucleation (Hendrickson, 2013, Fennema et al., 2008). Homogenous nucleation does not require any solid surface but considerable super cooling. It occurs spontaneously if the super cooling is increased. Nucleation occurring in the presence of a foreign surface (e.g. container wall, seed crystals) is known as heterogeneous nucleation. Homogenous nucleation occurs spontaneously in bulk emulsion but is very rare in food emulsions, because the impurities act like a solid-liquid interface and hence decrease the energy that is necessary for nucleation.

#### **2.2.1.2. Crystal growth**

Crystals continue to grow after the stable nuclei are formed, till the melt and crystalline state reaches the thermodynamic equilibrium (Hartel and Hartel, 2001). The growth begins with the migration of crystallizing TAGs' molecules (either by diffusion or convection mode). Once the diffusion occurs, the molecules need to rearrange or orient so as to locate a site to consolidate into lattice structure. After this process, the liquid phase removes the latent heat of fusion by means of conduction and convection (Hartel

and Hartel, 2001). Until the system ends up having a constant solid fat content, the crystal growth keeps going. The growth of the crystals is influenced by parameters like agitation, rate of cooling, number of nuclei and temperature. The growth is directly proportional to the rate of cooling. This growth leads to contraction, by replacing 90% volume of liquid fat by solid fat. The extent of contraction depends on the polymorph; the more stable polymorph will be denser.

### **2.2.2. Crystals' arrangement in emulsion**

Crystals have the tendency to move freely at an interface and their contact angle (at dispersed  $\theta_o$  and continuous phase  $\theta_w$ ) can be determined by the interfacial energies acting on it. The 2D representation of the solid particle at the interface is shown in **Figure 6** showing the contact angle. Along with the crystal position, the surfactant properties (such as type, concentration) can alter the interfacial energies (Fredrick et al., 2010).

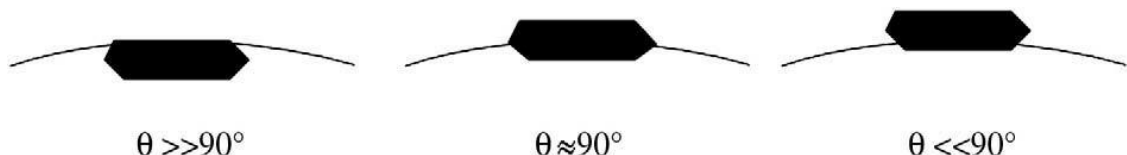


**Figure 6.** Arrangement of the movable crystals at the interface (Fredrick et al., 2010).

The study of fat crystals was further extended and explained various arrangements of the crystals as shown in **Figure 6** (Fredrick et al., 2010). The needle type (N-) globules have crystals arranged in the network whereas (L-) types have the crystals which are arranged tangentially. (M-) types can have the mixed arrangement while (K-) types contain thick crystals which do not follow the curvature and hence can even extend the oil globule interface.

### **2.2.3. Crystal size and polymorphism**

Arrested coalescence is also influenced by the size of crystals. The stability of the emulsion is observed to be reduced with an increase in the size of the crystal. With the size increase, the chances of partial coalescence will also increase as the larger crystal can cover large distance by protruding through the interface (Fredrick et al., 2010).

The polymorphic forms explain all possible arrangements of crystals, including their orientation, angle and packing. Fat crystals have three polymorphs –  $\alpha$ ,  $\beta'$  and  $\beta$  (**Figure 7**). The alkyl chains form hexagonal structure in the  $\alpha$  form, where they have no angle tilt, and maintain distance (which prevents the packing from its zigzag nature). In  $\beta'$  form, the structure formed by chains is orthorhombic, which being non-parallel prevents it from packing closely. Whereas in  $\beta$  form, the chains are packed more closely as they are parallel to each other (Himawan et al., 2006).

These polymorphs have stability in the following sequence. Being wetted by the oil, the crystals  $\alpha$  and  $\beta'$  are more polar as compared with the  $\beta$ . So the polymorphism can alter the position of crystals and thus can vary the structure formed with the different arrangements (Fredrick et al., 2010).  $\alpha$  being the least stable has the minimum surface energy and minimum heat of crystallization. The nucleation rate gets affected by minor differences occurring in the surface energy.  $\alpha$  can change to  $\beta'$  or  $\beta$  depending upon the thermal treatment. The  $\beta'$  form, being metastable, is desirable for the production of butter and margarines as it provides textural properties to the system because of its optimum crystal network. The  $\beta$  form is the most stable form and has large plate like crystals, which ultimately makes poor crystal network hence not suitable for butter and margarine. However, it is suitable for confectionery fats (Sato, 1999, Sato and Ueno, 2011). **Figure 8** shows various possible crystal structures in an emulsion.

#### 2.2.4 Crystallization of fat in an emulsion

There are two types of nucleation that can help in crystallization of fats: homogeneous and heterogeneous. There is significant difference in the nature of fats that crystallizing in oil-in-water emulsion as compared to the bulk. Of the two nucleation types, heterogeneous nucleation occurs in bulk systems, whereas in oil-in-water emulsions both types help in crystallization of fat. Since emulsion has polydisperse droplets, the catalytic impurities get unevenly distributed through them (**Figure 9**). This leads to isolation of impurities that either causes heterogeneous nucleation with an increased super cooling or homogeneous nucleation with an increased under cooling (Awad and Sato, 2002).

Depending on the sites or locations of impurities, nucleation can be divided into three types (**Figure 10**) (Awad and Sato, 2002):

- a) volume or bulk nucleation, is initiated by randomly distributed catalytic impurities in the oil phase when heterogeneous and by supercooling when homogeneous
- b) interfacial heterogeneous nucleation, which occurs when molecules of emulsifier provide templates at the oil-water interface, further helping crystallization
- c) interdroplet nucleation, which occurs because of the interactions between solid and liquid droplets.

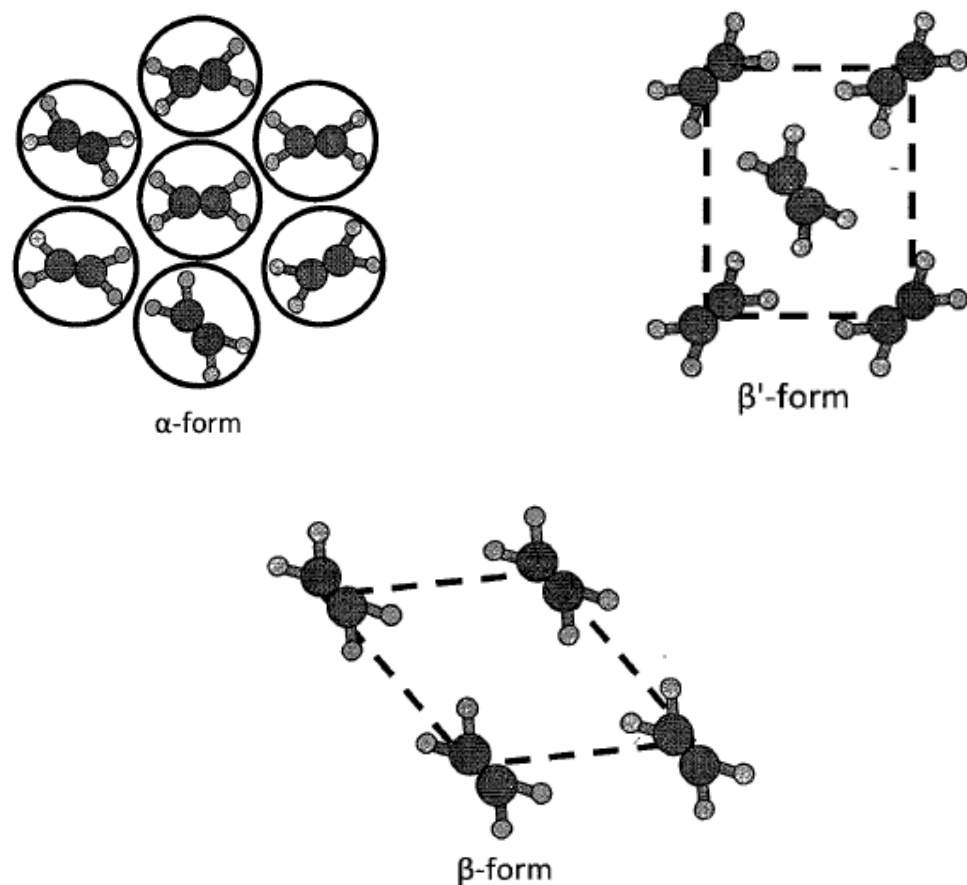


**Figure 7.** Subcell structure of tree polymorphs (Sato, 2001).

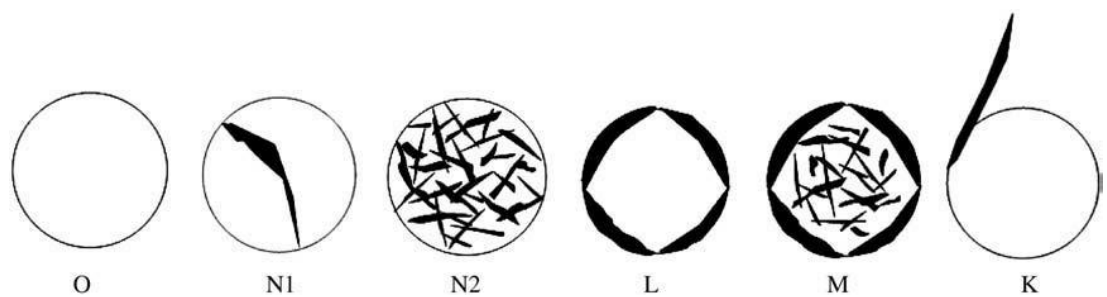


**Figure 8.** Arrangement of the semi-crystalline globules in O/W emulsion (Fredrick et al., 2010).

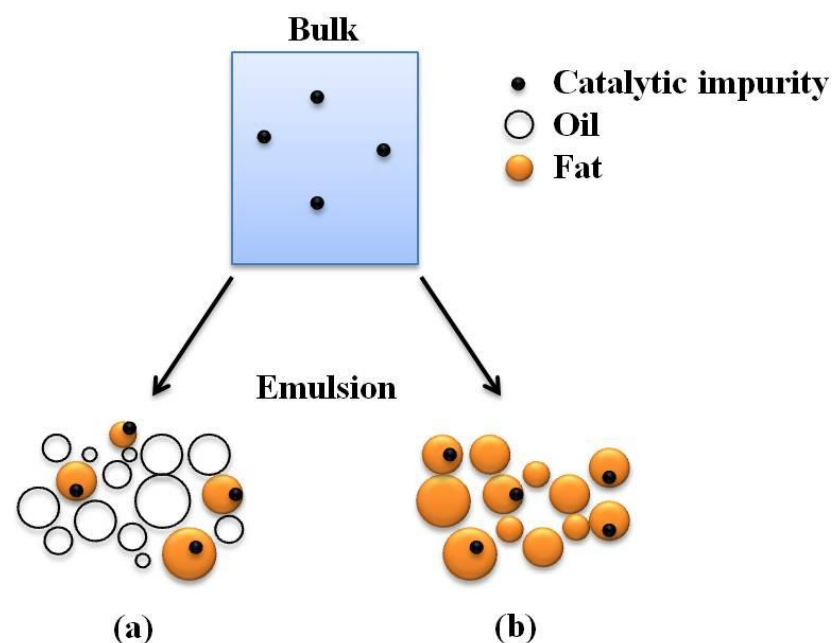


**Figure 9.** Fat crystallization in oil-in-water emulsions: a) without hydrophobic additives, b) with hydrophobic additives (Awad and Sato, 2002).

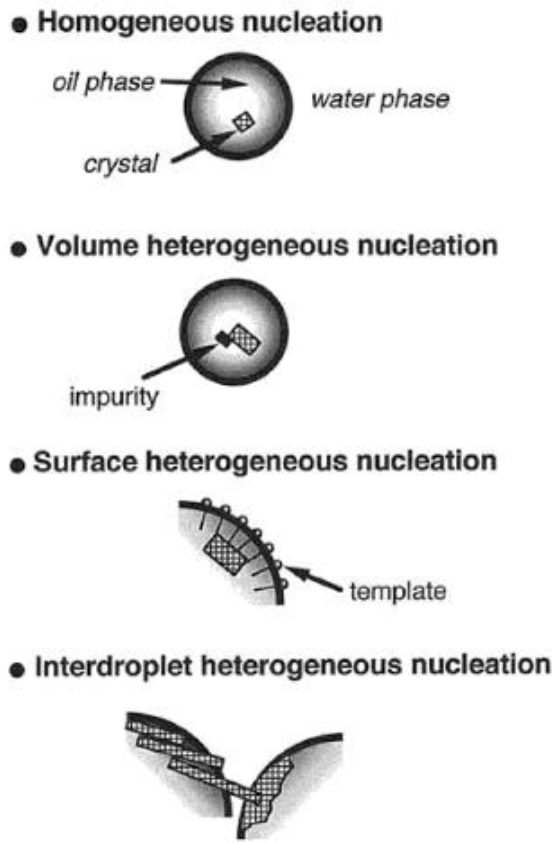


**Figure 10.** Types of nucleation in oil-water emulsions (Awad and Sato, 2002).

### 2.3 Pickering emulsion

Pickering emulsion droplets are liquid droplets stabilized by solid particles at the interface instead of by surfactant molecules (Ramsden, 1903, Pickering, 1907). One such droplet is shown in **Figure 11** (Chen et al., 2013), the red solid particles form a particle shell that separates the inner water phase colored in green with the outer oil phase marked by the black color.

Pickering emulsions have been intensively studied in the last decade, and may find broad applications in lots of important areas, due to their remarkably controllable permeability, mechanical strength and biocompatibility (Velev et al., 2000, Dinsmore et al., 2002, Lee and Weitz, 2008). For example, Pickering emulsions can be used to encapsulate drugs and then be delivered to infected areas in the drug-delivery (Simovic et al., 2009) industry. They can also be applied to facilitate oil recovery (Eow et al., 2001) in the oil industry: Pickering emulsions are often used in oil-field operations to

enhance oil recovery efficiency by altering the surface tension between water and oil in the reservoir, mobilizing oil which would otherwise remain in the reservoir as residual. The well-controlled coalescence in Pickering emulsions can also promote material mixing and profit the field of chemical and biochemical assays (Ahn et al., 2006).

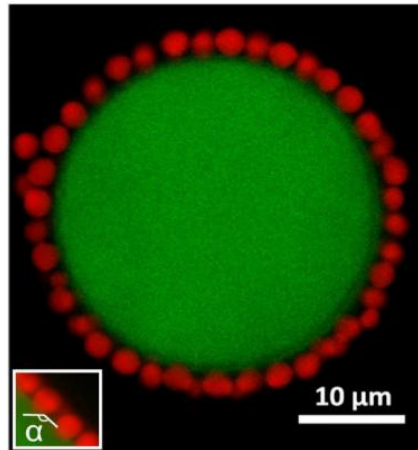


**Figure 11.** A 2-Dimensional confocal slice showing a typical Pickering emulsion droplet. The large saltwater droplet is dyed in green and coated by the small PMMA particles which are dyed in red. The particles have the diameter  $d = 3\mu\text{m}$  for this particular sample. The magnified image in the inset shows the contact angle of particles at the interface:  $\alpha = 133 \pm 5^\circ$  (Chen et al., 2013).

### 2.3.1. Stability of Pickering emulsion

Because of these broad applications, people are highly interested in the stability of Pickering emulsions, which is closely related to their coalescence behaviour. If the Pickering emulsion droplets can merge spontaneously just like ordinary water droplets, they are highly unstable; and they are very stable for the opposite situation. Therefore to understand the stability of Pickering emulsions, we must illustrate how such droplets coalesce, which still remains poorly understood. More interestingly, the existence of an extra structure - particle shell - may bring fundamentally different merging physics and enrich the classical coalescence research. Consequently, there is a great scientific and practical significance to clarify the coalescence of Pickering emulsion droplets. If the surface of Pickering emulsion droplets is poorly coated, they can coalesce automatically and form supracolloidal structures (Studart et al., 2009, Subramaniam et al., 2005), such as the case shown in **Figure 12**. Complicated dynamics and structure of particles are observed during merging, because of the combined effects of charge, surface tension

and liquid flow (Stancik et al., 2004). The numerical simulation further indicates that the repulsion between particles, the particles' ability to attach to both droplet surfaces, and the stability of the liquid film between droplets are essential for coalescence behaviours (Fan and Striolo, 2012).

Coalescence barely occurs if the surface is covered and stabilized by closely packed particles. However, stability of the droplets can also be influenced by other factors. For instance, inspired by the strong influence of electric field, which can deform liquid surface into conical tips (Taylor, 1964, Collins et al., 2008, Brazier-Smith et al., 1971, Stone et al., 1999), one can create liquid jets out of these tips (Collins et al., 2008), induce electro-coalescence between two isolated droplets (Brazier-Smith et al., 1971) or among a large population of droplets (Zhang et al., 1995), and even protect droplets from coalescing (Bird et al., 2009).

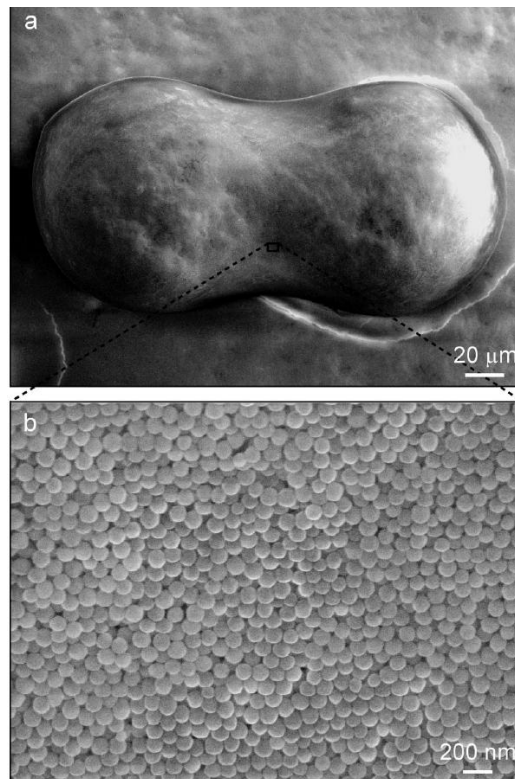


**Figure 12.** (a) Nonspherical supracolloidal structure formed by the arrested coalescence of droplets, (b) highlighting the jammed particles in the neck region between partially coalesced droplets (Studart et al., 2009).

## 2.4. Adsorption of particles

There are various studies, from Pickering (1907) to Ma et al. (2017), that have investigated the adsorption of particles at droplet interfaces. Levine et al. (1989) and

Aveyard et al. (2003) investigated the stability of the emulsion stabilised by monodisperse solids particles at interface of droplets. The studies showed strong dependency of stability of emulsion on the angle of adsorption of solid particles. Solid particles having  $<90^\circ$  contact angle at the interface contribute in oil-in-water emulsion stabilisation, whereas, solid particles having  $>90^\circ$  contact angle at the interface contribute in water-in-oil emulsion stabilisation. Binks et al. (2007) further examined the stability of emulsions by means of silica nanoparticles and pure cationic surfactant. Both were observed to stabilise the emulsion, however, at high pH very limited stability was provided by particles. Whereas, surfactant led to higher stability when used in high concentrations. Since many studies investigated the kinetic stability of emulsion, Sacanna et al. (2007) and Kraft et al. (2010) investigated thermodynamic stability of emulsion to be a function of addition of monodisperse droplets ranging from 30-150nm, and a combination of stabilised particles and amphiphilic ions, respectively.

Some researchers (McLean and Kilpatrick, 1997, Simon et al., 2008) studied the relation between surface and volume properties by adsorption of asphaltenes aggregates on to the surface of silica droplets. And, it has been observed that the monolayer of asphaltenes aggregates promoted the stability of the emulsion. Whereas, other studies (Hodge and Rousseau, 2003, Hodge and Rousseau, 2005, Nadin et al., 2014) showed association between wax crystals and stability of emulsions. A strong impact was observed, as wax crystals enhanced the stability of the emulsion by inhibiting the coalescence of the droplets.

Similarly, Ma et al. (2017) examined the adsorption of wax on paraffin oil-water droplets with and without surfactant. The study showed synergistic effect between the wax and surfactant that caused wax, having no interfacial activity, to get adsorbed on the droplets interface. This phenomenon was found to have direct impact on the interfacial storage modulus and interfacial viscosity. The study also investigated the influence of temperature, wax content and surfactant on the extent of adsorption and hence rheological properties. Temperature and elastic modulus are inversely proportional, whereas wax content and elastic modulus are directly proportional to each other. While in case of surfactant, it is observed that the elastic modulus is higher in the samples with surfactant as compared to the sample without surfactant. This is because

the wax and surfactant have a synergistic effect, that leads to the formation of a compact structure.

## 2.5. Arrested coalescence

The fusion of two droplets in such a way that it freezes at an intermediate stage before forming a spherical shape, is known as arrested coalescence. The presence of the fat crystals is essential to achieve such conditions (Fredrick et al., 2010). As explained earlier, it is the most demanding approach in the present time as it serves the best in achieving good quality of food products, for example, in dairy products like ice cream and whipped cream. Also it might be helpful in various packing arrangements in soft matter.

### 2.5.1. Theories on arrested coalescence

For achieving the arrested coalescence, studies on semi-crystalline fat were done (Van Boekel and Walstra, 1981). This concluded that the presence of crystals (at an interface) influences instability in an emulsion. Further research was done on O/W emulsions to understand the effects of fat (Boode and Walstra, 1993, Boode et al., 1993). This presents the mechanism of the arrested coalescence as shown in **Figure 13** (Fredrick et al., 2010). Initially, crystals being free in a droplet can relocate themselves at the interface. The van der Waals forces make the crystals aggregate and form a crystal network during crystallization. Hence, the crystals lose the tendency to move freely and stay in their position at the interface, which later on pierce through the interface when two droplets approach each other leading the droplets to coalesce. It does not lead to total coalescence, but arrested or “partial” coalescence, because the structure gets fixed as the rigid network of fat crystals is formed (Van Boekel and Walstra, 1981).

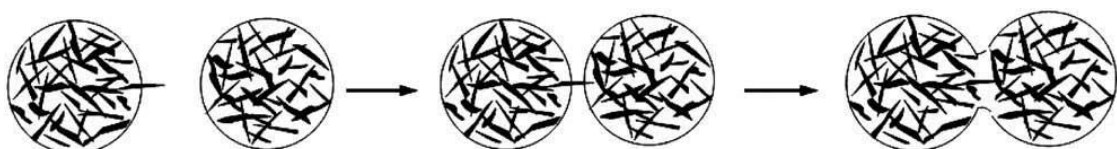


**Figure 13.** Mechanism of arrested coalescence (Fredrick et al., 2010).

Later on, another mechanism of arrested coalescence was described, which presented the use of model of balancing the energies for achieving such conditions (McClements, 2007a). According to this study, the two energies- interfacial and elastic energy can be

balanced to arrest the coalescence at particular point. And the sum total energy in the system can be calculated by summing these two energies (**Figure 14**) (Pawar et al., 2012).

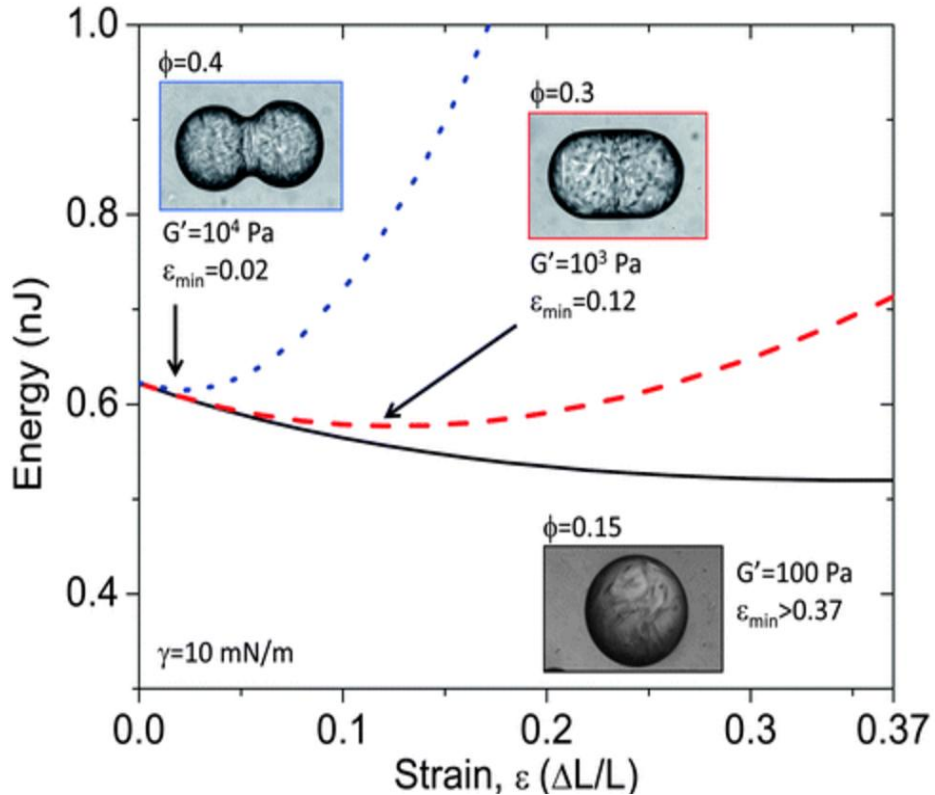


**Figure 14.** Variation in the energies during the different coalescence stage. The minimum strain is represented in the graph at zero for the highest arrest (arrest at high level of solid content) while maximum strain is observed to be at 0.37 for total coalescence of the droplets (Pawar et al., 2012).

For obtaining the specific results of arrested coalescence, some parameters require attention like: composition of emulsion, conditions during preparation, and properties of dispersed and continuous phase. As the crystals may be present in the dispersed phase or in continuous phase, it may lead to different situation during arrested coalescence.

### 2.5.2. Dispersed phase

As explained earlier, the SFC is most important in achieving the arrested coalescence. SFC leads to an increase in partial coalescence in most of cases but only up to a certain limit (McClements, 2007a). This is believed to decrease with the further increase in SFC. Various arrested coalescence levels are observed by varying the SFC

(McClements, 2007a) (**Figure 15**) (Pawar et al., 2012). It is observed that at the minimum solid content (0.15), there occurs total coalescence while the start of coalescence is restricted at the highest solid content (0.50). This research shows that arrested coalescence increases with a decrease in the SFC and vice versa.

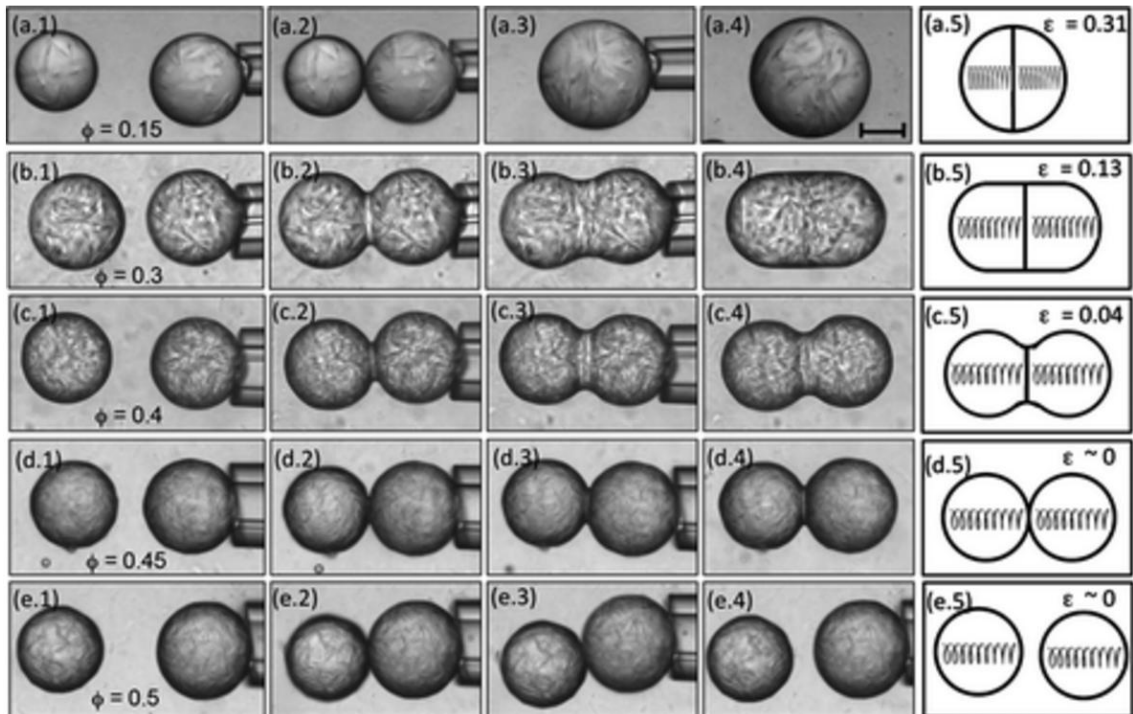


**Figure 15.** Coalescence arrest at different level of solid fat content (SFC). Right column represents the strain associated with each situation (Pawar et al., 2012).

## 2.6. Colloidal particles

Colloidal particle systems are at the heart of many products we encounter every day. Colloidal suspensions range from biological liquids such as blood and milk to technologically relevant materials such as house hold cleaners, paint and lubricating materials (Borówko, 2000). A colloidal system consists of two phases which *appear* to consist of only one phase to the naked eye - or did so under the microscopes of the day in 1861 when British chemist Thomas Graham coined the term “colloid” to describe a solution containing particles in suspension. Around the turn of the century, such famous scientists as Rayleigh, Maxwell, and Einstein also studied colloids (Edelstein and Cammaratra, 1998). As explained in **Table 1** (Goodwin, 2009) there are several possible phase combinations where either phase could be a gas, a solid or a liquid (two gas phases will mix on a molecular level and do not form a colloidal system) (Goodwin,

2009). The particle dimension in the dispersed phase has traditionally been considered to be in the range 1 nm-1 um, although unique behaviour of colloidal particles can still be observed with particle sizes up to 10 um (Goodwin, 2009). A homogeneous mixture in which the particles are larger than 1 um in at least one dimension (i.e., larger than the range for colloidal particles) is classified as a suspension (Brady and Senese, 2008). Colloidal systems contain at least one or more substances that have at least one dimension in the range between  $10^{-9}$  m ( $10$  Å) and  $10^{-6}$  m ( $1$  mm) in size (Hiemenz, 1986). On the smaller end of this scale, there are no distinct boundaries between the phases, and the system is considered a solution. On the larger end of this scale, particles will begin to fall to the bottom due to gravitational force, and the phases are separated. Aggregation involves the association of particles to form clusters, and depends on two distinct influences: (1) particles must move in a way that collisions occur, and (2) particles that repel each other are said to be stable, since they do not form aggregates. Colloids interact with each other at an extremely short range, (usually much less than the particle size), so that particles have to approach very close to each other before any significant interaction is felt. The interaction may be attractive (van der Waals) or repulsive (electrostatic repulsion, steric). There are many important properties of colloidal systems that are determined directly or indirectly by the interaction forces between particles. Colloidal particles are dominated by surface properties. If the surface area to volume, or surface area to mass of a spherical particle is considered, the dependence on the particle radius is  $S_A/V \sim 1/r$ . This relationship shows that as particles decrease in size, the surface properties of the particle become increasingly important (Fisher, 1998). The measurement of particle size is also a defining property. Colloidal particles dispersed in liquids can be the desired end-product (e.g., pigment particles in paint) (Kozan, 2007) or the product of a chemical reaction in the process (e.g., aqueous reduction of metal ions in electronic applications) (Chow and Gonsalves, 1996).

| <b>Phase</b> | <b>Gas (bubbles)</b>   | <b>Liquid (droplets)</b> | <b>Solid (particles)</b>  |
|--------------|------------------------|--------------------------|---------------------------|
| Continuous   |                        |                          |                           |
| Gas          | -                      | Liquid aerosol (mist)    | Solid aerosol (smoke)     |
| Liquid       | Foam (shampoo)         | Emulsion (mayonnaise)    | Sol (ink)                 |
| Solid        | Solid foam (packaging) | Solid emulsion (butter)  | Solid sol (stained glass) |

**Table 1.** The colloidal dispersions types (Goodwin, 2009).

Aggregation has become increasingly significant during the last twenty-five years. Industry has become progressively more interested in controlling the microscopic properties of particles, such as composition, shape, surface roughness, surface characteristics, and porosity. It has been estimated that 70% of all industrial processes involve dealing with fine particles at some point in the process (Bushell, 2011). Characterization of these particles helps us to understand and predict or control their behaviour in many processes. In industry, the properties of particles determine whether or not a dust is a respiration hazard, whether granular materials will mix or segregate when agitated, and whether material in a hopper will flow in a controllable fashion, behave like a liquid, or not flow at all. Many of the traditional particle characterization techniques make assumptions about the shape or physical structure of the particles being measured. The extraction of linear-size parameters from laser scattering measurements generally assumes that the particles are spherical. This assumption is normally made because it probably is not important to the technique being used, but often it is because it is a difficult problem. Almost every particulate system involves to a greater or lesser extent some particles that are aggregates of smaller particles in the system. This may be unimportant for systems such as the handling of bulk ores, but in processes such as drinking water filtration, it is the dominant structure. These aggregates are often wispy, tenuous entities that are absolutely unlike spheres, plates, or other familiar geometric forms.

Aggregation is a physical process in which the dispersed elementary units, which make up the aggregate, stick to one another irreversibly under the influence of interparticle forces to form tenuous structures. The two main considerations in the study aggregation

of fine particles are the reaction kinetics of the process and the morphology of resulting aggregates. The reaction or aggregation kinetics have been studied in depth since Smoluchowski in 1916. On the other hand, characterization of particles with irregular geometries has been a cause of much discussion and an agonizing task for scientists and engineers in diverse fields of research (including combustion, astrophysics, atmospheric sciences, and materials science among others). A breakthrough in mathematics came about with the introduction of the concepts of “fractal geometry” which was eventually applied to irregularly shaped particles. What seemed as a peculiar geometrical tool at first, was soon shown to be able to describe not only the complex macroscopic geometrical patterns in nature (snowflakes, clouds, coastlines, and rivers), but also the seemingly random structures of aggregates of fine particles. After the first experiments that explicitly investigated and revealed the fractal nature of aggregated particles in a metal smoke (Forrest and Witten Jr, 1979), the 1980s witnessed an avalanche of experimental and theoretical studies of the fractal description of aggregates in colloidal and aerosol systems.

### 2.6.1. Multiple connections of droplets

In the simplest case of equal spheres, a pair of particles would form a dumbbell. A third particle can attach in several different ways, and the greater number of aggregates, the number of possible structures rapidly increases. **Figure 16** (Elimelech et al., 1997) shows different particle configurations for an increasing number of primary particles. In most aggregative processes, the number of particles within a particle cluster may be on the order of hundreds or thousands, therefore, an understanding of the nature of the cluster structure is important. Aggregates are recognized as fractal objects.

Euclidean geometry is primarily the study of straight lines and smooth curves. In nature, (the earth) straight lines and smooth curves are the exception rather than the rule. Rugged profiles exist everywhere, from the clouds in the sky, to the outlines of trees and mountain ranges, and the stars in the sky. Fractals are characterized by a non-integer power law dependence of a measurable quantity upon the length of the object (or upon time) (Mandelbrot and Pignoni, 1983). The areas and perimeters of fractals are infinite.

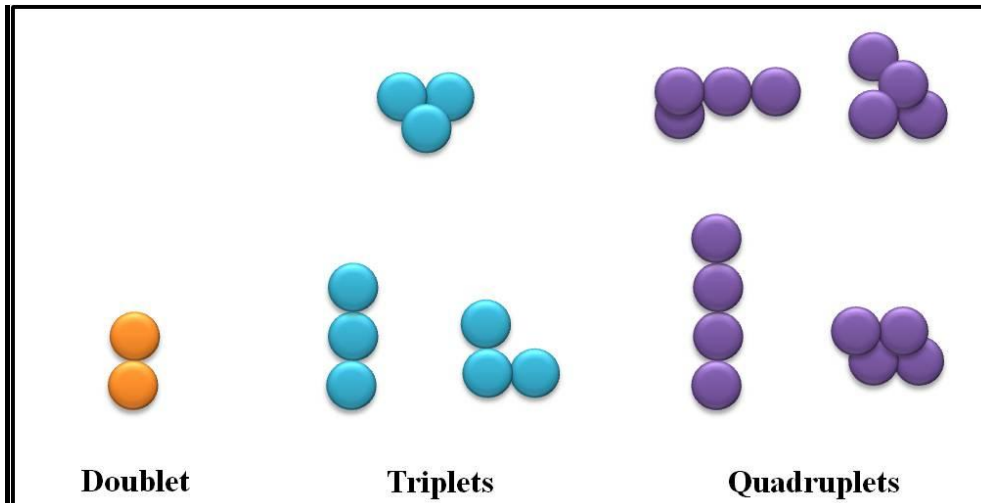


**Figure 16.** Different arrangements of various number of primary particles (Elimelech et al., 1997).

The connections or aggregates formed by arrested droplets might change rheology of the emulsions, as they determine the mechanical strength of the system (Oberdisse, 2006). For example, restructuring, occurring because of aggregate sintering (coalescence), may change the properties of emulsion by modifying the size of polydisperse primary particles. The average primary particle size increases as restructuring takes place, which narrows down the primary particle size distribution (Eggersdorfer and Pratsinis, 2013, Tsantilis and Pratsinis, 2000). Restructuring not only increases the average cluster (particle) density but also increases the fractal dimensionality by decreasing the floc size (Koos et al., 2014, Selomulya et al., 2003, Eggersdorfer et al., 2012). However, Meakin and Jullien, (1988) have shown direct dependence of density on the angle at which the particles are located. Restructuring can also be encountered in flocs of monodisperse polystyrene latex microspheres, where mixing triggers the relocation of the particles and hence leads to structural changes (Clark and Flora, 1991). The rate of mixing directly effects the rate of change in floc structures. For instance, excess mixing leads to less porous structure, where compaction suppress the structure to pack closely (Klimpel and Hogg, 1986). In capillary suspensions also, restructuring is noticed for very long times, which well enough fit a power law. Koos et al. (2014) showed variation caused by restructuring in a network in capillary suspensions both at rest and under applied shear deformation. Another research supports such structural changes in aerosol materials (like silicone dioxide and polymers) where fractal-like aggregates leads to the formation of compact structures

during material synthesis and energy generation, where high temperatures are being used (Eggersdorfer et al., 2011). Because at high temperatures, the rate of chemical reactions is faster in aerosol processes the overall changes in the structure or aggregates is influenced by particle collision and coalescence. These changes lead to formation of compact aggregated which later can even undergo restructuring and break-down (2011, Eggersdorfer et al., 2010). The structural changes in the aggregates for various fractal dimension,  $D_f$ , are presented in **Figure 17** (Eggersdorfer et al., 2011), where 256 monodisperse particle were generated by diffusion limited cluster-cluster (DLCA,  $D_f = 1.79$ ), diffusion limited (DLA,  $D_f = 2.25$ ), and ballistic particle-cluster (BPCA,  $D_f = 2.73$ ) agglomeration. This clearly shows that more compact structures sinter faster. These DLCA, DLA and BPCA provide direct and more detailed understanding about the structures of the real aggregates formed under appropriate conditions (Weitz and Oliveria, 1984, Weitz et al., 1985). The structure of the colloidal suspensions can range from aggregates to more compact yet vast structures through gelation (Jaquet et al., 2017). Jaquet et al. (2017) have studied shear-induced gelation of colloids, where they found coalescence to be a strong factor that affects the gelation, above glass transition temperature. It was observed that when both coalescence and shear-induced aggregation were combined the system can either delay gelation as coalescence decreases fractal clusters volume or hasten gelation as partial coalescence can make the bonds between the particles even stronger. Hence the result of shear-induction depends on characteristics time of aggregation and coalescence. There are various studies done on gelation in liquid-liquid dispersions and highly viscous droplets (Placin et al., 2003, Philip et al., 2000, Philip et al., 2001), which showed that sintering can be a novel route to transform emulsion from initially liquid to a dense and viscous emulsion.

## 2.7. Droplet size distribution

Controlling the droplet size of an emulsion is one of the ways to induce certain functionality, it influences important emulsion properties mainly stability and shelf life (Henry et al., 2009). The food industry most frequently encounters polydispersed emulsions, resulting in a distribution of droplet sizes.

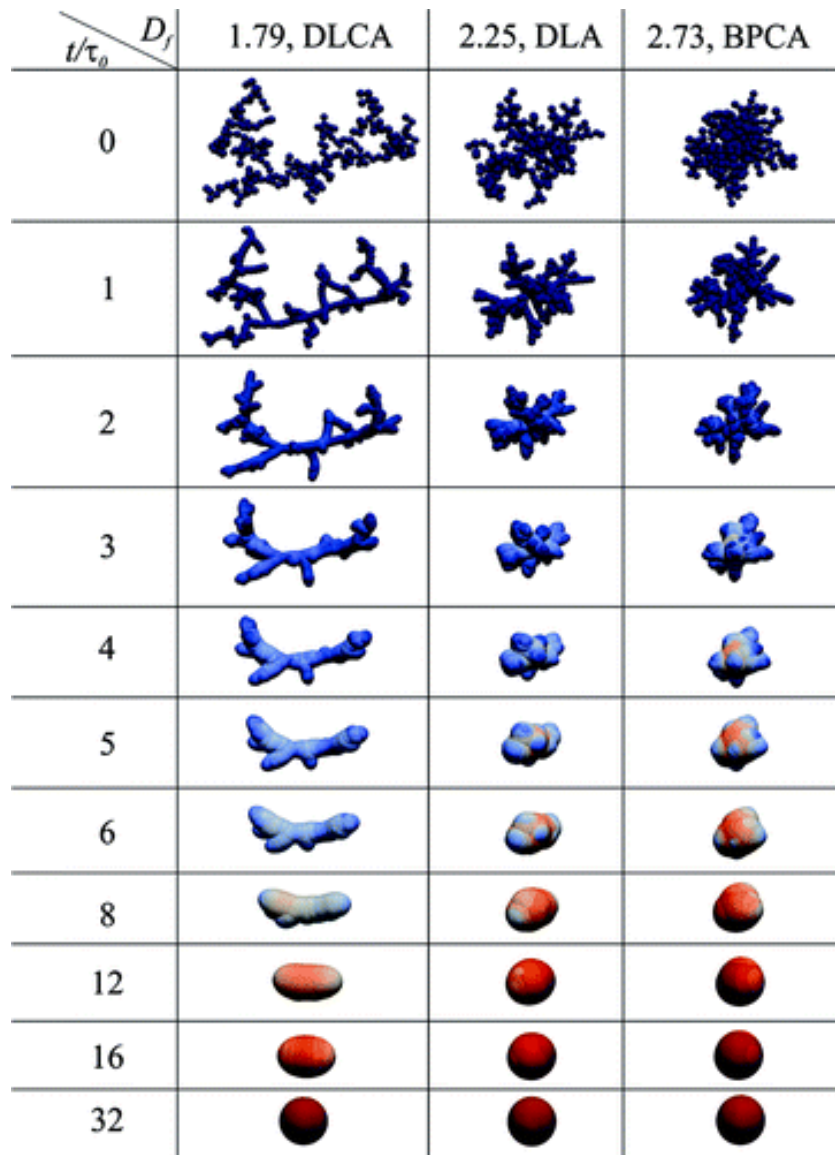


**Figure 17.** Structural changes in aggregates of 256 monodisperse primary particles with the passage of time. Blue and red color represents: large and small aggregate curvature, respectively (Eggersdorfer et al., 2011).

The understanding of structure of emulsions becomes important as it provides information about the elasticity of bulk emulsions, which is ultimately helpful in designing a product. Emulsions having droplets of the same size are referred as ‘monodisperse’ while the emulsions (almost all real emulsions) having a wide range of droplet sizes are referred as ‘polydisperse’ (**Figure 18**). A common approach of investigating emulsions is to utilize just the mean droplet size and the width of distribution (Hunter, 1986, McKenna, 2003). The droplet size distribution is normally presented in the form of a continuous histogram of volume frequency of known size-

class of droplets. A number of procedures exist to calculate the mean droplet size. Each of these methods results in the mean droplet size in units of ‘length’, however each emphasizes different physical properties of the emulsions. The equation for mean droplet diameter ( $d$ ) and standard deviation ( $\sigma$ ) can be used to characterize the particle size distribute of an emulsion; e.g.:

$$d = \sum \frac{n_i d_i}{N}$$

$$\sigma = \sqrt{\frac{\sum n_i (d_i - d)^2}{N}}$$

where  $n_i$  is the number of droplets with diameter  $d_i$  and  $N$  is the total number of droplets.

For a fairly monodisperse emulsion, the values of different mean diameters are similar, however, with an increase in polydispersity they vary more. Thus for an emulsion with a wide distribution of particle size the width of the distribution also needs to be reported. The width of a particle size distribution can be conveniently expressed by the standard deviation weighted with the particles’ surface area, divided by  $d_{32}$  (Walstra, 2003a). The range of width of distribution in food emulsions is generally between 0.5 to 1 (Walstra, 2003a). If the width of the distribution is large, the shape of the distribution should also be described. (e.g., skewed, log-normal, truncated or bimodal) (McClements, 2004).

The packing of the droplets also strongly influences the properties of an emulsion (from monodisperse to polydisperse). The elasticity of viscoelastic droplets gets affected by volume fraction of the dispersed phase. As the volume fraction increases, the rigidity of the droplets increases, which is strongly influenced by the droplet size distribution. Monodisperse emulsions tend to have ordered structures, while polydisperse emulsions have more disordered structures (Mason et al., 1996). Considering the aggregated emulsions, the rheological properties of the emulsion do not only get affected by droplet interactions but also by the structure of the emulsions. The pressure difference between the fluids also plays an important role in predicting the properties of an emulsion, as summarized by Mason et al. (1996). Evaluation of an emulsion prepared from

monodisperse droplets is much less challenging than more polydisperse ones (Mason et al., 1996).

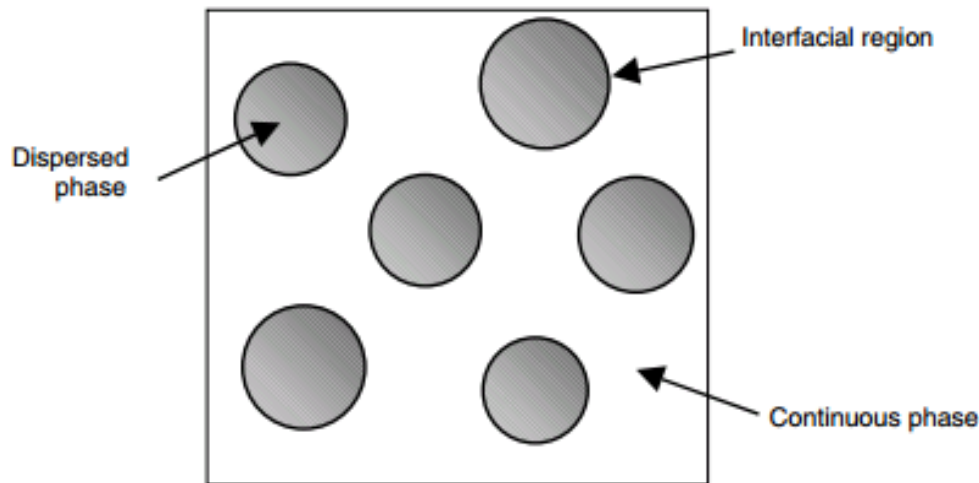


**Figure 18.** Polydisperse oil-in-water emulsion containing oil droplets dispersed in continuous phase (McKenna, 2003).

Manoharan et al. (2003) showed an impactful way of studying packing by using microspheres, through which they tried to explain a way to understand packing of finite and infinite number of identical spheres; which has always been a concern for researchers. The equal-sized polystyrene particles were used to disperse into toluene and water, which were brought together by evaporating oil. For less than 15 number of spheres, the structure always results into polyhedra; be it identical or unique; where they act as hard sphere. The packing was not found to be purely dependent on the particle-particle interactions. (Lauga and Brenner, 2004, Manoharan, 2006).

### **2.7.1. Instruments for determination of particle size distribution:**

Several different instruments have been developed to measure particle size distribution of food emulsions. Of these some of the most commonly used techniques are microscopy, static and dynamic light scattering, Electric sensing zone (i.e., Coulter counter), sedimentation, and ultrasonic spectrometry (McClements, 2004). The instrument used in the present work is based on static light scattering or laser diffraction light scattering technique. In this method a monochromatic light beam (generated by a He-Ne gas laser,  $\lambda=0.63 \mu\text{m}$ ) is passed through a sample cell containing the diluted emulsion (oil volume fraction  $< 0.05\%$ ) and the light scattered by the droplets of the emulsion is collected by an array of photosensitive detectors. The intensity of the

scattered light is measured as a function of scattering angle and analyzed by a computer. Generally the smaller the particle size of droplets, the more the scattered light would be (McClements, 2004). Finally using the Mie theory approximation the particle size distribution is calculated that gives the best fit with the experimental scattering data (Kerker, 2013). The use of Mie theory requires the refractive index of the dispersed phase and the continuous phase. In modern light scattering instruments a number of additional techniques are used such as more than one laser source and measuring intensity of backscattered light so that the instrument can be used for a wide range of emulsion droplet size (typical range of 0.02 to 2000  $\mu\text{m}$ ) (Rawle, 2001).

## 2.8. Emulsion Rheology

The study of deformation and flow of a material under applied stress or strain is termed rheology (McClements, 1998, Barnes et al., 1989). To understand the relation between these two parameters, stress is applied on some material (which is to be tested) and strain is measured, or vice versa. Food emulsions, being compositionally and structurally complex in nature, may behave differently, ranging from solid, liquid, plastic to viscoelastic (McClements, 2005). Rheology of food products relates to its density, viscosity, surface tension and physical properties. Consider two different materials: an ideal solid and a Newtonian liquid. Out of these two, the first is elastic. When it is sheared, stress and strain are proportional to each other. Hooke's law,  $\tau = G'\gamma$ , explains the simple relation for elastic solids, where  $G'$  is elastic shear modulus. For Newtonian liquids under shear:  $\tau = \eta\gamma$ , where stress is directly proportional to strain rate  $\gamma$ . Fluids containing gels, emulsions, polymers and are categorized as 'viscoelastic', possessing time-dependent rheological behaviour.

Rheological properties originate from material composition and from their physical properties. These can be used as tools for designing products with desired texture and flow properties. The results obtained from rheological measurements can also empower scientists to relate product quality to viscosity, elasticity, deformability, shelf life and interactions between molecules and also to assess mixing efficiency, power consumption and pumping rates (Barnes, 1994). For instance, **Figure 19** (McKenna, 2003) shows disruption in droplets structure, and hence shear-thinning behaviour.

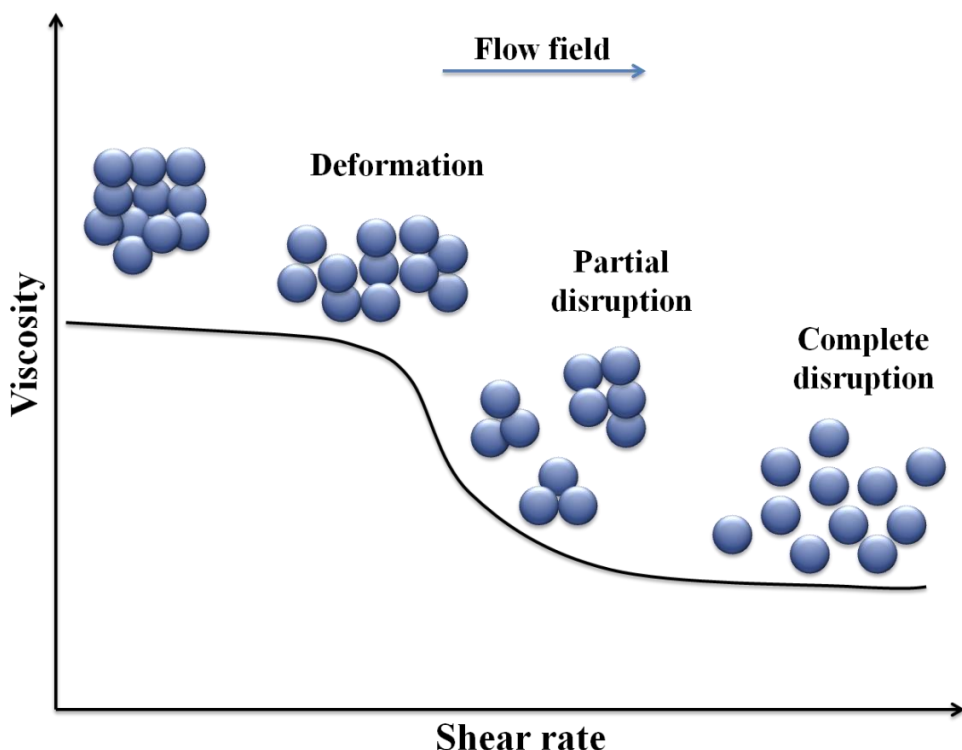


**Figure 19.** Droplets exhibiting shear thinning behaviour in an emulsion (McKenna, 2003).

There have been various studies conducted on emulsion rheology. The rheology does not only provide an understanding about the emulsions' deformation or flow properties but also about the internal strength or characteristics of droplets, which has a great influence on bulk behaviour. Elastic ( $G'$ ) and loss moduli ( $G''$ ) are parameters used to investigate a material's elasticity and viscosity, respectively, both in food (Goff and Hartel, 2013, Drelon et al., 2006) and model emulsions (Thivilliers et al., 2008). Thivilliers et al. (2008) showed direct relation between  $G'$  and thermal treatment, and hence gelling of emulsion. The emulsion was tempered at 4°C before examining its elasticity and viscosity.  $G'$  increased significantly because of tempering, however, this mainly depends on the droplet size and the ratio of surfactant and protein present in the continuous phase (Dickinson et al., 1997, Dickinson et al., 1999), which either leads to jamming or partial coalescence in the system.

Frostad et al. (2014) recently used a, Cantilevered-Capillary Force Apparatus (CCFA), for measuring force between two solid-in-oil-in-water (S/O/W) droplets. This method also measured rheological properties of individual droplets. As droplets containing wax dispersions have a yield stress (Pawar et al., 2012), upon compression they show stress

relaxation that holds similar properties to a bulk system. Waxy crude oil, as studied by Chang et al. (1998), have rigid solid-like properties when small stresses are applied, however it changes to a completely flowing fluid when higher stresses are applied. This is also supported by other research in edible fats (Bell et al., 2007), where  $G'$  was observed to be decreasing during crystallization because of constant stirring. The fat showed less dependency on the oscillation frequency. This provides us great information about the reaction that a system can give under two different stresses or situations. Rheological insights help us predict the structure of multiple droplet networks, if the individual droplets can withstand the forces occur during mixing and use. Parameters from rheological experiments are interlaced, and represent characteristics of formulations during manufacturing, processing, storage of emulsion. Hence, thorough research and deep understanding of structural properties of emulsions is crucial.

## **2.9. Conclusion**

The arrested coalescence is an important mechanism that has attracted growing research attention for its utilization in stabilization and formulations. In these studies, different methods of forming anisotropic shapes were exposed, which serve the purpose of stabilization of an emulsion. However, research in this area is still at preliminary stage. There is still generous amount of research yet to be conducted. Arrested coalescence in bulk emulsions was one of the least studied area. However, researchers have studied colloidal or aggregates formation in bulk, which is very distinct from what we studied now. Restructuring is also reported in the bulk emulsions studied earlier, but very little research was done to quantify this mechanism. Additionally, very little is known about the effect of size distribution on droplets deformation. This PhD research is hence focused on expanding the knowledge on arrested coalescence, from just two identical droplets to bulk mono and poly-disperse droplets.

## **CHAPTER 3 Arrested coalescence of viscoelastic droplets: polydisperse doublets**

### **3.1. Introduction**

Emulsions form the basis for common commercial products, such as foods, cosmetics and pharmaceutical formulations, but also find broad use as templates for advanced materials and unique controlled release systems. The stability of emulsions can govern the success of a product, and a key phenomenon is coalescence: when two droplets combine to form a single, larger, one.

Coalescence is undesirable when it increases the average droplet size in an emulsion, and can result in phase separation when the process is fast. Depending on the rheological properties of the droplets coalescence can be halted after initiation, but before completion, resulting in arrested, or partial, coalescence structures. In dairy foods, milk lipids are present in both solid and liquid forms, resulting in emulsion droplets containing solid crystals (Boode and Walstra, 1993, Fredrick et al., 2010) that impart a viscoelastic response that is responsible for the observed arrest (Pawar et al., 2012). Arrest contributes to the formation of three-dimensional networks of droplets in emulsions and is distinct from coagulated or flocculated droplet clusters (Torza and Mason, 1969, Princen, 1984) because the droplets are not connected simply by electrostatic or wetting interactions but by a common liquid bridge or neck because of the initiation of coalescence. Very viscous emulsions can coalesce on very long time scales (Philip et al., 2000, 2001) but are distinct from the droplets studied here that possess an elasticity able to stably offset the driving force of surface area reduction and halt coalescence at an intermediate state.

Arrested coalescence can be useful or beneficial to food products, for example, stabilizing whipped cream by a fat globule network that suspends small air bubbles. It has also been suggested to play a role in gas cell stabilization of doughs and batters (Brooker, 1993, 1996) and be a possible mechanism for stabilizing thin liquid films and coatings (van der Kooij and Sprakel, 2015). The robustness of arrested coalescence also allows creation of shaped droplets by assembly of spherical drops (2012, Pawar et al.,

2011) or by moulding techniques to produce unique structures that change shape due to external triggers (Caggioni et al., 2014, Caggioni et al., 2015). The formation of anisotropic droplet shapes is also relevant to the production of solid particles with non-spherical shapes, e.g. ‘snowmen’, which has been achieved using different wetting, cross-linking and adhesion approaches on polymer melts or emulsions (Torza and Mason, 1969, Pawar and Kretzschmar, 2010, Park et al., 2010, Sacanna and Pine, 2011, Walther and Müller, 2013, Zhang et al., 2014, Jung et al., 2000).

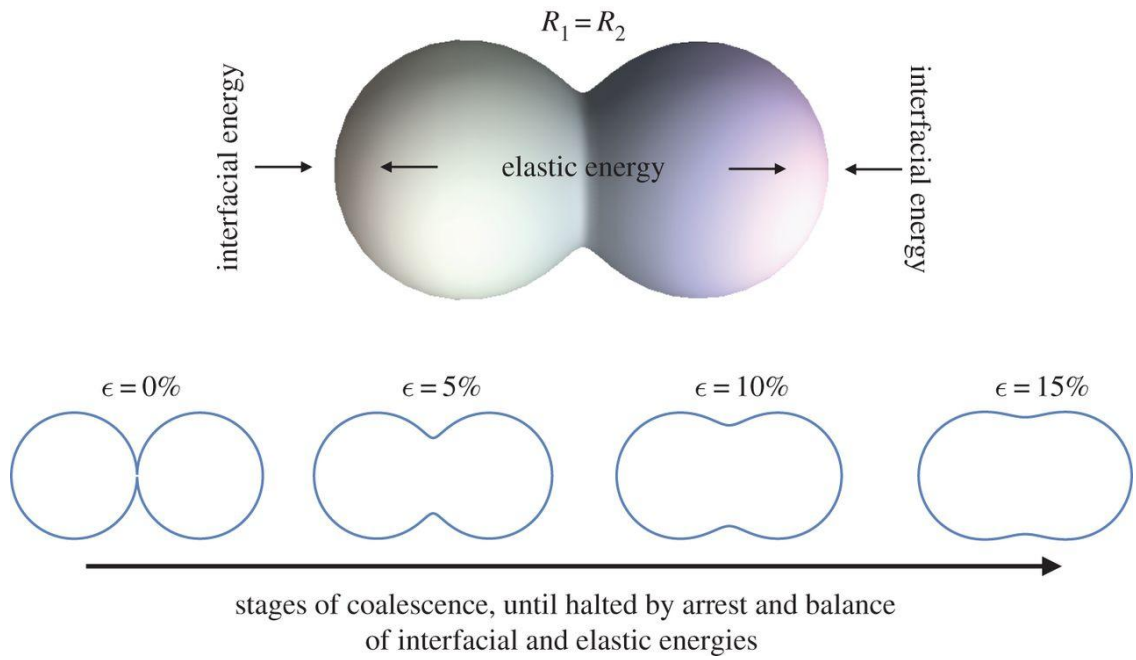


**Figure 20.** Conceptual model of droplet coalescence arrest, where the driving force bringing droplets together to reduce surface energy is offset by the resistance to deformation of the elastic energy storage capacity of the structure. The predictions of equation (3.1) are also shown for monodisperse droplets at different strain levels consistent with different stages of the coalescence process.

When two droplets arrest and form a pair, or doublet, the process can be described by the simple physical model of the opposing phenomena shown in **Figure 20**: interfacial tension-driven reduction of surface energy, and the elastic resistance to droplet deformation by the internal network of solid crystals (Pawar et al., 2012). If surface energy dominates, the droplets will completely coalesce into a sphere. If elastic energy dominates, the droplets are unable to even initiate coalescence and are stabilized by a sort of three-dimensional Pickering emulsion effect. Arrest occurs, however, when

coalescence can begin but not complete because surface and elastic contributions balance one another at an intermediate state of coalescence. The resulting droplet doublets can vary in shape depending on the state of coalescence when arrest occurs. Pawar et al. (2012) developed a model of the arrest process using an empirical measure of the decrease in droplet surface area and the linear deformation of the doublet as a function of the dispersed phase bulk rheology.

The model described the driving force of coalescence using an empirical fit of doublet surface area obtained from successive high-speed images of two monodisperse oil droplets at different stages of coalescence (Pawar et al., 2012). The model predicted the existence of an arrested state that changes with variations in droplet solids concentration, consistent with experimental results, but is only applicable to doublets formed from same-sized, monodisperse, droplets because of the specificity of the fitted area. Emulsions are usually polydisperse and the coalescence of two polydisperse droplets is expected to differ from the behaviour of the monodisperse case given the differences in surface area possible across a typical lognormal distribution of droplets.

We develop a more generalized form of the model of Pawar *et al.* (2012) that incorporates a theoretical description of droplet doublet shapes and their surface areas. The model is evaluated and compared to the predictions of the previous model and experimental data on polydisperse doublets with varying size ratios and solids concentrations. The work forms the basis for a broader effort to model the impact of arrested coalescence on bulk emulsion microstructures, enable the design of structured emulsion rheology, create novel colloidal shapes and develop innovative formulations using structured emulsions.

## 3.2. Experiment

### 3.2.1. Emulsion preparation

Equal volumes, 5ml each, of oil and aqueous phase was mixed. The dispersed oil phase contains hexadecane (99%, Sigma-Aldrich) and wax (Petrolatum, Unilever) in a ratio set by the desired solids concentration. The aqueous continuous phase consists of 0.5 wt% microfibrous cellulose (CP Kelco) and 10mM sodium dodecylsulfate (99%, Fluka) surfactant solution (Pawar et al., 2012). The emulsion is prepared by combining dispersed and continuous phase, then heating to 75°C and shaking for 10s by hand. The

resulting emulsion is polydisperse and stable against sedimentation as a result of the yield stress of the continuous phase. Initially, the dispersed phase is homogeneous but, as the temperature goes down, the wax (m.p. $\sim$ 45–60°C) inside the droplets forms irregular flat solid crystals in the hexadecane. Emulsions with different solids content (15–45%) are prepared to form various partially crystalline droplets. In all cases studied, the equilibrium state of the droplets is one in which the liquid fraction completely wets the crystals inside. The resulting droplets are viscoelastic in their bulk rheology (Pawar et al., 2012, Caggioni et al., 2015) and possess a continuous fluid surface with no particles adsorbed at the liquid–liquid interface.

### 3.2.2. Microscopy

Doublets were formed and studied using micromanipulation stages and microcapillaries to grasp and move droplets into contact to initiate coalescence (Pawar et al., 2012, Pawar et al., 2011). Borosilicate glass capillaries (1mm outer diameter and 0.5mm inner diameter, Sutter Instruments) are pulled with a Micropipette Puller (Model P-97, Sutter Instruments) to form microcapillaries with tip size smaller than the droplets manipulated by a factor of at least two. The other end of the capillary is attached to a syringe containing water using transparent tubing (Tygon). Adjusting the height of the water reservoir varies the hydrostatic pressure to enable grasping and manipulation of a droplet. The capillary is connected to a 3-axis coarse manipulator (Narishige International) mounted on a microscope to enable direct study of the coalescence and arrest process. A 1ml sample of emulsion is placed on a glass slide and the capillary tip aligned to the droplet height. By applying negative hydrostatic pressure with the water reservoir, the droplet is drawn towards the capillary tip and grabbed without deformation. The droplet is then brought through the continuous phase to contact a second droplet and initiate coalescence. Observation of contacted droplets continues for at least 15 min to map the stages of coalescence and any arrest (Pawar et al., 2012). Imaging is performed using a Motic AE31 inverted optical microscope with custom-mounted micromanipulator attachments. Digital images are obtained using a Moticam 10MP camera and image analysis carried out using IMAGEJ software (Schneider et al., 2012).

### 3.3. Theory

The shape history of polydisperse doublets can be approximated using the below ‘empirical analytical function’ that has been validated by comparisons with finite-element simulations of droplet neck growth during coalescence (Yadha and Helble, 2004). The model can map the outline of two droplets at most stages of coalescence (Yadha and Helble, 2004, Mbanga et al., 2014), as shown by the four calculated curves in **figure 20**:

$$r(\theta) = \sqrt{4bc} \sqrt{1 - b \sin^2(\theta)} + k \cos(\theta), \quad (3.1)$$

where

$$k = \frac{N-1}{N+1} (2 - b^{1/N})^N, \quad (3.2)$$

$$c(b) = \frac{3b}{1+N^3} [\sqrt{b} (\frac{5}{3} - b) + \frac{k^2}{\sqrt{b}} (1 + b) + \frac{(1-b)^2(b-k^2)}{4b} \ln(\frac{1+b+2\sqrt{b}}{1+b-2\sqrt{b}})]^{-\frac{2}{3}} \quad (3.3)$$

and

$$N = \frac{R_1}{R_2}; \quad (3.4)$$

and  $b$  is a parameter that indicates the degree of coalescence, varying from a value of 1 for no coalescence to 0 for completeness (Yadha and Helble, 2004). We do not carry out calculations over the entire range of  $b$  values, instead starting at  $b \sim 0.9$  and ending at  $b \sim 0.2$  to avoid small unrealistic changes in the doublet shape at extreme  $b$  values. Here, the convention used is that  $R_1$  is always the larger droplet radius when a polydisperse doublet is studied. We perform our calculations for a unit reference sphere and scale the dimensions accordingly for area and energetic determinations. The maximum strain of polydisperse doublets, that is, the amount attained after complete coalescence, is found by geometry and volume conservation to be

$$\epsilon_{max} = 1 - \frac{\sqrt[3]{1+N^3}}{1+N} \quad (3.5)$$

which is easily shown to reproduce the result of Pawar et al. [3] for the monodisperse case when  $N = 1$ :

$$\epsilon_{max} = 1 - 2^{-2/3}. \quad (3.6)$$

A surface integral of equation (3.1) can also be used to calculate a doublet surface area at each stage of coalescence to compare relative driving forces for different doublet proportions. A simple description of the total energy,  $E_{tot}$ , of a coalescing pair of spherical droplets accounts for the reduction in surface area driven by interfacial tension and the resistance to compression by the elastic microstructure of the droplets is (Pawar et al., 2012)

$$E_{tot} = \gamma A(\epsilon) + \frac{3}{2} G' \epsilon^2 V, \quad (3.7)$$

where  $\gamma$  is the liquid–liquid interfacial tension of  $10 \text{ mNm}^{-1}$  (Pawar et al., 2012),  $A$  is the total doublet surface area,  $G'$  is the elastic modulus of the droplet phase,  $V$  is the total droplet volume and  $\epsilon$  is the linear strain of the doublet, defined by

$$\epsilon = \frac{L_0 - L}{L_0}, \quad (3.8)$$

where  $L$  is the instantaneous / final doublet length and  $L_0$  is the initial doublet length. We assume here that the two droplets behave as ideal isotropic elastic springs so that, even for polydisperse doublets, the overall length of the doublet is the only significant contribution to strain. As in (Pawar et al., 2012), we link the droplet solids content to its elasticity using a power-law fit to the experimental bulk rheology data of (Pawar et al., 2012):

$$G' = 2.8 \times 10^5 \phi^{4.8}. \quad (3.9)$$

All calculations are carried out using MATHEMATICA software v. 10.0.

### 3.4. Results and discussion

At any moment during coalescence, the surface area of the droplets is an indicator of how far away the system is from its final state of total coalescence. Accurate representation of the surface area thus enables calculation of the process driving force. In addition, because arrest halts the progress of coalescence at an intermediate state, predicting droplet area also predicts the arrested shape produced when viscoelastic droplets are used. **Figure 21** shows the evolution of doublet area as it is reduced by the process of coalescence for the experimental fit of (Pawar et al., 2012) and compares it

with the calculation of equations (3.1) – (3.4). Overall the same exponential decay in area with strain is seen for experiment and theory, indicating the rapid relaxation of a doublet into a spherical droplet. Both results end at the maximum strain for monodisperse droplets,  $\epsilon = 0.37$ . The experimental fit from (Pawar et al., 2012) in **Figure 21** under-predicts the theoretical normalized area reduction for most strain values, possibly because the continuous phase fluid used in (Pawar et al., 2012) has a small yield stress that can affect the relaxation of the droplets. The area change predicted in **Figure 21** can now be used to calculate the change in energy as coalescence proceeds and then determine the point of minimum energy in order to assess the completion, arrest or prevention of coalescence.

Using equations (3.1) – (3.4) to determine the doublet surface area and the elasticity data from (Pawar et al., 2012), and substituting these into equation (3.7) as a function of strain, the curves in **Figure 22** are obtained. The calculations in **Figure 22** are performed assuming monodisperse droplets with radius  $R=50\mu\text{m}$ , an interfacial tension,  $\gamma = 10 \text{ mNm}^{-1}$ , and a droplet solids volume fraction,  $\phi = 0.4$ . The doublet area decays exponentially as coalescence proceeds from high to low strains, while the elasticity increases by a power law with exponent 4.8 (Pawar et al., 2012). Because of the opposing natures of the two functions, a minimum in the total energy curve exists, representing the intermediate arrested state. If either surface or elastic energy dominate the coalescence process, the drops will either fully coalesce or not coalesce at all, respectively. Pawar et al. (2012) used the model to predict the limits of arrest, as a function of droplet solids level and interfacial tension, but worked with only a single size of droplets and did not explore the effects of varying droplet size on arrest.

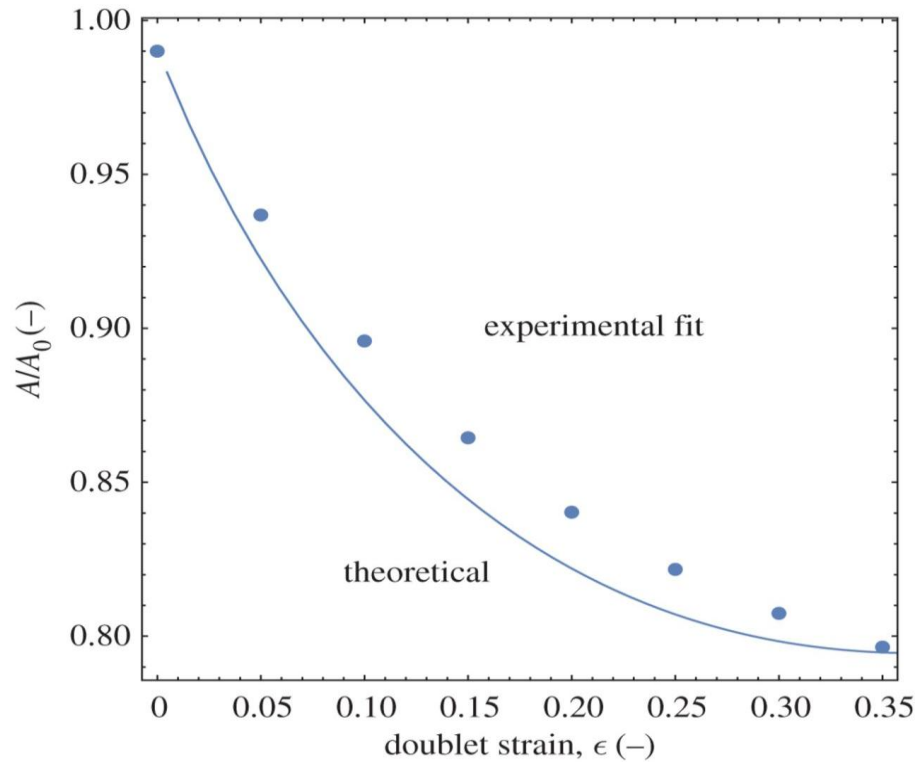


**Figure 21.** Comparison of analytical and empirical fit results for monodisperse droplet area change during coalescence.

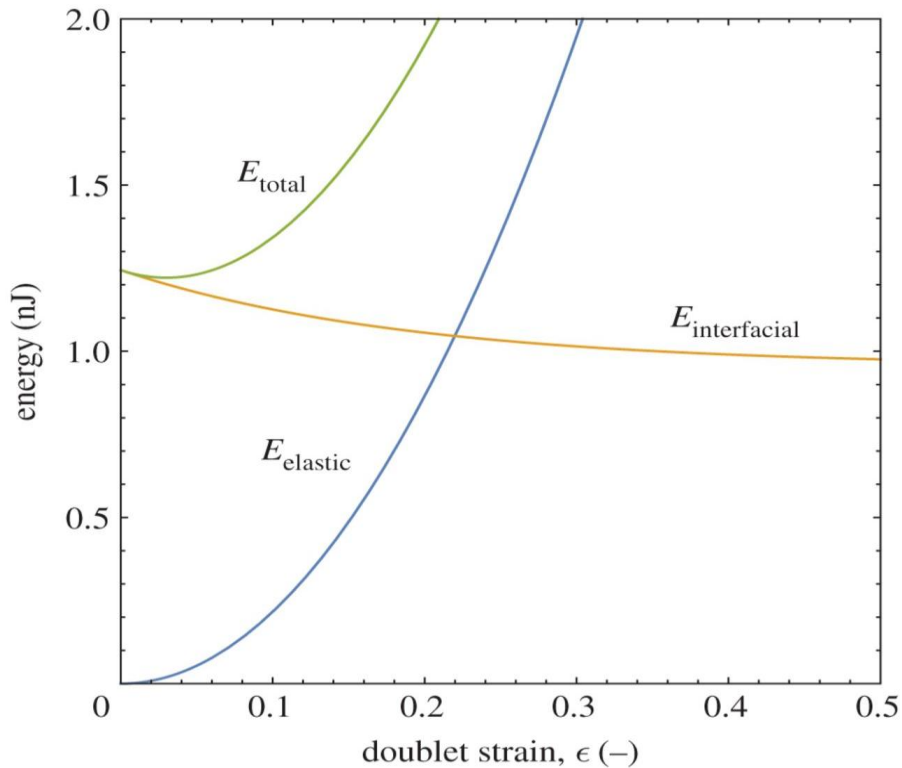


**Figure 22.** The total energy of the doublet is the sum of its interfacial and elastic contributions. The minimum in the total energy curve determines the doublet's ultimate stable arrested state.

Examples of arrested doublet structures are shown in **Figure 23** for several different individual initial droplet sizes and their resulting strains. In **Figure 23**, the same solids content,  $\phi = 0.4$ , is used in each doublet but the interfacial area varies with the droplet radii. At large radii, the strain approaches zero, the onset of no coalescence, while at low radius it approaches the maximum strain of  $\epsilon_{\max} = 0.37$  achieved during total coalescence. Such a result is consistent with our intuition regarding the effects of interfacial curvature on interfacial, or Laplace, pressure. More highly curved, smaller droplets exhibit a higher strain than larger droplets because the higher interfacial pressure squeezes the two drops more closely together. A prediction of the model is also plotted in **Figure 23** and follows the same inverse dependency on droplet radius but over-predicts the droplet strain. The larger strain found from the model could result from differences between the experimental system and our description of droplet elasticity. All elasticity measurements were made using bulk volumes of the droplet phase, but the droplets are much closer to the size of the internal crystal network building blocks. If the droplet elasticity value, or its elastic response, differs significantly at smaller length scales from the bulk value, a difference in strain would be observed. It is clear from the equilibrated microscopy images of representative doublets in **Figure 23** that the internal structure is not destroyed by the compression, as the droplets never fully coalesce. Given the strong influence of droplet size on arrest in these emulsions, and the likelihood that practical emulsions will contain relatively broad distributions of droplet sizes, it is of interest to more broadly explore how changing droplet size can affect arrest.

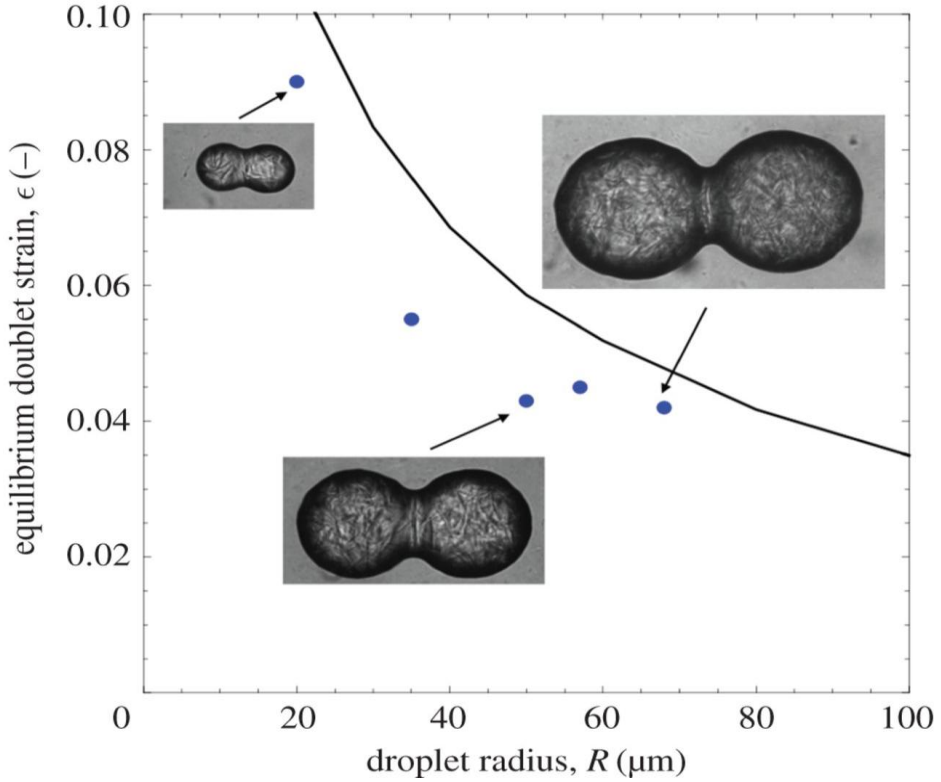


**Figure 23.** Arrested doublets have larger strains at smaller droplet radii as a result of the increased interfacial curvature and Laplace pressure that drives the droplets together. Higher pressures further compress the internal elastic structure, resisting complete coalescence. The line is a plot of the prediction of the physical model showing the strong effect of drop radius on the ultimate doublet arrested strain.

The generality of the description of doublet shapes in equations (3.1) – (3.4) (Yadha and Helble, 2004) enables us to predict their shape during coalescence, as demonstrated in **Figure 24**.

**Figure 24** shows a rendering calculated for a doublet with one droplet 60% the radius of the larger one and several shape profiles for different values of the total doublet strain. For polydisperse droplets, we assume only linear strain is significant and so define strain as we did for the monodisperse case, using equation (3.8). Any change in length of the doublet is thus normalized to the starting length in order to avoid biasing the calculations by the change in radius of one of the droplets. As for monodisperse doublets, a ‘neck’ is formed between the two droplets once coalescence initiates and the smallest drop determines the size of the neck. Polydisperse doublets will have a smaller total surface area as the size ratio increases and the dynamics of area loss will be different as well. As before, we use the model to calculate doublet surface area, as a

function of the stage of coalescence, and use that as input to equation (3.7) in order to understand the competing effects of surface and elastic energy on the process.

**Figure 25** shows the calculated relative decay of different doublets for a range of radius ratio values. As expected, increasing the radius ratio decreases the final maximum reduction in area of a doublet at the point of complete coalescence, from the monodisperse case of 79% of the initial area to nearly 87% for a value of  $N = 2$ . Similarly, the reduction in area is higher at a given strain for higher  $N$  values. A lower reduction in area with increasing radius ratio translates into a smaller driving force for coalescence and, potentially, a lower arrest strain for the polydisperse cases.

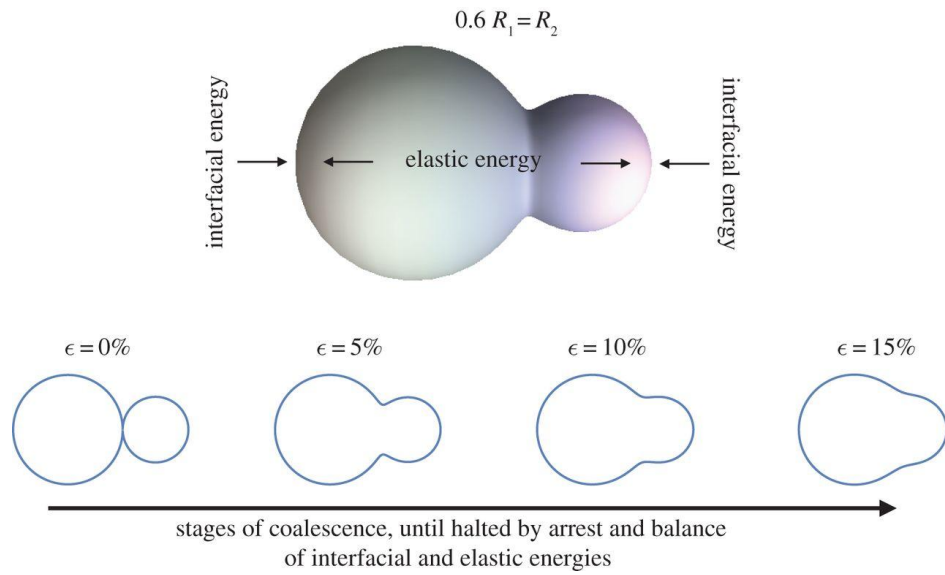


**Figure 24.** Coalescence of two different-sized droplets. The analytical model (Yadha and Helble, 2004) describes the shapes of Polydisperse doublets at all stages of coalescence.

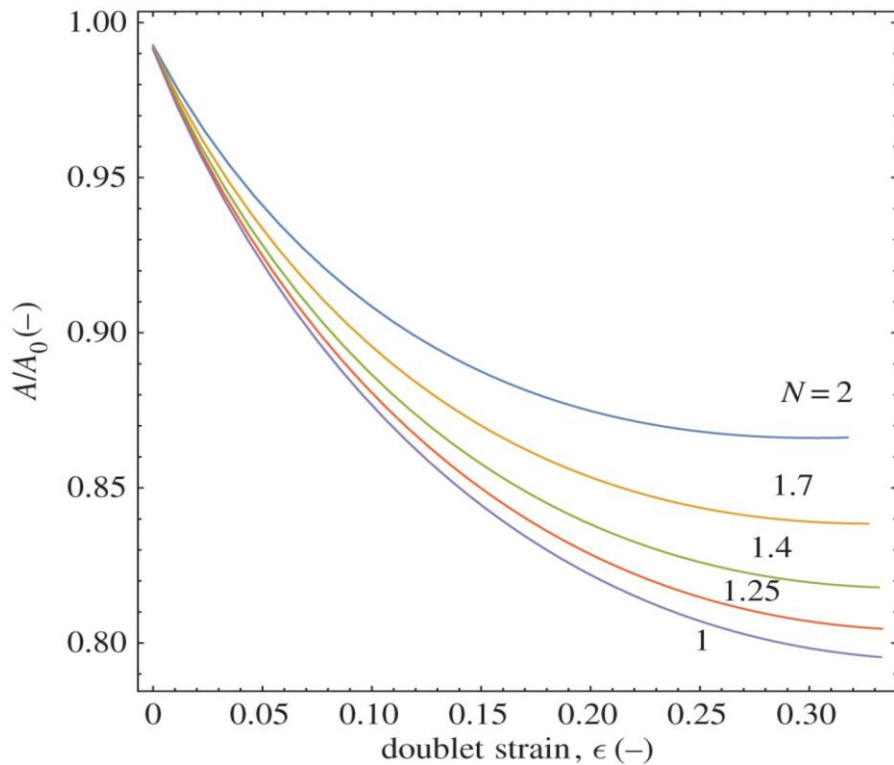


**Figure 25.** Decay of area, normalized by its initial value, for doublets with increasing radius ratio,  $N$ , as their strain increases and coalescence is approached. Higher polydispersity within a doublet reduces the amount that area can decrease during the coalescence process.

Calculating the arrest strain of polydisperse doublets as a function of radius ratio and solids concentration for a given larger droplet radius,  $R_1$ , the overall map in **Figure 26** is obtained. As suggested above, increasing the radius ratio decreases the arrest strain by bringing the doublet closer to its final state by starting from a lower initial area. The model also predicts a lowering of stable arrest strain with increasing solids level. The higher elasticity at higher solids loadings causes a stronger resistance to the surface energy-driven coalescence, leading to arrest at an earlier stage of coalescence and a similarly lower strain. For  $\phi = 0.35 - 0.4$ , the arrest strain changes very little for values of  $N \sim 1 - 3$ , indicating strong resistance and a low driving force (**Figure 26**). Also,

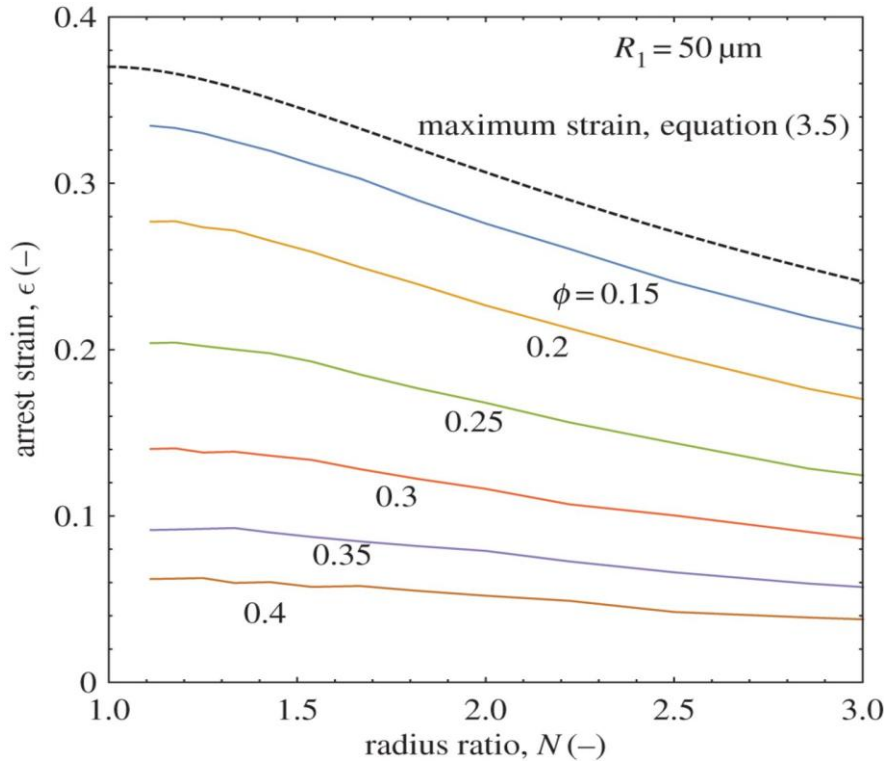


**Figure 26.** Changes in doublet polydispersity and solids level alter the resulting doublet arrest strain by changing the amount of area reduction that can occur and the droplet elasticity, respectively.

plotted in **Figure 26** is the maximum strain for polydisperse doublets, equation (3.5), in order to check the model predictions but also to bound the observed behaviour. The general shapes of the curves are the same, with a sigmoidal decay in arrest strain seen as a function of radius ratio. As solids concentration is decreased, the curves more closely approach the limiting value of equation (3.5) as it is equivalent to a coalescence process for droplets containing no solids and possessing no elasticity. The model agrees quite well with the geometric prediction when it is run using a zero elasticity. Increasing the overall doublet size, by repeating the above calculations using a reference droplet size of  $R_1 = 300 \mu\text{m}$ , produces a similar set of curves in **Figure 27** but with distinctly lower strain values. The larger droplets have a greater volume contribution to the arrest strain, increasing resistance to deformation and reducing its relative driving force. **Figure 27** shows an approximately 10% lower strain is predicted for  $R_1 = 300$  versus  $50 \mu\text{m}$  at a solids level of 15%.

There is also almost constant strain predicted at high solids levels, with little change for  $\phi = 0.35$  and the  $\phi = 0.4$  line not shown as it is flat and overlaps most of the  $\phi = 0.35$

line. It is also of interest to observe the experimental formation of polydisperse doublets to verify that their arrest is as stable as the monodisperse case and is affected by similar physical constraints.

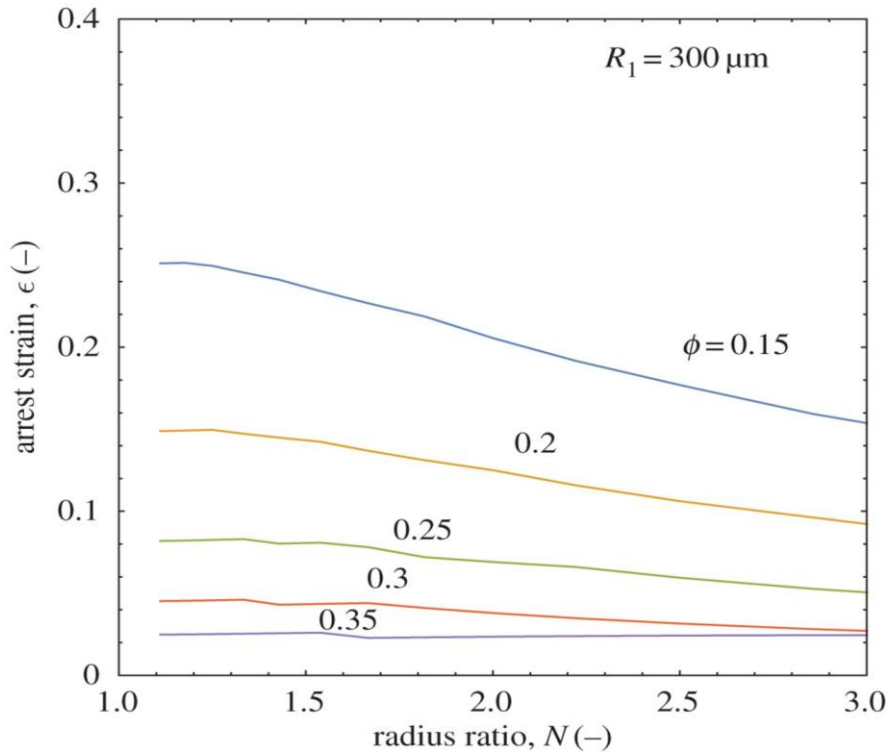


**Figure 27.** Increasing the overall doublet size decreases the strain of the structure for all solids levels.

A summary matrix of micrographs of polydisperse doublets with varying solids loading and radius ratio is shown in **Figure 28**. The images show equilibrated arrested doublets for a wide range of solids levels and dimensions, all of which form stable, axisymmetric shapes that are not significantly distorted by the arrest process. The broad range of shapes possible is evident, indicating not only the potential for simple synthesis of anisotropic colloids by such a process, but also the fact that such structures will form a rich array of connections within more complex emulsion microstructures. The shapes of the doublets show smooth, continuous borders that indicate the fluid-like behaviour of the droplet surfaces. Although almost solid-like in their static appearance because of the stabilization of shape by internal elasticity, the structures retain their fluid interface. Similar to monodisperse systems, higher solids levels decrease the doublet arrest strain because of an increased elastic resistance to coalescence and its associated compression. Even at the lowest solids concentration of 15%, the lack of

perfect spherical shapes is indicative of the fact that the internal elastic network of the droplet is arresting full coalescence. Also seen in most cases is the smaller strain predicted at higher radius ratios. Validation of the above predictions is necessary to evaluate the accuracy of the model and the significance of the predicted effects on shape and structural arrangement.

Because a wide range of droplet sizes and properties is examined, an aggregate comparison is made of the strains predicted by the model and observed experimentally.

**Figure 29** compares the experimental and theoretical values for droplets with radii between  $R_1 = 100$  and  $500 \mu\text{m}$  and solids levels between  $\phi = 0.15$  and  $0.45$ . Although variations in drop size and solids level will cause variations in strain, we see the model predictions are in reasonable agreement with experiment at low strains, meaning the larger droplets and higher solids levels. In such cases, the small deformation is more consistent with the assumed linear elastic behaviour. Still, the data are broadly distributed around the theory line and we note that the emulsion droplets we produce are polydisperse not only in size, but also in their crystallization history because differently sized droplets cool at different rates to form their inner crystalline networks. The resulting changes in crystal orientation and packing can cause variations in mechanical response and the experimental variability we see at low strains. The variability observed may also be the result of larger errors in image analysis measurement of small strains. Above strains of 20%, the model under-predicts the strain observed experimentally. No clear pattern with respect to drop size ratio was seen. We do know, however, that higher solids level have lower strains, hence the conclusion is that there is more error at high solids loadings. If the droplets exhibit nonlinear elastic deformation, its effects are more likely to be significant at the large deformations seen at lower solids levels and smaller droplet sizes.

Differences between the observed doublet shapes and the model are likely the result of a more complex rheological response of the viscoelastic droplets than the bulk rheological response of the droplet phase. More work is needed to ascertain whether the droplets exhibit a small degree of nonlinear elastic response, which could cause the observed discrepancy.

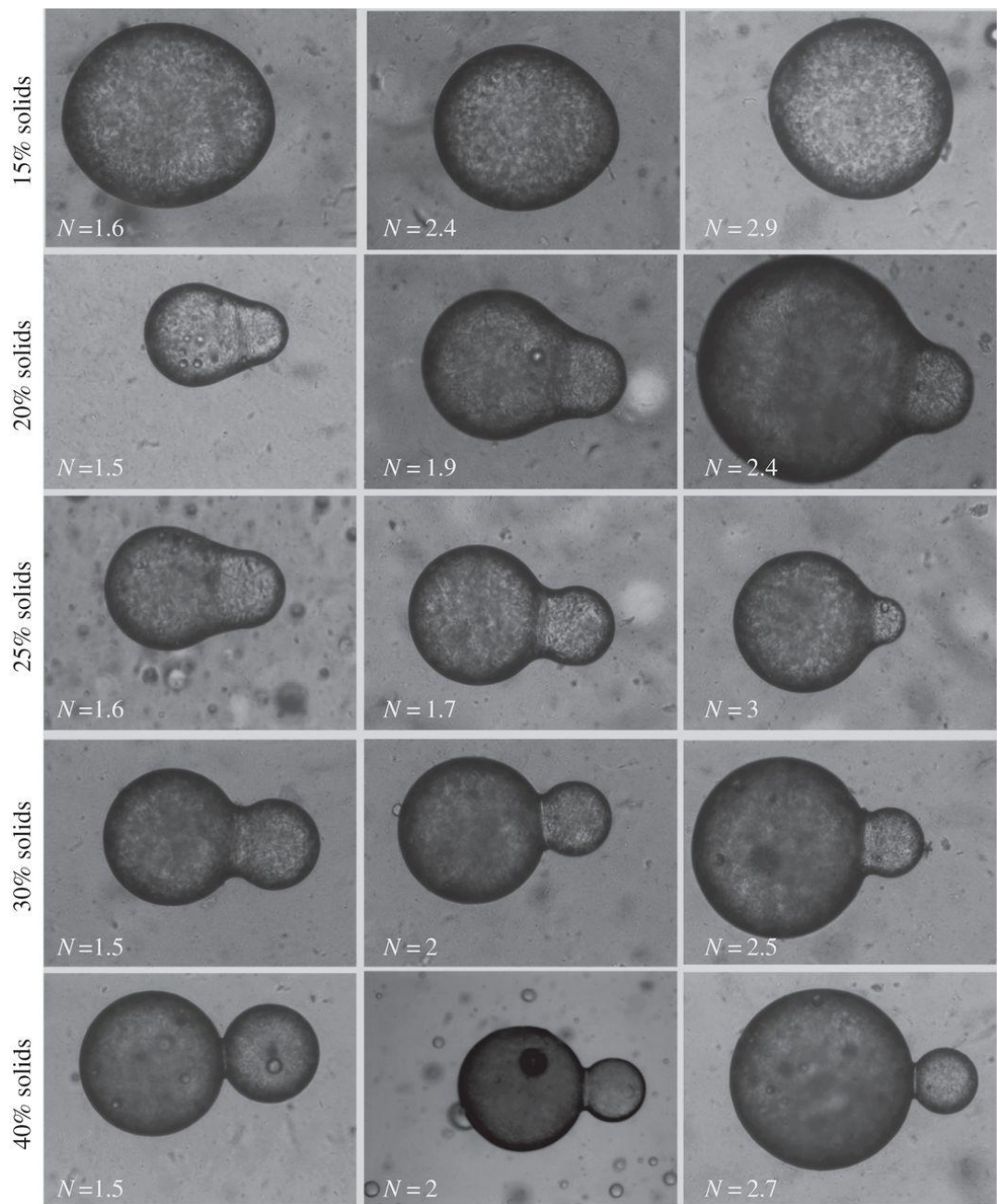


**Figure 28.** Examples of polydisperse doublets arrested by different solids levels for different values of the radius ratio, N. The height of each individual image is 250 $\mu$ m.

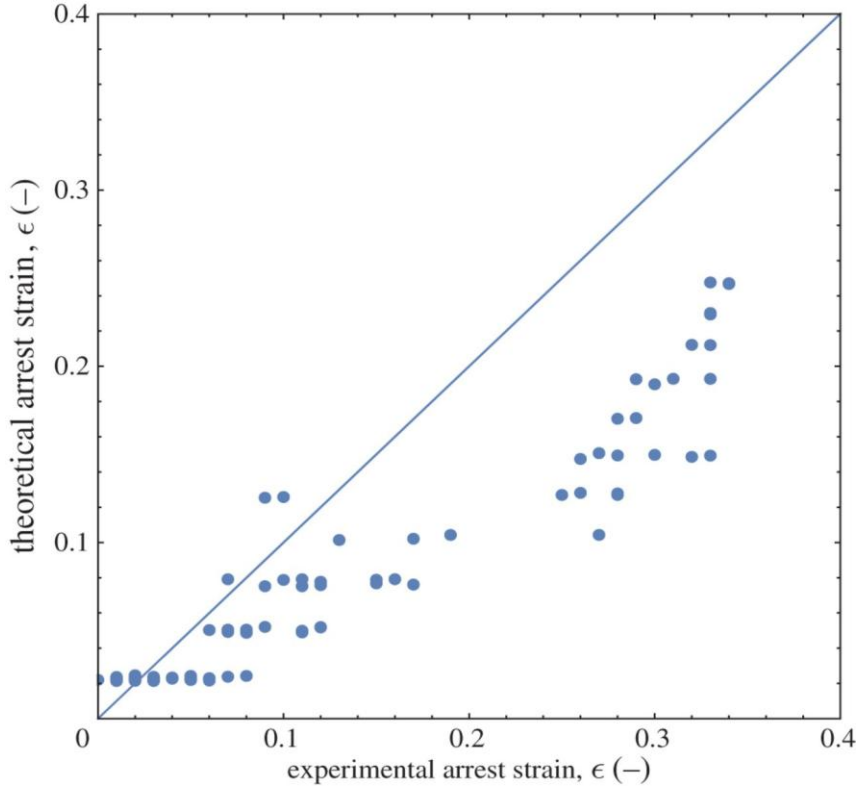


**Figure 29.** A comparison of the predicted level of strain and the experimentally observed value shows reasonable agreement at low strains but poorer agreement at high strains. The droplets may deform following more nonlinear elastic dynamics at high strains, causing disagreement with the simple model used here.

One mechanism of non-ideal elastic response is structural rearrangement during deformation. A preliminary evaluation of whether such structural changes occur suggests a way to evaluate individual droplet response, as it is expected to differ from the bulk fluid behaviour. Our model approximates the doublet's elastic response to deformation experienced during coalescence and arrest as linear, but we can explore this response in more detail by examining the deformation's reversibility and dynamic nature. The presence of surfactant around the doublets lowers their interfacial tension to  $\gamma \sim 10 \text{ mNm}^{-1}$ , so localized dilution with deionized water will raise the interfacial tension by a factor of at least two. **Figure 30** shows the initial formation of an arrested doublet from two individual droplets. The resulting doublet is then held in place and flushed with deionized water to temporarily dilute the surrounding and adsorbed surfactant. The response is immediate: the deformation increases by 5 – 6% as the local interfacial tension increases the Laplace pressure. Several minutes after flushing, the interfacial tension has decreased again to its original value and the doublet has

equilibrated at a new deformation slightly less than during rinsing but significantly more than prior to dilution. It is likely that some restructuring took place within the doublet, or the step change in stress caused an irreversible deformation, whereas more reversible behaviour might be expected for less brittle structures like hydrogels. **Figure 30** demonstrates the responsiveness, at small deformations, of viscoelastic structures to subtle changes like dilution but also suggests an approach for triggering an irreversible shape and structural change at larger deformations (Caggioni et al., 2014, 2015). It also suggests the need for more detailed study of individual droplet response to deformations experienced at different strain levels.

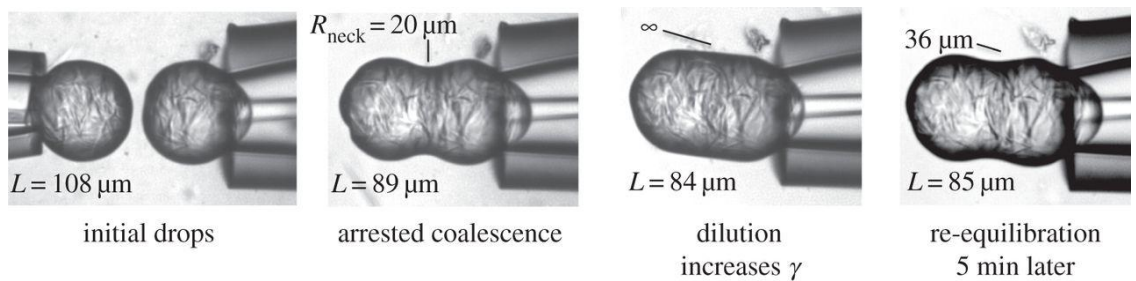


**Figure 30.** Microscopy images of a doublet changing its strain, and thus shape, in response to a dilution-induced increase in the local interfacial tension. As surfactant diffuses back in to re-equilibrate the local concentration, the strain increases but the droplet does not return to its original strain, probably because of structural rearrangements that cause hysteresis in the droplet's rheological response.

### 3.5. Conclusion

The coalescence, and arrested coalescence, of polydisperse viscoelastic droplets has been studied and the resulting structures compared to an energetic model based on the relative importance of droplet elastic energy and surface energy as coalescence proceeds. The model predictions are consistent with experimental observations of the stable arrest of polydisperse doublets over a wide range of solids concentrations and radius ratios. Doublet shape is a strong function of the droplet polydispersity, with final arrest strains decreasing significantly as the smaller droplet of the pair decreases in size. Variations in droplet polydispersity are typical for most emulsions and, if microstructure formed by significant arrested coalescence is present, the structural integrity and material rheology are likely to be strongly affected by the efficiency of connected droplet packing and the resultant load-bearing response (Giermanska et al.,

2007, Thivilliers et al., 2008, Thivilliers-Arvis et al., 2010). Future work will study the individual droplet deformation response in more detail, explore polydisperse droplet arrest in more complex droplet aggregates, and improve understanding of how such structures contribute to emulsion rheology and flow.

## **CHAPTER 4 Arrested Coalescence of viscoelastic droplets: Triplet shape and restructuring**

### **4.1. Introduction**

Emulsions are mixtures of two immiscible liquid phases, where one phase exists as dispersed droplets in the second, continuous, phase as long as the system is stabilized against coalescence: the recombination of the dispersed phase into a single liquid region. Coalescence can be prevented by a number of mechanisms, but one common to many complex fluids like foods is the arrest resulting from colloids that provide an offsetting rheological resistance (Boode and Walstra, 1993, Dickinson, 2012, Vanapalli and Coupland, 2001). Arrest occurs once coalescence is initiated but cannot complete because of a halt in the ability to reduce droplet surface area (Stratford et al., 2005, Studart et al., 2009, Pawar et al., 2011) or increase deformation (Pawar et al., 2012, Dahiya et al., 2016a) to minimize system energy. While both types of arrest play a role in practical microstructures, the surface, or Pickering, type can have significant limits on the number of connections formed between droplets (Wu et al., 2015) because the end result is essentially a solid interfacial shell. Droplets with an internal viscoelastic resistance are more flexible in their ability to form multiple connections between droplets, even after an initial arrest event.

Previous work showed that droplets containing an elastic network of crystals can initiate but not finish coalescence, creating a range of anisotropic intermediate droplet shapes, (Boode and Walstra, 1993, Fredrick et al., 2010) but only recently has a physical model of the process for uniform (Pawar et al., 2012) and non-uniform (Dahiya et al., 2016a) droplet pairs been developed. Essentially the interfacial pressure driving two droplets to minimize their area must be offset by the internal elasticity to stably arrest coalescence at an intermediate state: a liquid doublet rather than a sphere (Pawar et al., 2012). In such cases the exact doublet shape represents one of a number of intermediate points between the beginning state of two discrete droplets and a completely coalesced single sphere and is determined by the level of solids in the droplet and the point at which coalescence is arrested (Pawar et al., 2012). We extend that work here by examining the dynamic behaviour of an aggregate of three arrested droplets, a triplet, as multiple

connections are the basis for many fluid microstructures formed during the manufacture of food, coatings, and material templates like bijels (Mohraz, 2016). Unlike aggregated solid particles, however, arrested droplets are permeated by a liquid oil phase that can adhere easily to other surfaces and can form a neck that bridges the two droplets. It is this liquid bridge that determines connectivity between droplets and, by transmitting interfacial pressures that balance the internal elasticity of the droplets, the degree of deformation exhibited. When two droplets connect to form a doublet, the interfacial driving force for coalescence acts along the centre of each droplet and produces a rotationally symmetric shape. When an additional droplet is added, however, that symmetry is broken and more complex behaviour is expected.

These experiments report the dynamic behaviour of three viscoelastic droplets arrested at an intermediate stage of coalescence by internal elasticity. Micromanipulation and microscopic time-lapse imaging techniques are used to study changes in droplet deformation and order to investigate the path taken to a final droplet aggregate structure. We observe a significant degree of droplet restructuring from loose to dense packings as long as the droplet solids content and elasticity are low. We develop a physical model of the restructuring, resulting in a simple geometric criterion predicting the extent of densification as a function of system variables.

Our ultimate goal is to build on previous work on local deformations of structured emulsion droplets (Pawar et al., 2012, Dahiya et al., 2016a) to realistically simulate the formation of full-scale emulsion networks (Thivilliers-Arvis et al., 2010, Thiel et al., 2016) and more complex coalescence phenomena (Thiel et al., 2016). We increase the complexity of scrutiny here by studying triplets of structured droplets as these break the symmetry of the doublets previously examined, exhibiting new mechanisms of shape-change and construction. An understanding of the packing and connectivity within such structures is critical to predicting mechanical properties and dynamic performance of materials as diverse as foods, cosmetics, and 3D printed products (Thivilliers-Arvis et al., 2010, Thivilliers et al., 2006, Thivilliers et al., 2008). This work also demonstrates a new aspect of responsiveness and shape change: restructuring of an underlying elastic framework using the strong driving force of a liquid interface (Leong et al., 2007, Caggioni et al., 2015, Prileszky and Furst, 2016, Py et al., 2007, Roman and Bico, 2010,

Caggioni et al., 2014). We show that numerous complex shapes can be self-assembled even from simple droplet building blocks larger than the thermal limit.

## 4.2. Experiment

### 4.2.1 Materials and methods

Oil-in-water (O/W) emulsions are prepared by mixing 5 mL volumes of oil and aqueous phase. The dispersed oil phase is a mixture of hexadecane, 99%, Sigma Aldrich, and petrolatum, Unilever, in a ratio yielding the desired solids concentration (Pawar et al., 2012). The aqueous continuous phase is a neutralized 0.3 wt% Carbopol in a 10 mM sodium dodecyl sulfate, SDS, 99%, Fluka, surfactant solution. The emulsion is prepared by mixing dispersed and continuous phase, then heating to 75°C and gently shaking for 10 seconds. A non-uniform emulsion size distribution is formed, which remains dispersed and suspended due to the yield stress of the continuous phase. Initially, the emulsion droplets are a homogeneous liquid phase, but as the temperature reaches the wax melting point of ~40–60°C, elongated, flat, prismatic crystals form an elastic network inside the droplets, enabling arrest. Emulsions with different solid content, 15–45%, are prepared to explore the behaviour of various partially crystalline droplets. The droplet elasticity was determined by Pawar et al. (2012) and can be calculated from a power-law fit to their data:

$$G' = 2.8 \times 10^5 \phi^{4.8} \quad (1)$$

where  $G'$  is the droplet elastic modulus in Pascals and  $\phi$  is the dimensionless droplet solids mass fraction.

### 4.2.2. Microscopy

The doublets and triplets are formed and studied by micromanipulation experiments (Pawar et al., 2011, Pawar et al., 2012, Dahiya et al., 2016a, Thiel et al., 2016). A pre-pulled microcapillary is used to hold a droplet at its tip and then bring it into contact with another droplet to start the coalescence process. Borosilicate glass capillaries with 1 mm OD and 0.5 mm ID, Sutter Instruments, are pulled with a Sutter Instruments Model P-97 Micropipette Puller to form microcapillaries with tips smaller than the droplets under study. The capillary is attached to a small water reservoir by Tygon tubing. Adjusting the height of the water reservoir varies the hydrostatic pressure,

enabling the capillary to grab the droplet and manipulate it within the emulsion using a 3-axis coarse manipulator, Narishige International USA, mounted on a Motic AE31 inverted microscope.

An emulsion sample is placed on a glass slide and the tip of the capillary is aligned to the droplet under study while viewing through the microscope. Negative hydrostatic pressure is applied, using the water reservoir, to grip the droplet and then the manipulator used to move the drop across the continuous phase toward a second to form a doublet. The doublet is allowed to relax into an arrested steady state and then a third droplet is added to initiate coalescence and form a triplet, allowing us to observe arrest, and document any restructuring that occurs. Because some structural relaxation occurs slowly, the shapes formed are observed continuously for 15 minutes and then compared for up to 15 hours after formation.

All results are for droplets that have been brought together in the level focal plane of the microscope so no out of plane movements can bias the results. As the starting doublets are rotationally symmetric about their long axes, our results should apply to all starting orientations of the third droplet.

#### 4.3. Results and discussion

**Figure 31** shows an example of a multidroplet complex emulsion microstructure exhibiting varying degrees of arrested coalescence and droplet arrangements. Such structures are common in dairy food products where fat blends possess both solid and liquid components, providing the elasticity and interfacial forces needed for arrest to occur (Pawar et al., 2012). Lines drawn over the image in **Figure 31** indicate the orientation between droplet centres of mass and map the wide variation in packing efficiency possible in an emulsion where arrest is significant. Some droplets form triangular packings with  $\sim 60^\circ$  angles between them, a strong state based on hexagonal close packing, one of the densest possible arrangements of spheres. Others have much larger angles between them, indicating that arrest stabilized the droplet arrangement before it could reach close packing. In an effort to understand the formation of similar multi-droplet structures, here we expand on previous studies of two-droplet structures and investigate the effects of orientation on the final arrested state and packing

efficiency of viscoelastic droplets. The goal is to better predict how structures like those in **Figure 31** form and how they can be controlled and predicted.

#### 4.3.1 Elasticity-dominated structures

In **Figure 32a**, droplets containing 40% solids are brought into contact via micromanipulation, initiating coalescence and demonstrating the arrest of coalescence before it can complete formation of a larger spherical droplet. The droplets possess a significant elasticity, with a  $G' \sim 3$  kPa, so a low arrest strain is expected (Pawar et al., 2012) and found to be less than  $\epsilon \sim 1\%$  in **Figure 32a**. The neck connecting the two droplets in the third frame of **Figure 32a** is about 50  $\mu\text{m}$ , or about 20% of a single drop diameter, across because the high elasticity resists compression and exudes only a small amount of free oil to form the neck. This is sufficient, however, to join the droplets and arrest the doublet in a long term stable nonspherical shape (Pawar et al., 2012).

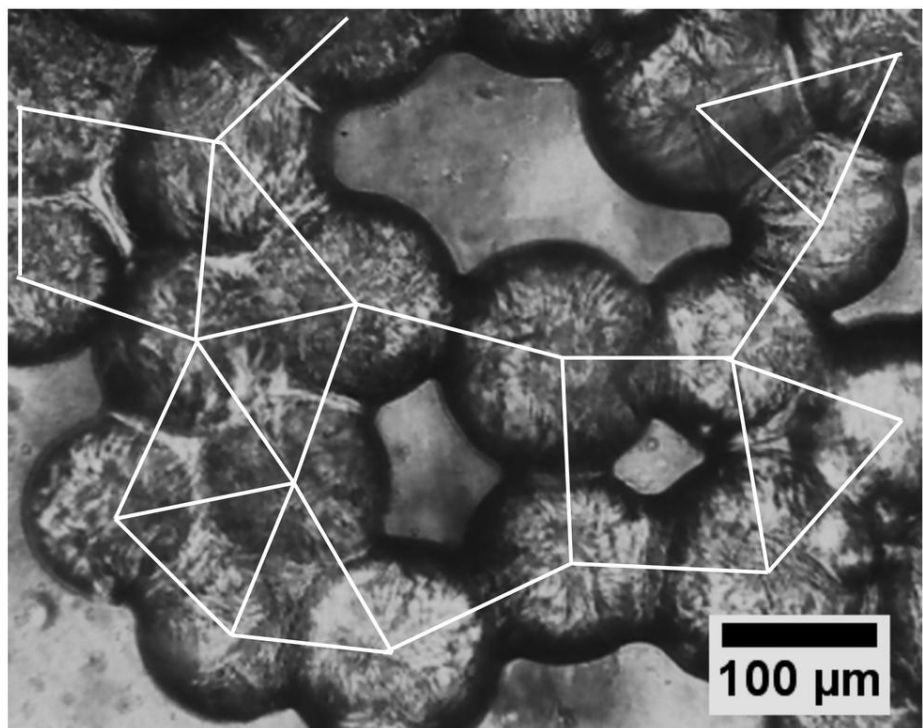


**Figure 31.** An emulsion exhibiting arrested coalescence of a number of droplets, with the connections mapped by white lines. A wide range of angles between droplets is visible. Some droplets are quite closely packed while others have a surprising amount of space between them.

Adding a third droplet requires formation of a second neck, necessitating further compression of the initial doublet to free up the fluid volume needed. We see this occurs in frames 4 and 5 of **Figure 32a**, with the strain increasing slightly to 1.2% and the neck width more than doubling to 117  $\mu\text{m}$ . Clearly the droplets are sufficiently adaptable to adjust and accommodate the addition of a new droplet as 60% of its mass is free liquid that can flow out of the porous microstructure during compression, like a saturated sponge. A fascinating aspect of this result is the ability of the drop aggregate to adjust to numerous shape configurations depending on the environmental conditions and interactions. An example of this was seen previously when the strain of a doublet oscillated between two deformation states because of changes in the local interfacial tension (Dahiya et al., 2016a), demonstrating significant degrees of reversibility and responsiveness (Caggioni et al., 2014, 2015).

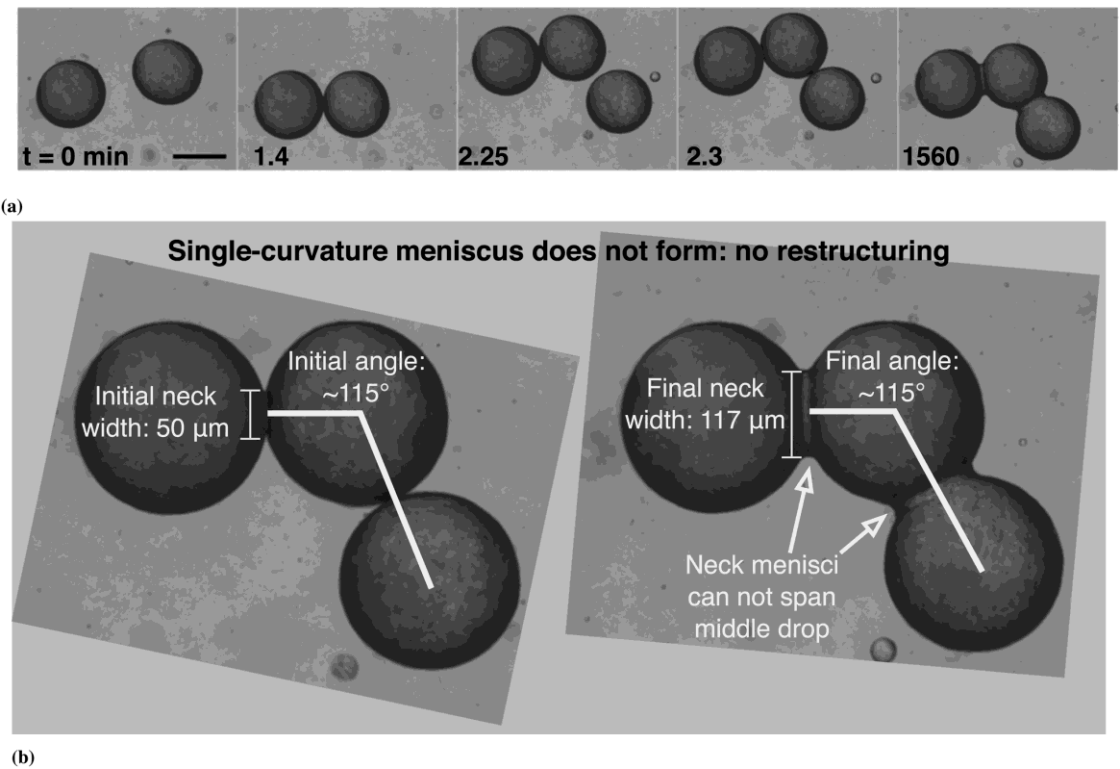


**Figure 32.** (a) Successive images of arrested coalescence of droplets at 40% solids level, showing changes in area and compactness of the shape. Scale bar is 200  $\mu\text{m}$ . (b) Close-up study of the changes occurring during triplet formation in (a), showing neck width growth and two separate meniscus regions.

A key feature of the formation of the stable triplet in **Figure 32a** is the dynamic behaviour of the liquid neck bridging the droplets. It is instructive to examine in closer

detail what sorts of changes occur to understand the driving force behind structure formation. **Figure 32b** shows a close-up view of frames 4 and 5 of **Figure 32a**, allowing observation of the liquid neck meniscus and its shapes at different stages of the process. Although the free liquid permeates the entire triplet, some of its greatest mobility occurs at the neck between droplets. We see in **Figure 32b** the meniscus transitions from a very small radius and a very highly curved state to a larger neck with a smaller curvature as the third droplet equilibrates into its final position. The two neck menisci remain distinct, with opposite curvature sign from the middle droplet surface, whereas full coalescence would likely have merged the two menisci and bridged the middle droplet. As a result, here the third droplet does not reorient because of the meniscus expansion, its final angle through the centre droplet is quite close to when coalescence began. If we now adjust the mechanical properties of the droplets, by decreasing solids level, we expect similar changes to those seen in **Figure 32a** but with increasing dominance of the interfacial driving force.

#### 4.3.2. Interface-dominated structures

For the case of droplets containing 30% solids, we see in **Figure 33** similar behaviour to **Figure 32a**, but with higher strains and neck widths. This is consistent with past work: doublet strain increases as solids level decreases (Pawar et al., 2012). A direct comparison with the results of Pawar et al. (2012) can't be made since larger droplets are studied here. Final doublet strain is the result of a balance between interfacial Laplace pressure and internal elasticity, so doublets made of larger droplets will have a smaller curvature, Laplace pressure, and strain (Pawar et al., 2012, Dahiya et al., 2016a). Also noticeable in **Figure 33** is the merging of the two neck menisci on the inside edge of the triplet, something that could not occur for the higher solids content case in **Figure 32**. Despite the formation of a single, lower curvature, meniscus from two higher curvature menisci on one side of the triplet, the overall triplet structure changes only a small amount due to restructuring. As in **Figure 32**, the strain of each connected droplet pair does increase with time, reflecting a similar need for additional compression to accommodate the creation of a second neck. Clearly a reduction in droplet elasticity lowers the resistance to interfacial pressures, enabling greater degrees of compression of the droplet microstructure and the beginning of restructuring behaviour that alters the shape of the final triplet from its beginning orientation. Since

such behaviour has the potential to significantly vary emulsion structure and rheology, we further investigate the restructuring by altering the balance between the two driving forces more in favour of interfacial dominance: by examining even lower elasticity systems.

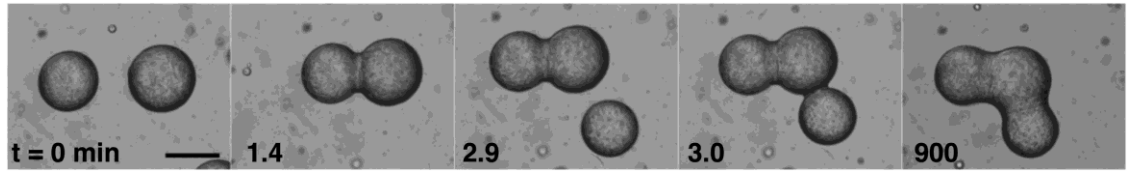
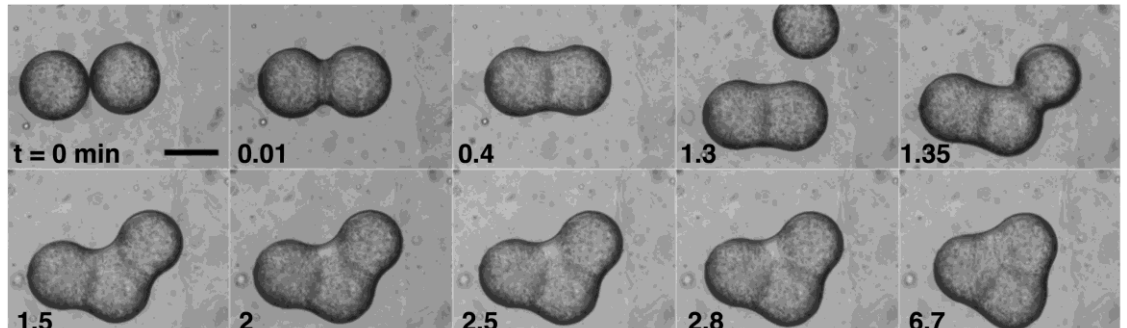


**Figure 33.** Arrested coalescence of droplets at 30% solids level, where changes in the meniscus between droplets can occur but are not strong enough to significantly restructure the triplet. Scale bar 200  $\mu\text{m}$ .



(a)

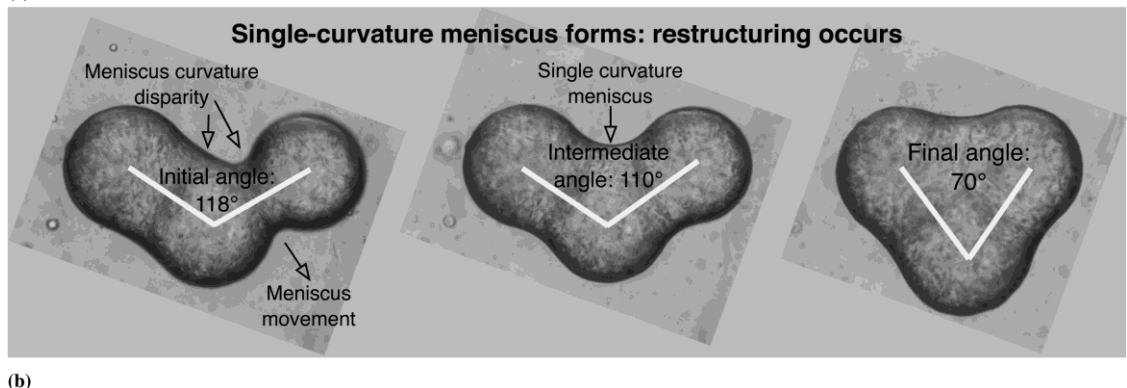


**Figure 34.** (a) Images of restructuring of droplets (25% solids) as a result of meniscus dynamics, the driving force to make the droplet relocate to a denser packing state. Scale bar 200  $\mu\text{m}$ . (b) Close-up study of triplet formation in (a), showing neck width growth and the merging of the two separate meniscus regions, resulting in a significant amount of restructuring.

**Figure 34a** shows the coalescence of droplets containing 25% solids, and they exhibit a similar initial arrest behaviour to the higher solids cases in **Figure 32a** and **33**. Here the

lower solids level and elasticity enables an even larger strain,  $\epsilon \sim 10\%$ , and thus a greater degree of meniscus expansion than the previous two concentrations. In **Figure 34a** the meniscus between the first and second droplet merges with the one between the second and third droplet between 1.3 minutes and 1.5 minutes, and the combined meniscus then continues its outward expansion. Between 1.5 and 2.5 minutes the fluid of the meniscus contains almost no solids, emphasizing the viscoelastic nature of these structures. After 2.5 minutes, **Figure 34a** shows a second way that addition of a third droplet dynamically modifies the droplet aggregate state: the third droplet is steadily pulled into a more compact packing through  $\sim 50^\circ$  of motion. Examining the restructuring transition in more detail in the close-up study in **Figure 34b**, we observe the importance of meniscus dynamics during triplet formation. Compression of the internal droplet solid network frees additional fluid to expand the menisci until they merge into one, single-curvature, interface. The third droplet then moves around the assembly until it reaches a lower angle with a much lower surface area and energy, while all meniscus curvatures have been reduced to a more uniform value throughout the triplet.

Such a change is significant: the initial state of the droplet connection would have, if retained as for the triplets in **Figure 32a** and **33**, created a more open, high fractal dimension, structure in a larger emulsion network. The meniscus-driven restructuring is a mechanism unique to this sort of system, balancing interfacial driving forces with elastic response and resulting in a strong means of actuating shape change. The movement represents a distinct pathway to structure formation in emulsion-based products. Typically, emulsion networks are assumed to form *via* fractal aggregation models, depending on the significance of transport rates and droplet interactions. However, a more compact structure is shown here to be possible as a result of restructuring of droplet aggregates, depending on the balance of elastic and interfacial forces. Such changes are expected to produce structures with varying degrees of compactness greater than expected for fractal systems. More compact droplet arrangements are expected to impact emulsion mechanical properties, given the strength imparted by constructing a network from compact triangular building blocks (Hsiao et al., 2012). The observation that the restructuring occurs at an intermediate solids level indicates a need to understand the balance between the interfacial and elastic forces in these systems, so we continue to reduce the solids level in order to explore the system extremes.

Creating a droplet with 20% solids continues the progression observed above of increasing dominance of interfacial forces over elastic resistance to deformation. The first two frames of **Figure 35** show the construction of a doublet with a significantly higher strain than seen in **Figure 32a–34a**. The lower elasticity of the droplets allows them to compress so far that the neck width is the same as the individual droplet diameter. When a third droplet is added to produce a triplet, we observe restructuring similar to **Figure 34a**, but at a more rapid pace than seen for 25% solids in **Figure 34a**. Here the movement of the third droplet resembles more of a flow than the rigid body rotation seen in **Figure 34a**, as the lower elasticity of the droplet prevents it from remaining in its initial orientation and shape. The large neck and flow-like behaviour of the restructuring suggests the droplet locally yields under the interfacial pressures while the higher curvature ends of the droplet indicate that regions of elastic structure remain.

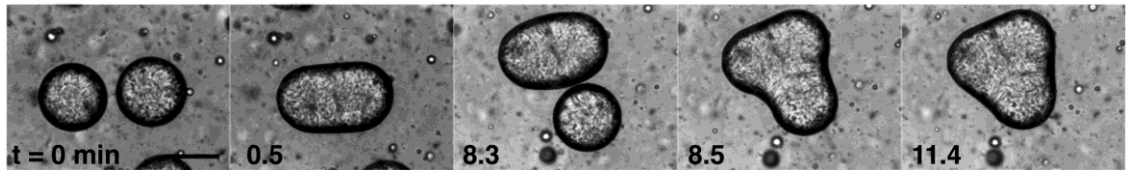


**Figure 35.** Restructuring of droplets (20% solids level), showing more extreme changes in area and compactness of the triplet shape. Scale bar 200  $\mu\text{m}$ .

Comparing the final state of the triplets formed in **Figure 32–35** demonstrates the increasing dominance of the liquid meniscus, transmitting interfacial pressure, in determining the final shape of the droplet aggregate. Increasing solids level increases elasticity and better preserves the individual spherical identity of the droplets. All experiments here have examined the behaviour of triplets formed in a single level plane of the surrounding fluid, allowing us to avoid any out-of-plane movement and track restructuring as it occurs for each droplet. There are a number of possible initial conditions that produce a triplet, and we would like to understand the variability of the restructuring phenomena observed for low-to-intermediate solids concentrations. A critical variable is expected to be the angle of approach by the third droplet, defined here as the angle the third drop's centre of mass makes with the long axis of the doublet, as in **Figure 32b** and **34b**. Varying this angle provides a way to study the relevant processes and forces involved in restructuring: movement of a droplet initially attached at a high angle of approach to a more compact packing arrangement.

### 4.3.3. Approach angle effects

Observations of droplet coalescence during triplet formation in **Figure 32–35** indicate the dynamic character of the triplet as a result of movement directed by the meniscus between drops. We hypothesize that the approach angle determines the degree to which the meniscus can alter the droplet from its initial position *via* restructuring. Experiments varying the approach angle for all four solids concentrations were carried out in order to determine the effect of the initial droplet orientation on its final state. Examples of several different initial angles are shown for 25% and 30% solids concentrations in **Figure 36**, along with the final angle attained after sufficient time allowed for restructuring. For the 25% solids case in **Figure 36**, the approach angles vary between 95–137° and only the highest approach angle avoids restructuring. For the case of the lower two angles, the third droplets are seen to be repositioned in the final state at an angle 25 – 52° lower, respectively, than their initial state. Between an approach angle of 112° and 137° there appears to be a threshold approach angle where the interfacial force exerted by the meniscus is unable to initiate, or significantly alter, the third droplet's orientation and the initial orientation remains stable. Interestingly, the two neck menisci overlap for 137° but the droplet does not restructure. Clearly some form of resistance exists and could be related to the increased compression droplets may experience at larger approach angles. At higher angles the interfacial force is directed more through the centre of the droplet and may create local connections, or bonds, as a result of compressive stresses versus cases when the meniscus force is directed off of the centre axis.

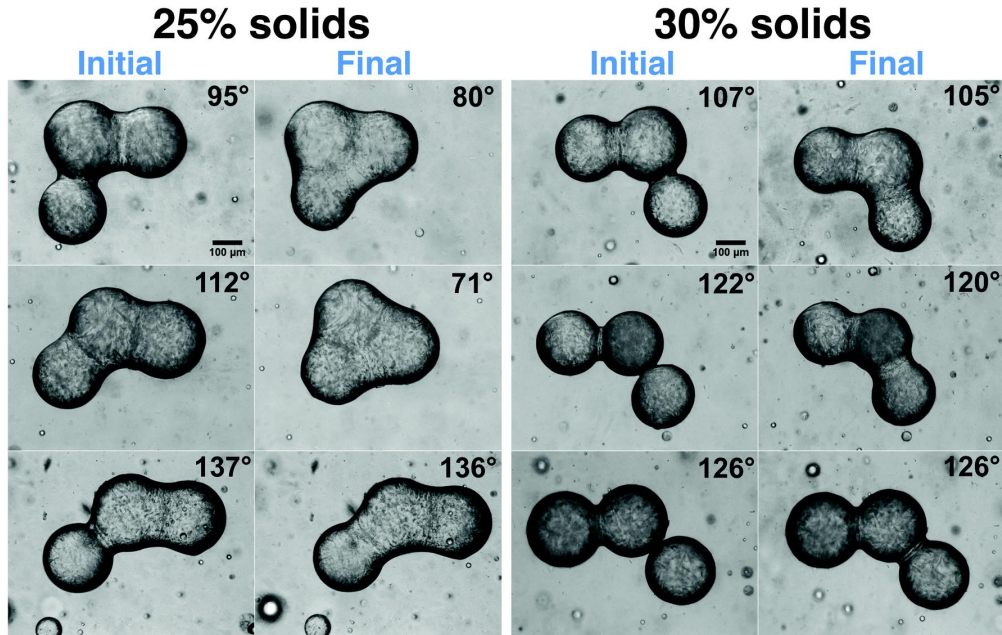


**Figure 36.** Images showing the effect of different approach angles on the restructuring of droplets containing 25% and 30% solid concentrations.

A slight increase in solids concentration to 30% mostly stabilizes the droplets against any restructuring, even for a similar angular range where significant restructuring is observed for 25% solids in **Figure 36**. If the fluid meniscus joining these droplets is responsible for transmitting the force that causes restructuring, the observed dependence on approach angle may occur because higher approach angles decrease the volume of meniscus in one region. The effect of solids level likely occurs because increased elasticity will decrease compressibility of the internal crystalline microstructure, making less free fluid available at higher solids levels and also reducing meniscus volume and ability to restructure. Following this reasoning, we examine the effect of approach angle for a wide range of solids concentrations in order to more closely map the boundary between stability and restructuring behaviour and to understand its origin.

**Figure 37** shows plots of initial and final approach angle for four solids concentrations, with a solid line drawn for  $\theta_{\text{initial}} = \theta_{\text{final}}$  to allow comparison of cases where restructuring occurs and the data deviate from the line. At 20% solids, we see that all triplets exhibited restructuring. The only change is a slight increase in final angle as approach angle is increased. This may indicate an increased resistance to restructuring at higher initial angles with some of the droplet mass spreading out as it flows into its final position. Similarly, at low initial angles the system converges to the state of most

compact packing. Increasing solids to 25% we see a clear transitional behaviour depending on approach angle. Restructuring occurs for lower approach angles, up to a value  $\sim 115^\circ$ , above which the droplets abruptly no longer change. We also see the final angle of the restructured systems, at solids levels of 20% and 25%, tends to level off near a value of  $70^\circ$ . The consistent value reflects the approach to a true spherical close packed value of  $60^\circ$ , differing only because the droplets' internal elasticity enables varying deformation, and some drag may reduce complete rearrangement. For solids levels of 30% and 40%, no restructuring is observed for any angle of approach and points in **Figure 37** all lie on the equality line. There are some outliers for 30% and 40% solids, where the final droplet angle is actually a bit higher than its starting value. Presumably these rare effects occur because of some bias in the crystalline microstructure that shifts the meniscus-driven movement of a third droplet away from the typical direction of restructuring into a more compact shape. As noted earlier, the strain of the initial doublet always increases when a third droplet is added. Above the critical angle, no dependency of strain on approach angle is observed, likely because the new meniscus volume does not vary with angle. We have observed that a critical angle of approach exists for intermediate level solids concentrations that determines whether restructuring occurs. The value of this angle is  $\theta_c \sim 115^\circ$ , from **Figure 37**, and may be a result of interaction of the two menisci joining the outer two droplets to the centre one in a triplet.

#### 4.3.4. Triplet restructuring theory

In order to better understand the transition angle at which triplets begin to restructure, as in **Figure 34a** and **b**, we develop a simple theoretical model of the phenomenon. Assuming that the primary driving force is interfacial tension, the restructured triplet should be the lowest energy state given its relatively small surface area. However, we assume that the triplet is capable of restructuring to achieve this state only if the two oil menisci, which bridge from the outer droplets to the centre drop, overlap. We assume that the oil bridge between droplets will take the shape of a catenoid, which is known to be a minimal surface between two loops that share an axis. Thus, a system of two droplets connected by an oil bridge can be represented in two dimensions by two circles connected by a catenoidal curve. The outer edges of two droplets whose centres lie on the x axis are,

$$\mathbf{r}_0^2 = \mathbf{x}^2 + \mathbf{y}_{d,0}^2 \quad (2)$$

$$\mathbf{r}_1^2 = (\mathbf{x} - (1 - 4\epsilon_1) \mathbf{r}_1)^2 + \mathbf{y}_{d,1}^2 \quad (3)$$

where  $r_i$  is the radius of droplet  $i$ , and  $\epsilon_i$  is the strain between droplet  $i$  and droplet 0.

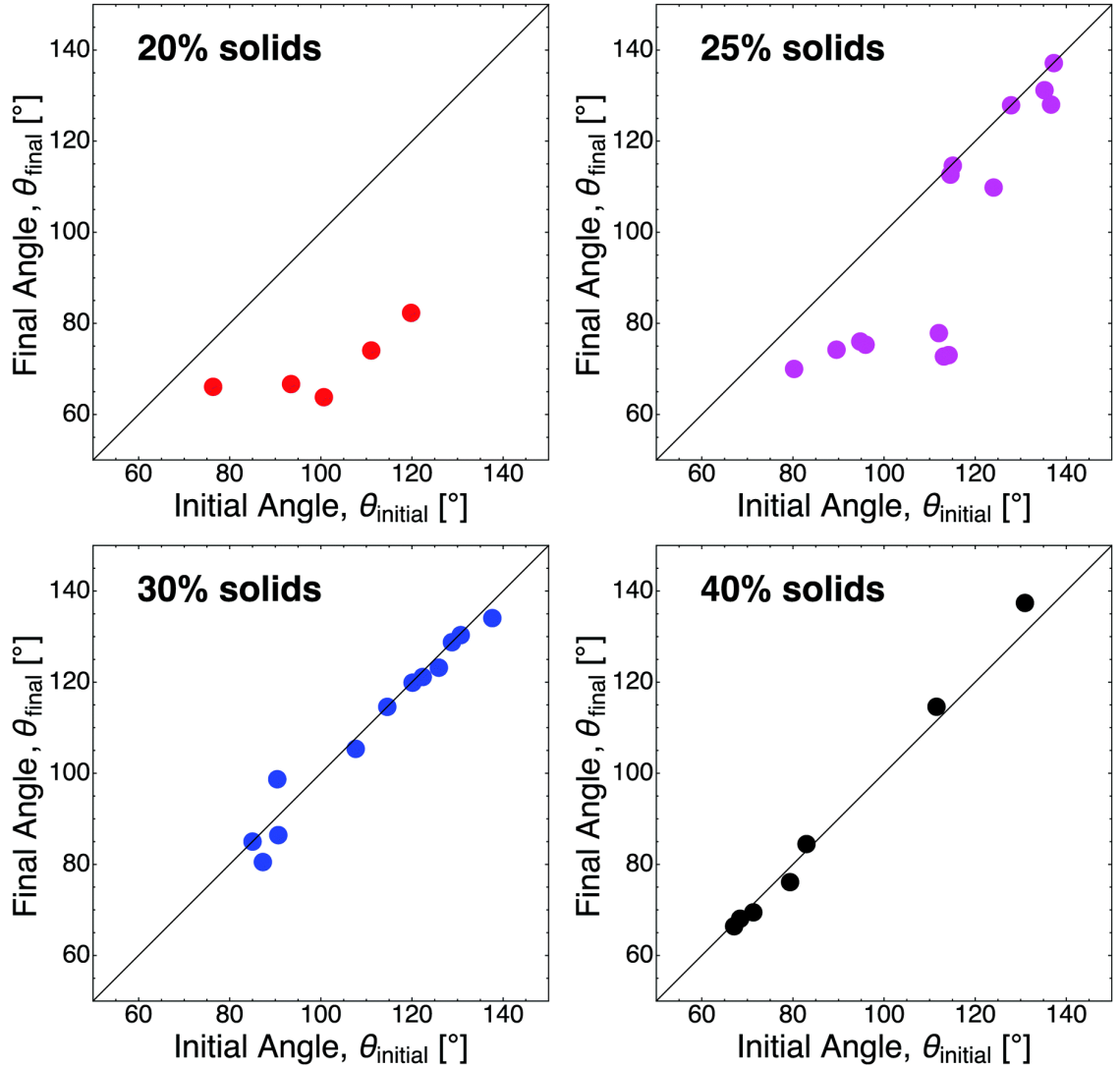


**Figure 37.** Results plotted for numerous triplet formation processes, mapping the initial and final angle between the third droplet added and the initial doublet. The diagonal line of equality indicates the cases when no restructuring occurs and deviation from the line maps the boundaries of the specific cases of restructuring.

The meniscus is written,

$$y_m = a \cosh \left( \frac{x-b}{a} \right) \quad x_0 \leq x \leq x_i \quad (4)$$

where  $a$ ,  $b$ ,  $x_0$ , and  $x_i$  are determined by assuming that the meniscus and each droplet connect continuously and smoothly.

This configuration appears in **Figure 38a** for  $r_1 = r_2$  and  $\varepsilon_1 = 10\%$ . For each pair of abutting droplets, the points  $x_0$  and  $x_i$  determine the size of the meniscus between the droplets. If the angle formed by the centres of mass of a triplet is less than some critical angle  $\theta_c$ , the two menisci of the triplet will overlap and restructuring should occur.

This analytical method provides an estimate of the transition angle for restructuring for any given droplet sizes and strain amounts. However, unlike the experimental system, this simple model does not conserve the volume of oil available to form the meniscus. In order to model a volume-constrained system with interfacial tension, we also perform simulations using the Surface Evolver (Brakke, 1992).

With Surface Evolver, we find a minimal surface subject to the level set constraints,

$$\mathbf{r}_0^2 \geq x^2 + y^2 + z^2 \quad (5)$$

$$\mathbf{r}_1^2 \geq (x - R_1)^2 + y^2 + z^2 \quad (6)$$

$$\mathbf{r}_2^2 \geq (x + R_2, +\cos\theta)^2 + y^2 + (z - R_2, +\sin\theta)^2, \quad (7)$$

and the volume constraint,

$$V = \frac{4}{3}\pi(r_0^3 + r_1^3 + r_2^3). \quad (8)$$

Here  $R_{i,\pm} = (1 - 4\varepsilon_i) r_i \pm r_0$  is the distance from the origin to the centre of sphere  $i$ , and  $\theta$  is the angle formed by the centres of the spheres comprising the triplet. Assuming interfacial tension is the dominant force that determines triplet shape, the minimal surface given by Surface Evolver should be the shape of the oil in and around the droplets.

Panels (b) and (c) of **Figure 38** visualize our volume-conserved simulations. In **Figure 38b**, we highlight the point of disconnection of the menisci for simulations with  $\varepsilon = 10\%$ . **Figure 38c** indicates that our simple interfacial tension-dominated model does very well to predict the shapes of the droplet triplets.

**Figure 39a** shows the surface area of many simulated arrangements as a function of triplet angle and for several different strains. For each series, the minimum energy,

which is proportional to surface area, is achieved at  $60^\circ$ , which corresponds to spherical close packing. The energy of a triplet at a given angle then increases with increasing angle before levelling off to a constant interfacial tension. The levelling off occurs exactly at the critical angle  $\theta_c$  that corresponds to the menisci becoming fully disconnected, as we theorized for the basis of our analytical model. In **Figure 39a** the critical angles are noted by a vertical solid line on each data series, solid for the volume-conserving simulation and dashed for the analytical results. Though second-order effects undoubtedly exist in this system, the simple approximation of an interfacial-tension-dominated set of overlapping spheres does well to model our experimental observations and confirm our physical intuition. The simulation is also consistent with the physical case, as lower solids levels have more overlap and greater amounts of free fluid available.

The effect of the volume constraint on the critical angle is evident from **Figure 39b**. Simulations with little strain have less oil available and therefore form narrow menisci that are less likely to overlap. Thus, the simulated results show a critical angle that is shifted below the angle predicted by the analytical construction that does not conserve volume. This helps to explain why restructuring is less common for stiffer droplets. Similarly, simulations with large overlap have more meniscus material available and thus exhibit a shift of the critical angle towards larger values than that predicted by non-conservative theory. For  $\epsilon = 10\%$ , the analytical model does coincidentally conserve volume, and no shift in the critical angle is observed.

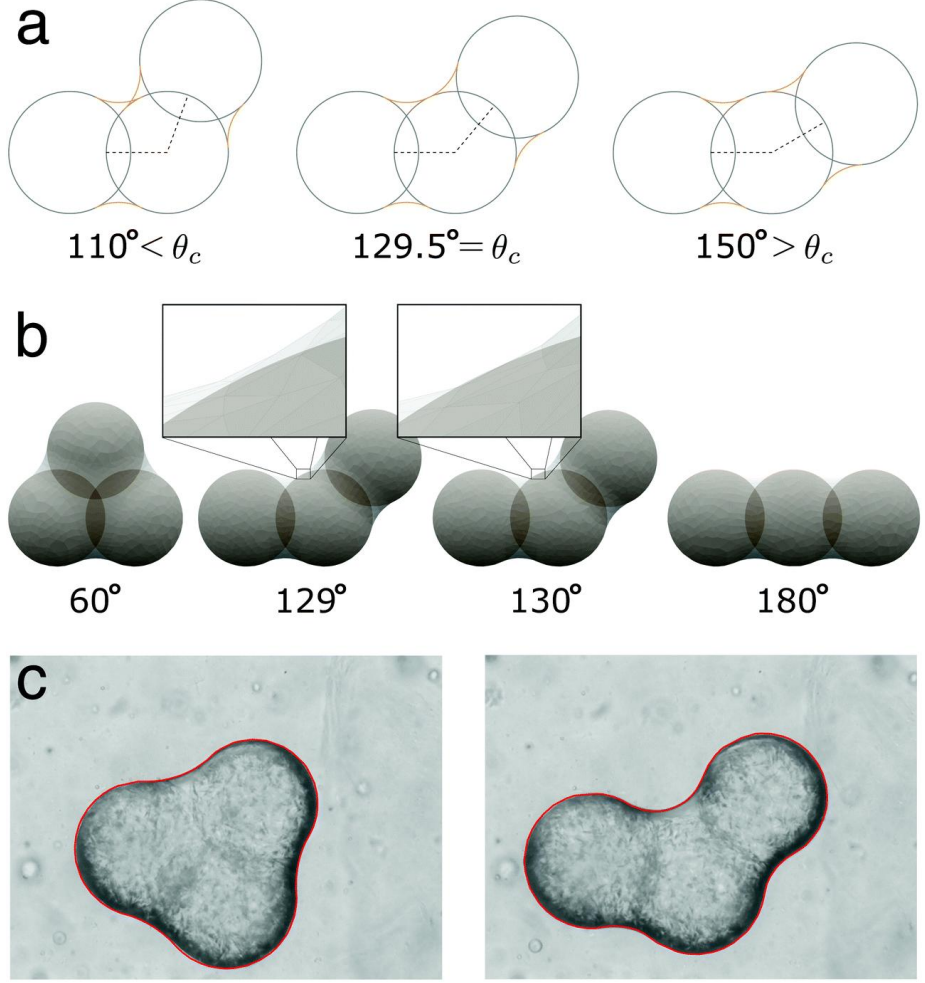


**Figure 38.** Panel (a) shows diagrams of our analytical model for angles less than, equal to, and greater than the critical angle  $\theta_c$  given equally sized droplets with a strain of 10%. In the diagrams, a catenoidal meniscus (orange) forms between two each abutting pair of droplets (gray). The angle formed by the centres of two droplets and the point at which the meniscus meets the droplet exterior is  $\theta_c/2$ . Panel (b) shows a series of simulation visualizations at  $\theta = 60^\circ, 129^\circ, 130^\circ$ , and  $180^\circ$  for the series  $\epsilon = 10\%$ . The zoomed in frames demonstrate the transition from overlapping to non-overlapping menisci that occurs at  $\theta_c$  between  $129^\circ$  and  $130^\circ$ . Panel (c) overlays the results of simulations (red outline) with experimental images for 25% solid triplets with angles of  $75^\circ$  (left) and  $115^\circ$  (right). The radii  $r_i$  and stains  $\epsilon_i$  were extracted from the experimental images and used as inputs to the simulations.

That we do observe a critical angle experimentally suggests that, even though restructuring is always favourable given the global energy landscape, the triplet is only capable of restructuring if the derivative of interfacial tension with respect to angle

overcomes some initial energy cost—likely due to mechanical friction. This explains the discrepancy between the critical angle observed experimentally and found by simulation, **Figure 39b**. Based on experimental evidence, droplets with 25% solids tend to have overlaps between  $\epsilon = 10\%$  and  $\epsilon = 15\%$ , corresponding to the third or fourth series from the top in **Figure 39a**, which suggests a critical angle of at least  $129^\circ$  and not  $115^\circ$  as observed. Though the interfacial tension produces some torque to restructure the triplet, the triplet only restructures if this torque overcomes the mechanical friction opposing it. This work has not explicitly examined the effects of droplet size but the fact that the restructuring behaviour seems to depend on a balance between interfacial and frictional forces indicates the phenomenon will be most important for droplets with sizes equal to, or smaller than, those studied here.

**Figure 40** shows a map of the main modes of arrested coalescence behaviour of the triplets studied here. Consistent with earlier observations, we see that three regions are possible: total coalescence and loss of individual shape, arrested coalescence with subsequent restructuring, and arrest without restructuring. Restructuring is possible where approach angles and elasticity are low, while sufficiently high approach angle or elasticity can prohibit restructuring and arrest. Some variability is noted in the observed trends, such as when we see merging of menisci between droplets but no significant restructuring, **Figure 33**. Such variations indicate triplets can vary in their resistance to restructuring, likely due to small differences in crystal microstructure and mechanical properties.

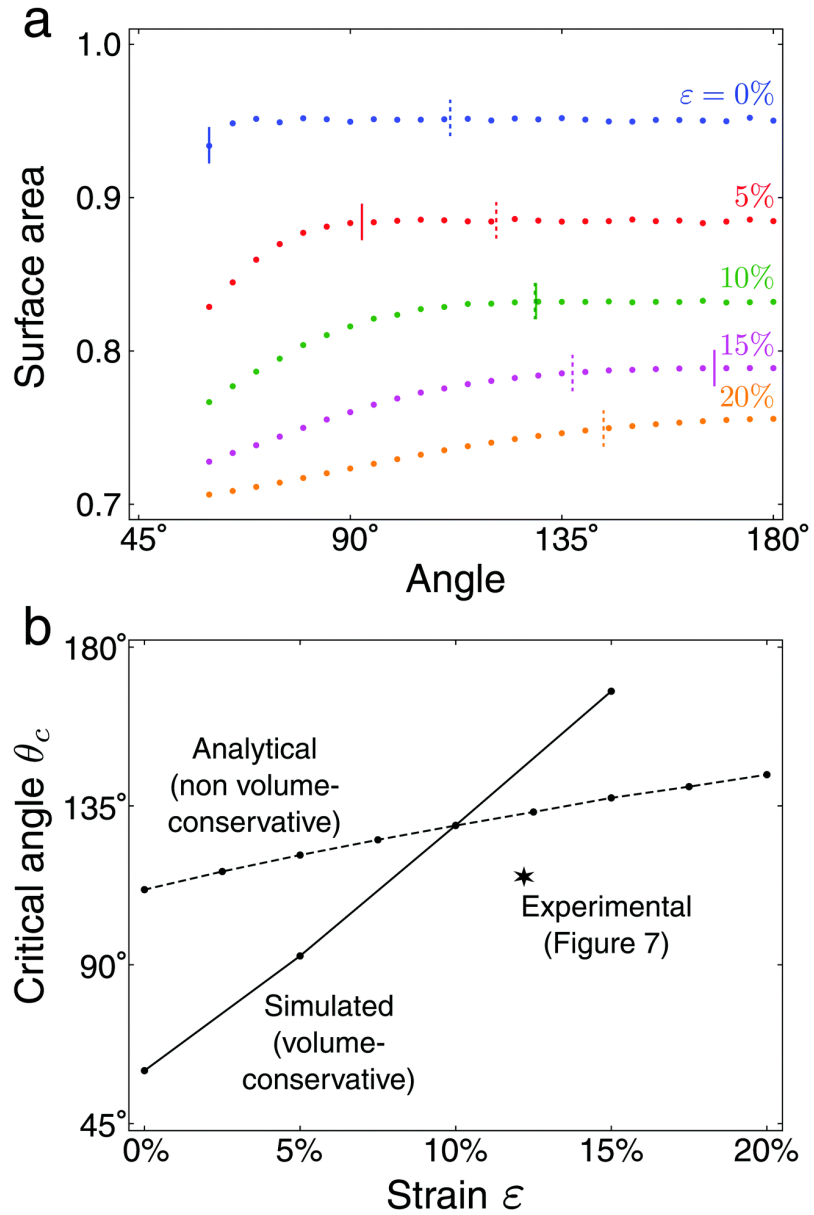


**Figure 39.** Panel (a) shows surface area, normalized by the surface area of three unconnected spheres, of several simulations runs for  $r_0 = r_1 = r_2$ . The different series represent different values of strain  $\varepsilon$ , while the solid (dashed) vertical line in each series gives the critical transition angle based on simulation (analytical) results. Panel (b) plots the critical angle  $\theta_c$  as a function of strain based on analytical results (dashed line) which do not conserve droplet volume and simulation results (solid line) which do conserve droplet volume. No critical angle exists for simulated runs at  $\varepsilon = 20\%$  because the volume available to form the menisci is large enough that the menisci are never disconnected.

Key example silhouettes of numerous final triplet shapes are also plotted in **Figure 40** as a function of their solids concentration and initial angle of approach. The mapping of shapes reveals the regions of concentration and trajectory where droplet geometries are stable or forbidden based on the balance of interfacial and elastic energies. One interesting effect is during approach angles of  $100 - 125^\circ$  for 20% solids: the system passes through a local maximum in surface-to-volume ratio with more compact shapes produced. Initially surprising, we assume this results from a change in the displacement possible for the third droplet: the longer the distance it is pulled the more it is fluidized and spread/compacted during interface equilibration, producing a more compact shape. At high or low approach angles the droplet travels almost no distance from its original contact point and less deformation occurs.

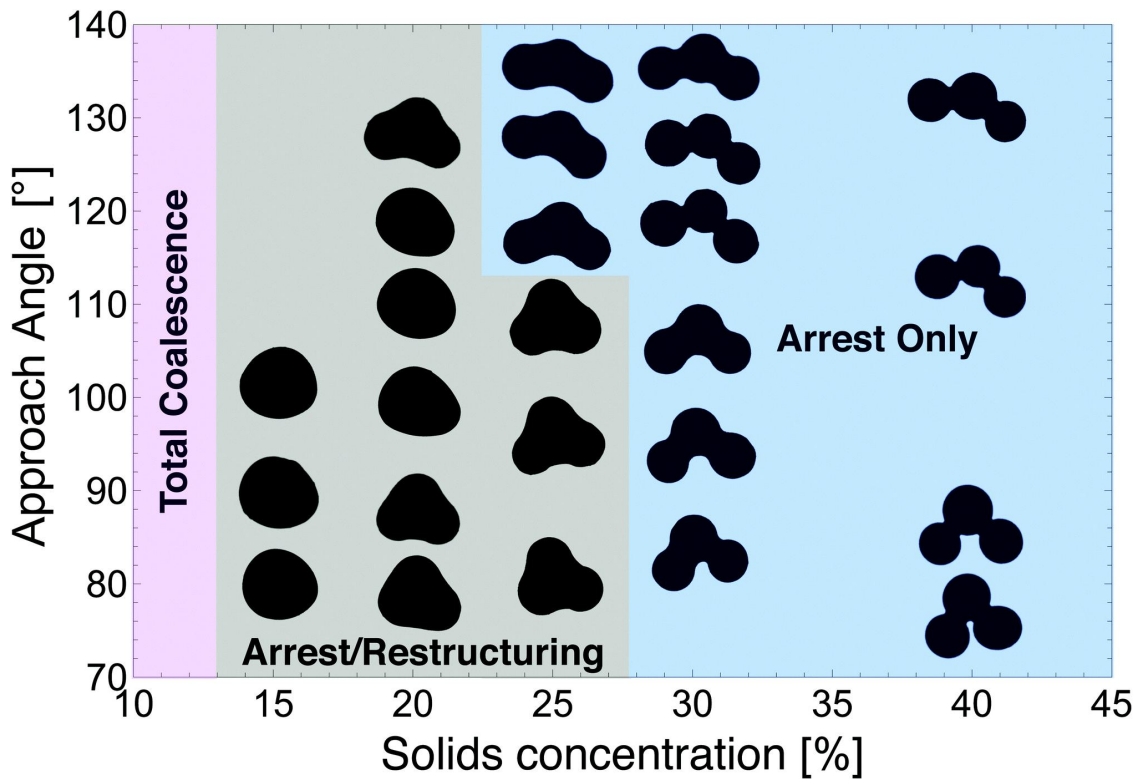


**Figure 40.** A design map of the possible shapes formed following the initiation of coalescence in an aggregate of three viscoelastic droplets. The shapes are a result of the balance between interfacial pressures and elastic deformation of droplet microstructure and indicate where shape complexity, stability, and dynamic behaviour is found.

#### **4.4. Conclusions**

Structural dynamics in aggregates of three viscoelastic droplets have been studied during arrested coalescence in order to understand the changes in microstructure wrought by interfacial and elastic driving forces in an emulsion. The experimental data depict the change in deformation of droplet doublets when a third droplet is added to the system. A central player is the meniscus of fluid between droplets as it connects the droplets and exerts the shaping and equilibrating force of the interfacial tension on the aggregate. The solids content of the droplet exerts an elastic opposition to the interfacial pressure and the ultimate balance between forces determines the final state of the droplet. There are two key effects observed for triplets that are unique from the doublet case and can be explained with simple physical arguments. The first is an increased width of the fluid neck bridging droplets that is a direct result of the redirection of liquid to create a second neck and connect the third droplet. A second behaviour has an even more profound effect on the droplet network structure and packing: the relocation of the third droplet to pull it into a more close-packed state and restructure the triplet from its initial position. None of the resulting structures are fully coalesced and their arrested state is a key factor in their formation, but this work shows that

there are additional relevant dynamics in this process than have been previously considered in the formation of three-dimensional emulsion structures. These observations are important in real emulsions as the flow trajectory and droplet addition history become particularly important to the final emulsion structure. Further research is needed to see the effect of restructuring in a system with larger, more realistic, numbers of droplets in bulk emulsions, as well as to account for droplet size effects on strain and ability to restructure. These results add to our physical model of arrested coalescence of droplets, moving us closer to the simulation of the three-dimensional networks formed during mixing and preparation of foods, pharmaceuticals, cosmetics, and coatings with targeted rheological properties. The restructuring mechanism also indicates a method to program varying shape formation and shape change into colloidal systems from generic starting conditions, adding to the symmetries possible in assemblies constructed from fully solid particles by a liquid interface (Manoharan et al., 2003, Meng et al., 2010, Kraft et al., 2009, Arkus et al., 2009). The restructuring studied here is a complex mix of deformation and movement of connected droplets so, although we know interfacial

tension is the driving force for the process, additional measurements of the mechanism and magnitude of resistance to restructuring are still needed.

## **CHAPTER 5 Arrested coalescence of viscoelastic droplets: Monodisperse multidroplet aggregates**

### **5.1. Introduction**

Nearly all the droplets in an emulsion are spherical, as surface forces dominate and produce the most compact shapes possible. However, non-spherical shapes can be of great importance in commercial applications. For instance, arrested coalescence is an enduring mechanism for producing microstructure in products like foods, pharmaceuticals and petroleum by making stable anisotropic shapes. Arrested coalescence can be desirable or undesirable depending on the final product. Say for ice cream, it helps in trapping the bubbles and hence enhances texture and mouth feel, whereas in crude oil, it is not acceptable because it leads to clogging of pipelines (Méndez-Velasco and Goff, 2012). Arrested coalescence is actually a collision of two droplets whereby they begin merging into each other but are halted at an intermediate stage before they form a single spherical droplet (Fredrick et al., 2010, Walstra, 2003b, Giermanska et al., 2007). The formation of such anisotropic shapes can be achieved by arrested coalescence of two spherical droplets with (Studart et al., 2009, Pawar et al., 2011) or without particles adhering to their interface (Pawar et al., 2012). The structures that we get from these mechanisms are three-dimensional, and are distinct from the structures formed by flocculated droplets (Torza and Mason, 1969, Princen, 1984, Bibette et al., 1993) because these are bridged by a liquid neck that varies depending on droplet rheology. In each case, we are interested in understanding the microstructure formed in an emulsion.

Fluid microstructure has become an essential parameter in determining the stability and rheological properties of complex products. Understanding the relation between droplet interactions and bulk properties requires a physical model of the relevant mechanics. And to have that, we need experimental data on structure formation and its changes during formation, processing and storage, with time (McClements, 2007b). Local changes ultimately affect the overall structure and rheology of the product.

In many fat products, solid content of the system determines the overall textural properties, of the 3D colloidal fat crystal network. When crystallized, fat crystals aggregate, like colloidal gels networks. Such structural hierarchy has been observed by many researchers (Van den Tempel, 1979, Juriaanse and Heertje, 1988, Heertje, 1993, Deman and Beers, 1987). The rate of droplet collision and coalescence is affected by fluid flow, viscosity, and interfacial properties (Leal, 2004, Janssen and Anderson, 2011). Previous work has studied arrested doublets from mono- (Pawar et al., 2012) and polydisperse (Dahiya et al., 2016a) emulsions when elastic and interfacial forces are balanced, but only examined static systems. This work builds on these examples to understand the dynamics of structures in flow where additional effects on structure and ordering may occur. Real emulsions contain a multitude of droplets and experience complex flows and interactions. We focus here on idealized droplets as they interact and arrest to understand the importance of phenomena previously studied in more isolated conditions (Dahiya et al., 2016b).

## 5.2. Experiment

### 5.2.1. Materials

The oil (dispersed) phase constitutes hexadecane (99%, Sigma Al-drich) and petrolatum (Vaseline, Unilever) in a ratio needed for a given solids concentration, while the continuous phase consists of 0.15 wt% Carbopol (Carbopol Lubrizol).

### 5.2.2. Formation of monodisperse droplets

Monodisperse droplets were generated using the glass microcapillary device sketched in Figure 1. In this design, a pulled round borosilicate glass capillary is fitted into a square capillary to facilitate the co-axial flow of dispersed and continuous phase through the device [adapted from (Benson et al., 2013)]. A square capillary with inner diameter (ID) of 900  $\mu\text{m}$  and outer diameter (OD) of 180  $\mu\text{m}$  was used. Whereas a round capillary with ID of 700  $\mu\text{m}$  and OD of 870  $\mu\text{m}$  was used to make it easy to align in the center of the square capillary. The round capillary was pulled with a Micropipette Puller (Model P-97, Sutter Instruments) to form tips smaller than 80  $\mu\text{m}$ . Both round and square capillaries were attached to syringes containing oil and Carbopol respectively. Syringe pumps were used to maintain the desired flow rates and control the size of the droplets. Once the droplets are produced, a 10 cm long plastic bag full of ice is placed

onto the square capillary for 15 minutes to hasten crystallization of the droplets. After crystallization, droplets produced in the device were released into a rectangular capillary with ID of 400  $\mu\text{m}$  which was connected to the device through a transparent Tygon tube (as indicated in **Figure 41**).

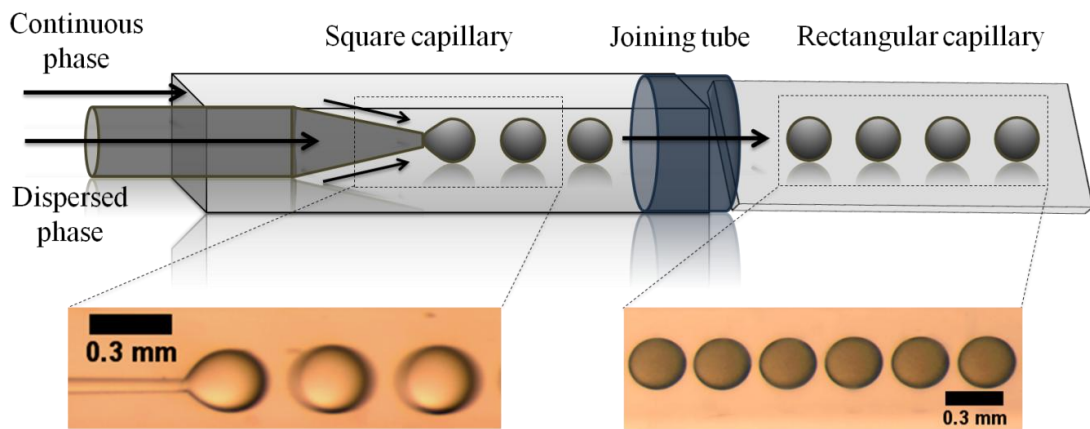


**Figure 41.** Schematic diagram of microfluidic made of borosilicate glass for the droplet production. Inset: images showing monodisperse droplets formed in square capillary [adapted from (Studart et al., 2009)].

### 5.2.3. Fabrication of capillary to induce flow

Once the desired number of droplets are in the rectangular capillary, it is detached from the device and sealed or glued from one end, to restrict air-liquid interface. The prepared capillary is then mounted vertically onto an empty petri dish that is later filled with 25 wt. % KCl solution, **Figure 42**. The salt solution flows at a velocity of  $\sim 0.0078$  mm/sec, and the droplets flow upwards with velocity of  $\sim 0.0046$  mm/sec. The velocities of droplets and salt solution can be calculated by tracing the position or distance travelled (by both droplets and salt solution) in capillary in every frame.

### 5.2.4. Microscopy

Droplet structure is formed and studied using a horizontally-oriented stereoscope. Once the set up is ready, the petri dish is filled with KCl solution, and the rectangular capillary containing emulsion is placed inside. Salt releases the droplets from the yield stress fluid by deswelling the microgel particles and allowing the droplets to flow up via buoyancy so they can collide and begin arrested coalescence. Observation of the

structure formation continues for at least 3 hours to map the formation dynamics as well as the resulting structure.

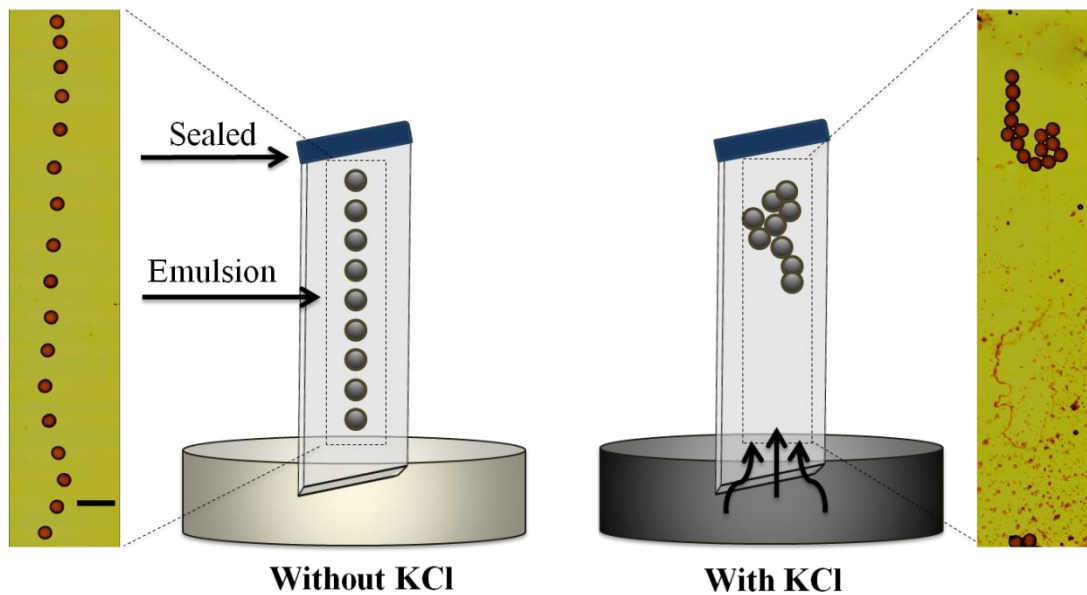


**Figure 42.** Schematic diagram showing arrangement of flat capillary for salt diffusion into the emulsion. Scale bar 500um.

### 5.3. Results and discussion

#### 5.3.1. Structure formation

**Figure 43** shows formation of microstructure in droplets having 50% solids content. Once the salt starts diffusing into the emulsion, the buoyant oil droplets flow upwards. As they touch the neighbouring droplets, they begin to coalesce. There is a viscosity gradient as the diffusion process is quite slow. We don't see significant effects on the coalescence process except to make it more orderly than in a more chaotic mixed system. Whereas previous work manipulated droplets into contact, this work allows natural transport and orientation to be observed. In past studies, 50% solids was too elastic to allow coalescence (Pawar et al., 2012). Here, however, the droplets form small necks of fluid and arrest weakly into aggregates with a maximum strain of 0.079. The discrepancy is likely because the flow here influences the energy of collision. The structure obtained in such a system is quite interesting, as it is quite open and porous. High elasticity prevents the droplets from progressing beyond early stages of coalescence before being arrested, so multiple variables affect the ultimate structure of droplets.

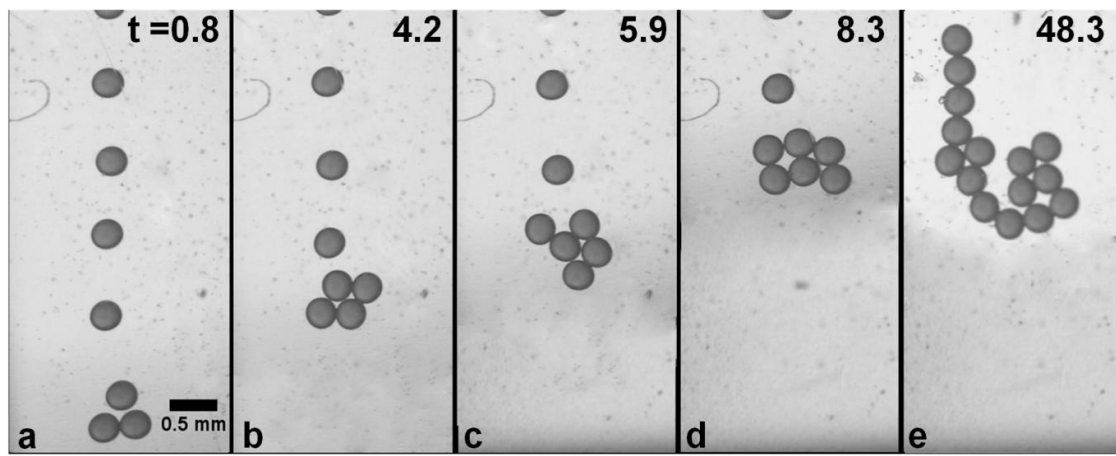


**Figure 43.** Microscopic images showing sequence of formation of structures for 50% solids. Time in minutes, scale bar 0.5 mm.

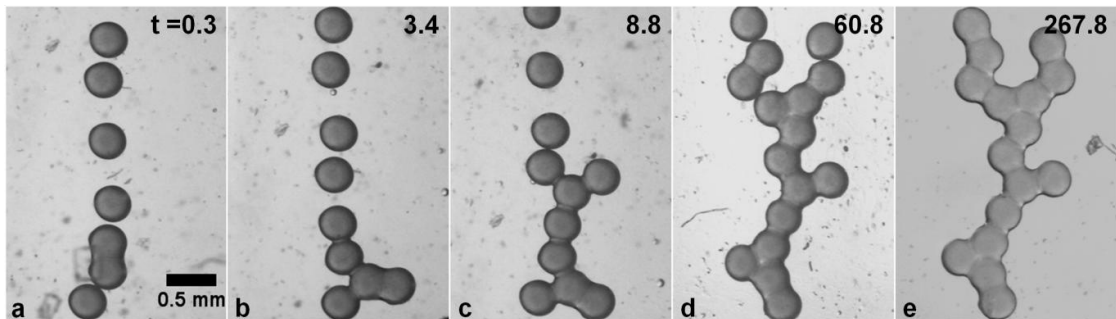


**Figure 44.** Microscopic images showing sequence of formation of structures for 40% solids. Time in minutes, scale bar 0.5 mm.

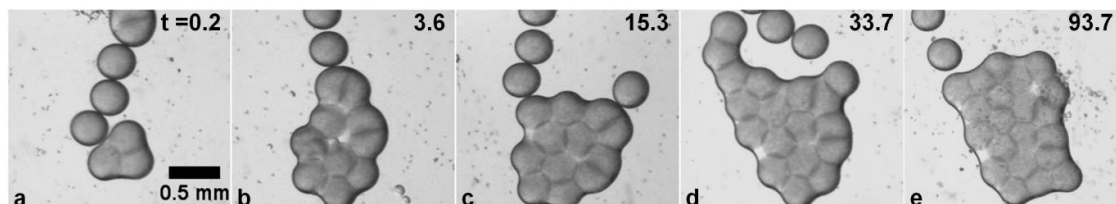


**Figure 45.** Microscopic images showing sequence of formation of structures for 30% solids. Time in minutes, scale bar 0.5 mm.

Droplets with 40% solids (**Figure 44**) have a microstructure that is more compact than the 50% solids case. The deformation of the droplets in **Figure 44** is higher than the doublets from previous work (Pawar et al., 2012), with a maximum value of around 0.26. **Figure 45** indicates further lowering the solids level to 30% produces an even more compact structure because of the low elasticity that allows much higher

deformation. The droplet boundaries are still visible, allowing us to identify the structure and connectivity without such aggregates.

### 5.3.2. Flow directions and mechanisms during the formation of multidroplet networks

Although essentially a two-dimensional flow is used to form these emulsion structures, the velocity profile across the capillary still allows vorticity to influence orientation of the droplets and their aggregates by causing rotation. **Figures 46, 47 and 48** highlight the directional changes in droplets during their flow up through the capillary. As seen in **Figure 46a - 46c**, the triplet has 90° angle rotation in the direction of flow, whereas in **Figure 46d - 46g**, the quartet has almost 180° angle rotation in the direction of flow. Similarly, in **Figure 46g - 46j**, the pentet show a 90° flip followed by upward motion. These results differ from earlier studies (Pawar et al., 2012) in that additional shear stresses influence droplet orientation and packing throughout the process.

As solids level is decreased, restructuring can also occur within the aggregate. For 40% solids the droplets display distinct rotations. In Figures **47a - 47d**, the doublet residing in between two single droplets does not begin coalescing when flow was initiated. It rotates almost 80° counterclockwise, and then begins coalescence with its neighbouring droplets, which is further followed by some slight rotations in **Figures 47f -47h**. As the structure formation progresses, the droplets are further deformed, as seen in **Figures 47i - 47l**. The deformation occurring in the droplets leads to oil extraction, which starts bridging the neighbouring droplets with liquid necks (**Figure 47i - 47k**) as explained in a previous work (Dahiya et al., 2016b). This liquid neck widens if the added droplet is at low angles, and restructures the droplets to make a compact structure (Dahiya et al., 2016b). The previous studies showed no evidence of restructuring of droplets above 30% solids but we see it here as a result of the inertia of the moving droplets. Flow rotates the structure as well as increasing the pressure during collisions and coalescence.

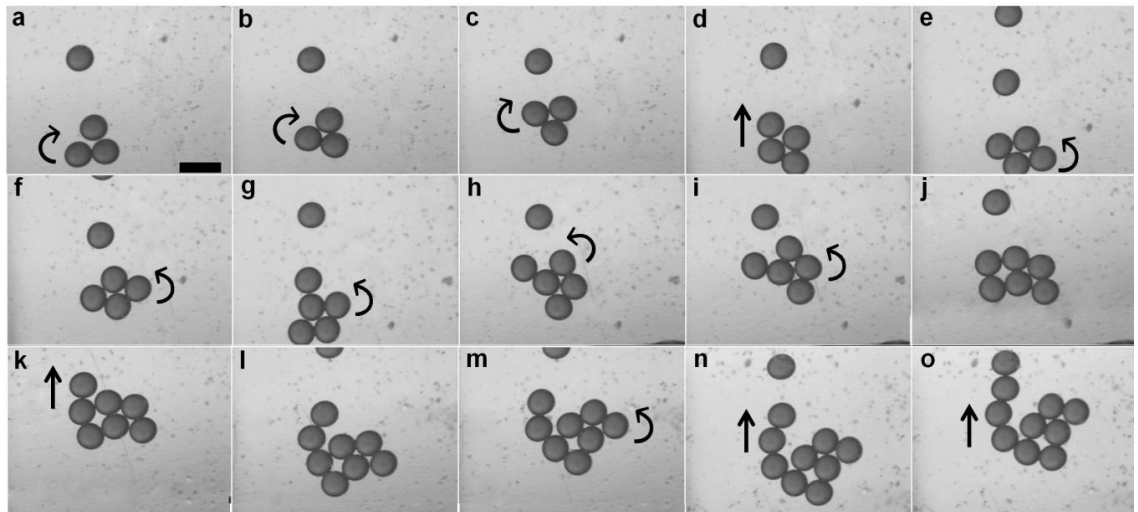


**Figure 46.** Microscopic images showing various rotations during network formation at 50% solids. Scale bar 0.5.mm.

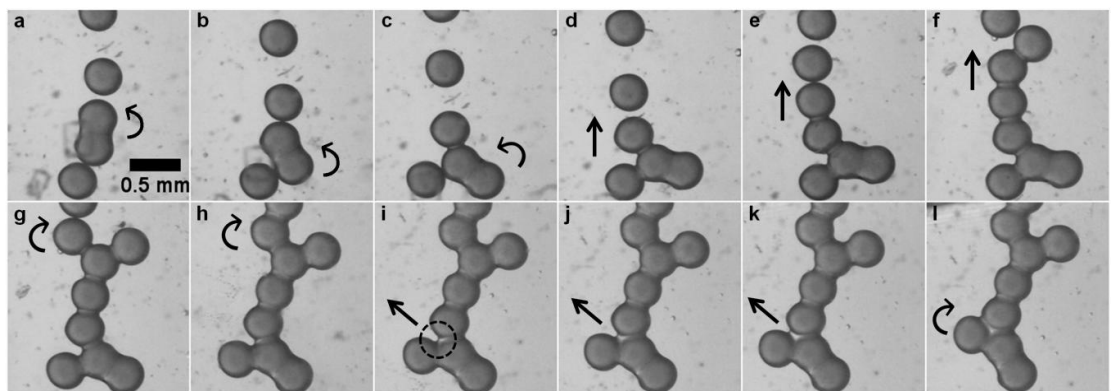


**Figure 47.** Microscopic images indicating individual rotation and restructuring events at 40% solids. Scale bar 0.5.mm.

**Figure 48** follows a sequence of droplet collisions that produces an even more compact aggregate. Here the aggregate is more compact than those formed at higher solids levels. Smaller changes in orientation are seen here. **Figure 48f - 48j** shows 30° clockwise rotation of the aggregate, whereas **Figure 48k - 48m** show 15-20° rotation. The movement of the entire structure during flow-induced collisions is important to its final packing as rearrangement is frequent and increases with decreased solids levels. Deformation of primary droplets is also significant, **Figure 48**, as their elasticity is quite low, and the stresses experienced here are higher than for micromanipulation experiments (Dahiya et al., 2016b, Pawar et al., 2012). These observations supplement

our ability to predict multidroplet structure formation in a system that undergoes low Reynolds number flows during processing or storage.

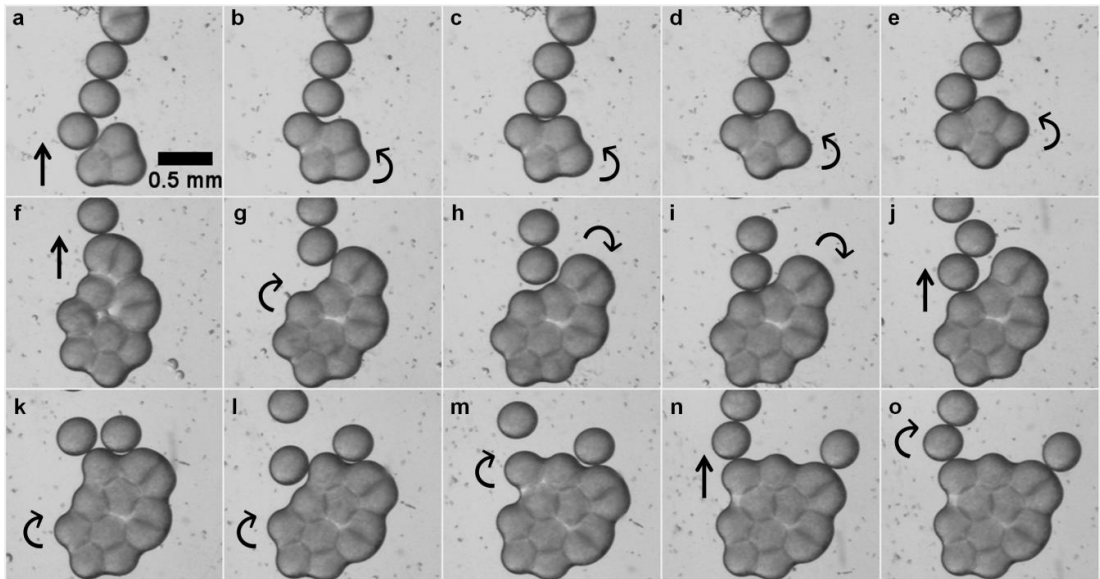


**Figure 48.** Microscopic images showing formation of a compact aggregate of droplets at 30% solids. Scale bar 0.5.mm.

### 5.3.3. Image analysis of the structure deformation and packing

The observations of droplets deformation and packing in **Figures 49-50** show the dynamics resulting from flow induced by droplet buoyancy. More quantitative structural characterization of the network provides us with insight into the types of structures formed by droplet aggregates. Packing efficiency and connectivity relate directly to the bulk rheology of such networks, so it is helpful to understand how to apply arrest to form more effective structures. **Figures 49A** and **49B** map the distribution of strain exhibited in the 40% and 50% networks. Colours indicate three different ranges of strain within a single aggregate, varying by as much as 13%.

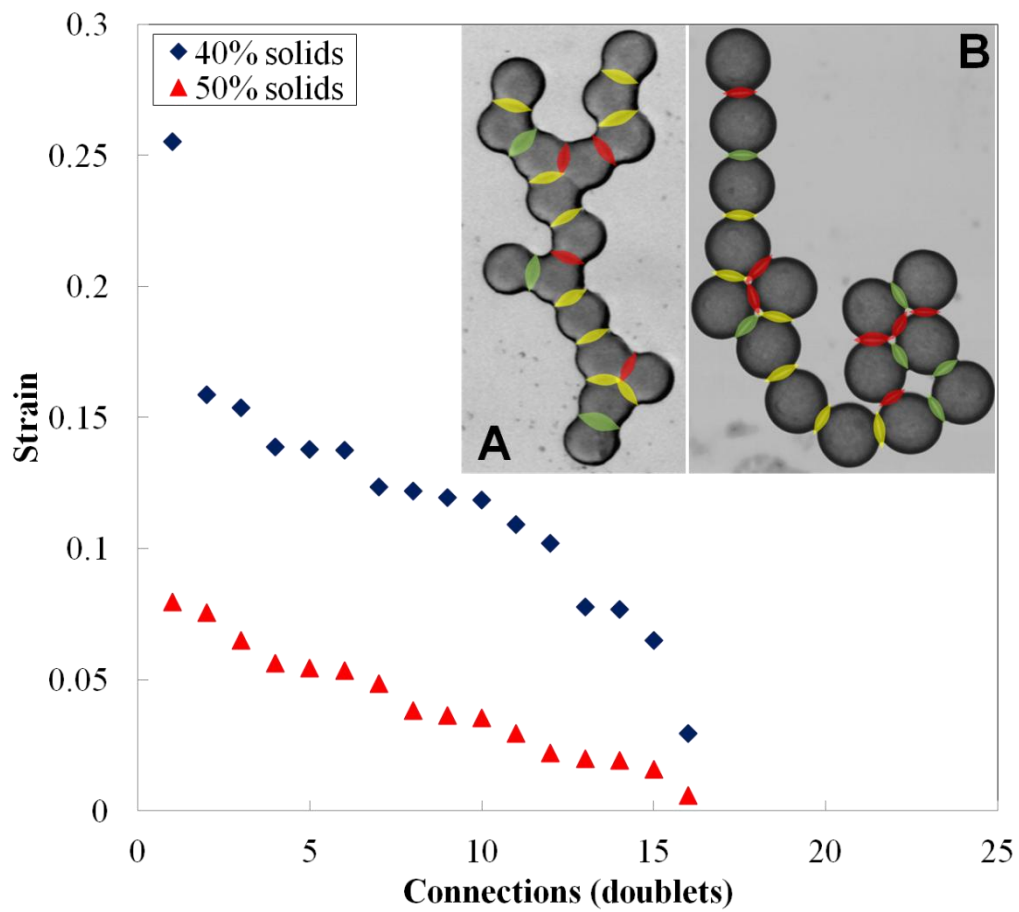


**Figure 49.** Microscopic images and graph showing strain of doublets varying throughout the network for A) 40% solids [ Green:  $\varepsilon > 0.15$ , Yellow:  $0.15 < \varepsilon > 0.1$ , Red:  $\varepsilon < 0.1$  ], B) 50% solids, [Green:  $\varepsilon > 0.05$ , Yellow:  $0.05 < \varepsilon > 0.02$ , Red:  $\varepsilon < 0.02$  ].

For both 40% and 50% solids, strain is distributed unevenly throughout the multidroplet structure. However, larger connectivity regions have larger strains, likely as a result of extraction of fluid to form multiple neck. No droplets residing at the very outside of the structure have high strain. Droplets at the outer edges have fewer connections and lower strain. Droplets' deformation is highly affected by the neighbouring droplets' position, that is, angle.

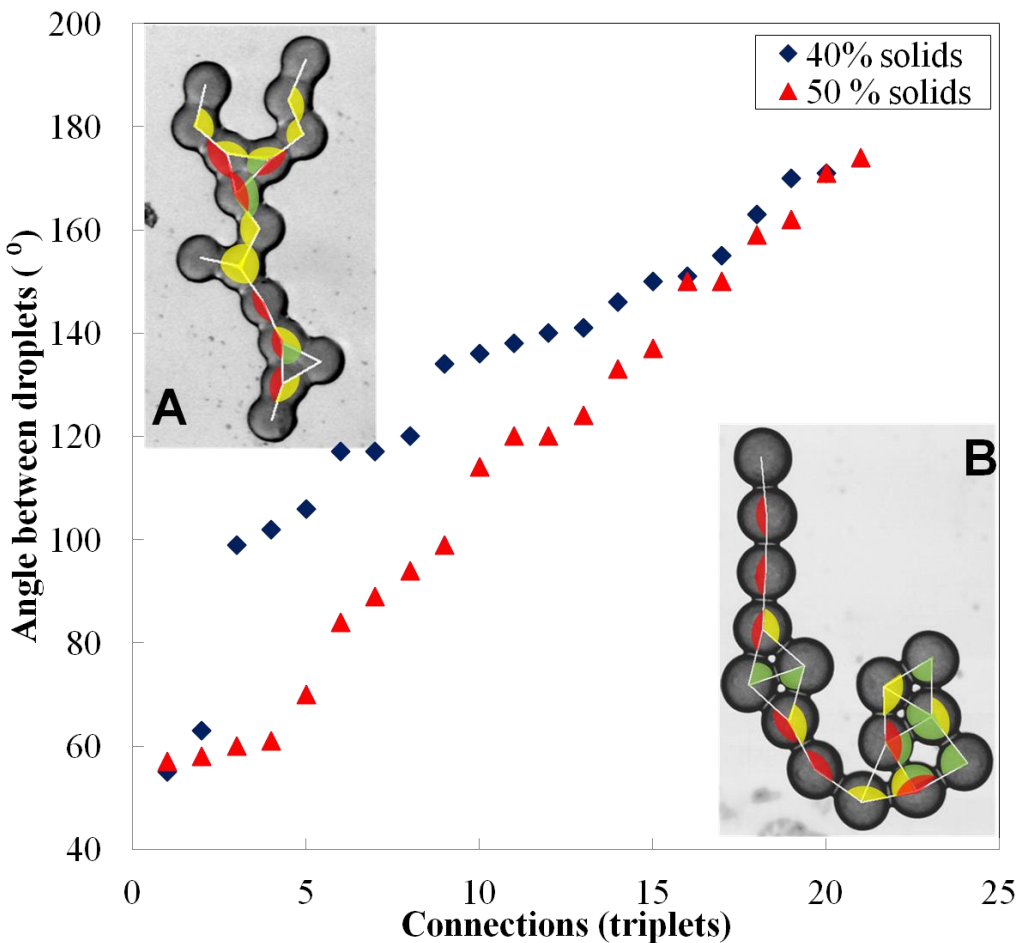


**Figure 50.** Microscopic images and graph showing the distribution of angles of triplets varying throughout the network for A) 40% solids, B) 50% solids, Green: angle below 100°, Yellow: angle between 100°- 150°, Red: angle above 150°.

**Figure 50** summarizes the bond angles between the aggregated droplets for 40% and 50% solids levels. A broad distribution of angles is seen, ranging from compact forms with angles < 60° to linear structures with angles ~ 180°. In **Figure 50A**, we can observe that there are two possible connections for triplets to get into the compact shape: represented as whole triangle. But when we compare **Figures 49A and 50A**, we find that the connections having lower bond angles might not always show higher deformation. That is probably because the droplet is connected with another droplets beyond just being in a triangle, and hence the compression in structure is spread to the whole network, not condensed just in triangle. In **Figure 50B**, the same trend is observed for 50% solids multidroplet structure as well. The packing of the droplets is very uneven throughout the structure. However, the structure formed by droplets having

50% solids is more porous as compared to the structure formed by droplets having 40% solids, because of higher elasticity, and hence higher deformation.

The multidroplet aggregates structures can be altered by varying solids concentration in the droplets. However, at 30% solids the resultant structure is too compact and deformed that is becomes difficult to analyze, as the droplets lose their identity. **Figure 51** shows differences in the structures for 50%, 40% and 30% solids formed by arrested coalescence and total coalescence. The orange circles represent the volume of all droplets undergoing total coalescence. The differences, in terms of porosity and compactness, in a structure are evident from **Figure 51**, that are caused by varying the elasticity of droplets. This helps to explain how higher deformation and restructuring can impact overall structures formed in bulk emulsions.

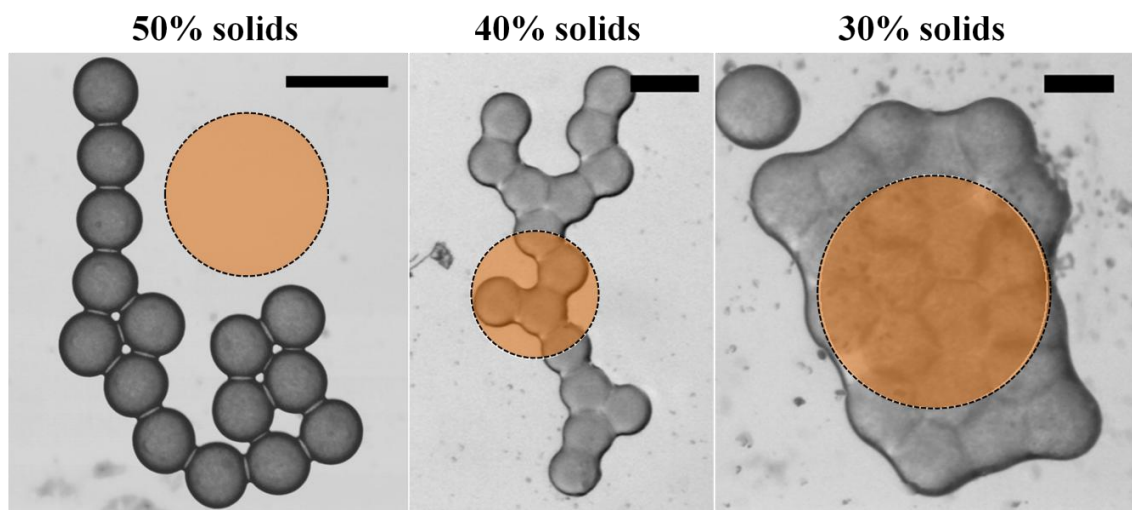


**Figure 51.** Final shapes exhibiting total volume, of all the droplets undergone coalescence to make final structures, for 50%, 40% and 30% solids. Scale bar 500  $\mu\text{m}$ .

#### 5.4. Conclusion

The evolution of viscoelastic monodisperse multidroplet aggregates has been investigated by microscopy and image analysis. The chains and disordered structures that result are analyzed for structural details like strain and bond angle to compare with previous work on aggregates of two and three droplets. High concentrations of solids in droplets lead to less deformed and loose microstructure, whereas lower concentrations of solids result in highly deformed and compact structures. Aggregates with larger numbers of droplets maintain a broad distribution of deformation and orientation,

preserving the history of their formation and additional changes wrought by flow. Increasing the solids level of droplets increases their elasticity, lowering their ability to restructure and deform. For lower solids concentrations, significant restructuring and rotation of droplet structures is observed. The effect of solids level on deformation of the evolving microstructure of monodisperse droplets is likely to have a strong impact on the rheology of an emulsion and this study provides a new means of studying this type of structure formation. Future work will investigate more complex multidroplet aggregates structures, formed by polydisperse droplets (**Figure 52**), along with their rheological properties.

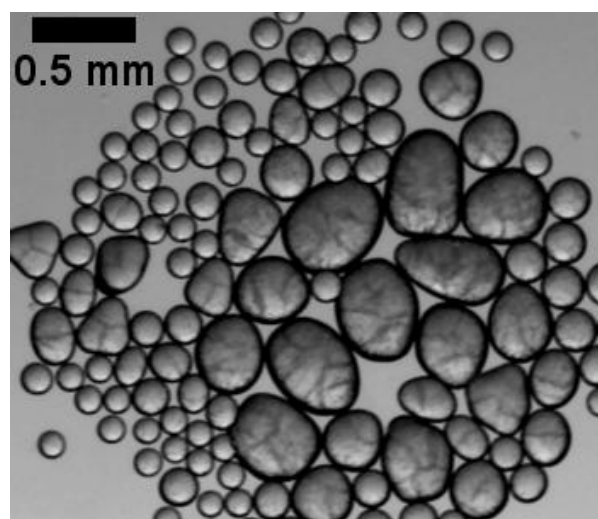


**Figure 52.** Microscopic images showing multidroplet network for: polydisperse droplets having 25% solids and monodisperse droplets having 50% solids concentration.

## **CHAPTER 6 Arrested coalescence of viscoelastic edible fat droplets: Effects of fat crystal partitioning**

### **6.1. Introduction**

A mixture of two immiscible liquids with one liquid dispersed in other liquid is known as an emulsion (McClements, 2007a, Vanapalli et al., 2002b, Cosgrove, 2010). Emulsions are thermodynamically unstable, and eventually undergo some changes or in their state due to the external forces like gravity or fluid shear (Cosgrove, 2010, Borwankar et al., 1992). Oil-in-water emulsions have oil droplets dispersed into an aqueous continuous phase, and in foods like dairy products the droplets may contain fat crystals. Fat plays a vital role in providing texture to many of food products, strongly influencing the food's microscopic and macroscopic properties. A food's mechanical properties, including spreadability, consistency, and mouth feel is often affected by solid fat content (SFC). For example, desirable spreadability of margarines is observed from 20 to 40% SFC (Wright and Marangoni, 2006). Fats can also provide firmness to a food product by forming a colloidal network that enables the liquid oil to be trapped in the structure (Blake and Marangoni, 2014, Patel et al., 2014).

Coalescence refers to the fusion of two droplets to form a single big droplet and results when the thin film at the interface of a neighbouring droplet ruptures and initiates merging. A spherical shape is formed because it minimizes the droplet surface energy (Cosgrove, 2010, Fredrick et al., 2010). Arrested coalescence occurs when the merging process is halted at an intermediate stage by some physical resistance like fluid elasticity. This is undesirable in some cases, like milk or cream as it causes flocculation of milk fat droplets (Petrut et al., 2016). However, in other cases, like butter, margarine, and ice cream, arrest is important as it increases mechanical strength by improving viscosity and thickening the system to resist phase separation (Van Boekel and Walstra, 1981, Boode et al., 1991, Vanapalli et al., 2002a). Previous work has shown that arrest of two droplets can be achieved by balancing elastic and interfacial energies (Pawar et al., 2012, Dahiya et al., 2016a). Recent work has shown that the structure formed by coalescing milk fat droplets can sometimes deviate from the energetic model developed for petrochemical-based emulsions (Thiel et al., 2016) and it would be useful to further

examine these phenomena to understand the mechanisms determining structure formation in more complex emulsions.

In the present study, we examine the anisotropic doublet shapes formed by coalescence of viscoelastic droplets in an edible system, where more complex crystallization phenomena are known to occur because of highly surface active materials present in natural fats. A key aspect we investigate here is the heterogeneity of crystal partitioning and location in an edible system, and its effects on arrest and resultant deformation. The heterogeneity of the structure is strongly influenced by fat crystallization (McClements et al., 1993, Malcolm, 1990, McClements et al., 1990). The goal of this research is to link droplet microstructure to more complex arrested coalescence phenomena and better understand and predict structure and rheology control in edible systems by building on previous work (Dahiya et al., 2016a).

## 6.2. Materials and methods

Coconut oil (Pacific Organics), Goose fat (Clos Saint Sozy) and duck fat (Clos Saint Sozy) are chosen as edible fats. The oil-in-water (O/W) emulsions are prepared by mixing separated liquid and solid fractions in different proportions to obtain different solids concentration emulsions. An aqueous phase containing 0.2% microfibrous cellulose (MFC) prepared from Nata De coco (Kara Marketing-M Sdn Bhd, Malaysia). Further dilution is carried out to experimentally study the arrested coalescence in droplets by micromanipulation.

### 6.2.1. Emulsion preparation

A Heraeus Pico 17 centrifuge was used to separate the liquid and solid fraction of each kind of fat at 25 °C. This was done to achieve the desired droplets' solids concentration by mixing the liquid and solid fraction in the desired proportion. Equal masses, of 35 g of each fat was weighed and centrifuged at 10000 RPM for 1 hour. Equal volumes (5 mL each) of oil and aqueous phase were then mixed to form an emulsion. The emulsion is prepared by mixing both dispersed and continuous phase followed by heating at 50° C and shaking for 10 seconds by hand. This leads to the formation of polydisperse droplets, which remain suspended due to the yield stress in the continuous phase. Emulsions are further diluted with 0.2 wt% MFC and stored at room temperature (23 °C) for at least 3 days before study.

### **6.2.2. Microscopic study**

The fat crystal structure of each oil was observed by mixing liquid and solids fraction, without dispersing into MFC. Further to this, the prepared samples were shaken manually for 20 seconds. Then 1 mL of each sample was put on a glass slide, and observed under a Motic AE31 microscope.

Doublets were formed and studied by micromanipulation experiments (Dahiya et al., 2016a, Pawar et al., 2012). A pre-pulled capillary is used to hold droplets at its tip and then bring them to another droplet to start the coalescence process. Borosilicate glass capillaries (1 mm OD and 0.5 mm ID, Sutter Instruments) are pulled with a Micropipette Puller (Model P-97, Sutter Instruments) to form microcapillaries. The other end of the capillary is attached to a water reservoir (10 mL open syringe) by transparent rubber tubing. Adjusting the height (upwards and/or downwards) of the water reservoir allows the hydrostatic pressure to push or grab the droplet and manipulate it. The capillary is connected to a 3-axis coarse manipulator (Narishige International USA) mounted on a microscope, which helps in positioning the droplet. The emulsion sample (~1 mL) is placed on a glass slide and the tip of the capillary is aligned to the droplet which is to be studied. By applying negative hydrostatic pressure using the water reservoir, the droplet is drawn towards its tip and grabbed, without removing any oil. To approach another droplet present in the continuous phase, the manipulator is moved to touch it with the grabbed droplet to observe their interaction. Motic software was used to capture the images every second while coalescence of two droplets occurred.

### **6.2.3. Differential Scanning Calorimetry (DSC) experiments**

The melting temperatures of coconut oil, goose fat and duck fat were studied by a differential scanning calorimeter (TA Instrument - DSC Q20). The range of heating for all three fats was set from 25°C to 95°C at 1°C/min rate. The holding time for the samples was 1 min, followed by cooling from 95°C to 10°C with a rate of 1°C/min.

## **6.3. Results and discussion**

### **6.3.1. Thermal stability**

**Figure 53** shows the range of melting temperatures for each fat. Coconut oil shows one sharp peak indicating that it has a narrow melting range. Goose fat shows two peaks and a broad

melting range from 27 ° to 41 °C. Compared to duck fat, there is a broadening of the curves and the melt regions moved to higher temperatures (**Figure 53**).

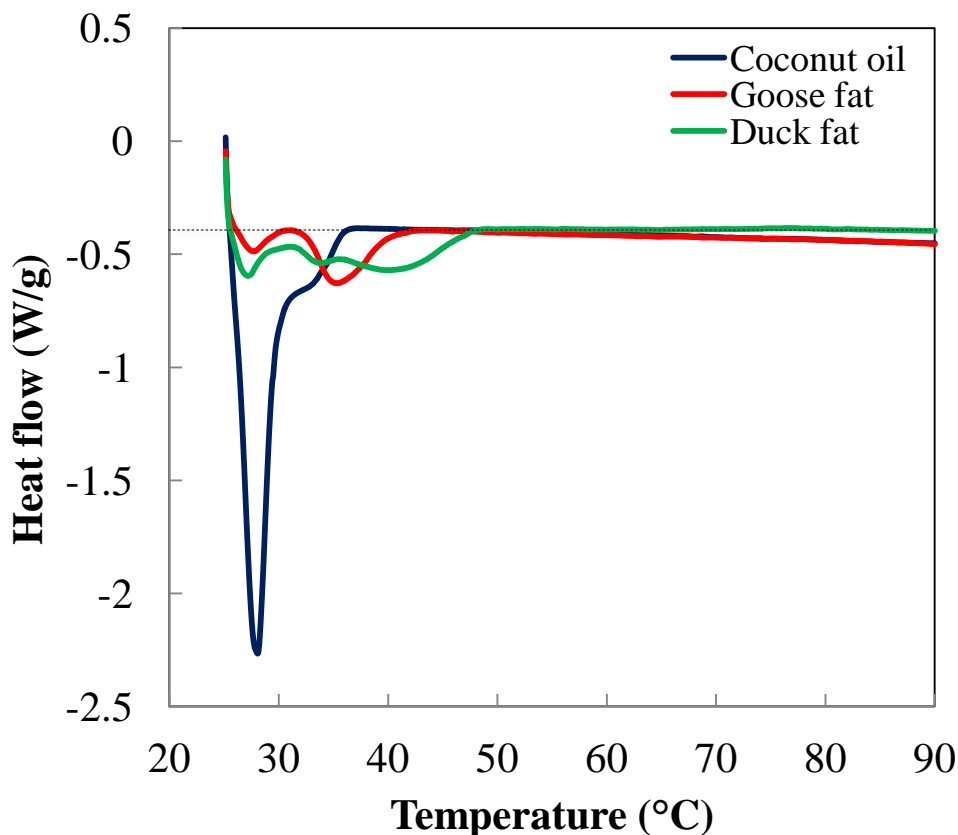


**Figure 53.** Melting point of coconut oil, goose fat and duck fat

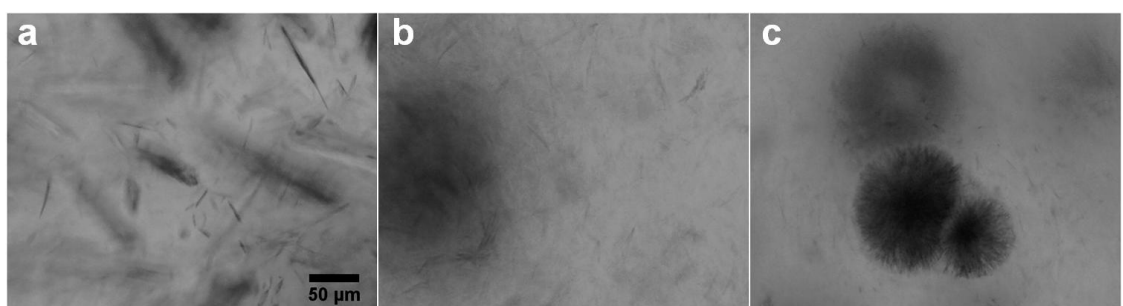


**Figure 54.** Pure fats: solid fraction dispersion in liquid fraction: a) coconut oil, b) goose fat and c) duck fat.

### 6.3.2. Crystal structure

The typical form of fat crystals in coconut oil, goose fat and duck fat is shown in **Figure 54**. All three fats form thin elongated structures which are mostly dispersed. Coconut oil tends to have larger crystals, on the order of 50  $\mu\text{m}$  long crystals. Usually, the size of the crystals depends on the size of droplets where they grow. Goose fat also has needle

crystals but much smaller than crystals present in coconut oil. Duck fat has clusters of crystals called spherulites. The maximum length of crystals dispersed individually in goose fat was between 8-20  $\mu\text{m}$ . Duck fat forms clusters 50 to 125  $\mu\text{m}$  in size.

### 6.3.3. Crystals' distribution or location: Internal vs External

Complex food emulsion droplets can have vastly different wetting properties of the crystals they contain because of natural surface active compounds present like monoglycerides. Unlike our previous work (Dahiya et al., 2016a) that formed smooth liquid surfaces in droplets containing crystals, **Figure 55** shows that coconut oil droplets have uneven surfaces, which means that these individual crystals are long enough to protrude through the interface from inside of the droplet or they tend to move or grow towards interface because of their wetting properties (Spicer and Hartel, 2005). In extreme cases shown ejection and growth of crystals beyond the droplets' interface can occur because of adsorption of surfactant. Goose and duck fat droplets have comparatively smooth surfaces. They both have crystals in the form of spherulites when dispersed in MFC that seem to be either just inside the interface or sitting at the interface of droplets. For instance, the duck fat droplet (**Figure 55c**) shows dewetting of crystals, which may even cause some crystals to cross the droplet oil-water interface. The distribution of the fat crystals strongly influences the ultimate shape of the droplet, and it is expected to strongly influence coalescence and arrest.

**Figure 55** also indicates that the crystal distribution varies with each fat. Coconut oil (**Figure 55a**) shows higher concentrations of needle like crystals at the bottom left of the droplet or even dewetting or outgrowth of crystals. Goose fat (**Figure 55b**) shows concentrated groups of spherulites at the top of droplet, causing less light transmission in those dense regions. Duck fat (**Figure 55c**) shows even distribution of clusters of crystals, which are separated by fairly regular distances between them. The distribution of crystals varies with individual droplets, even in the same fat sample, for all three types studied here. Three sets of droplets are presented in **Figure 56** to show the effect of solids concentration on crystals distribution in droplets of coconut oil, goose fat and duck fat, respectively. The distribution of crystals is one of the key factors that affects the coalescence of the droplets, as this affects whether free liquid contacts another, determining whether coalescence and arrest can occur.

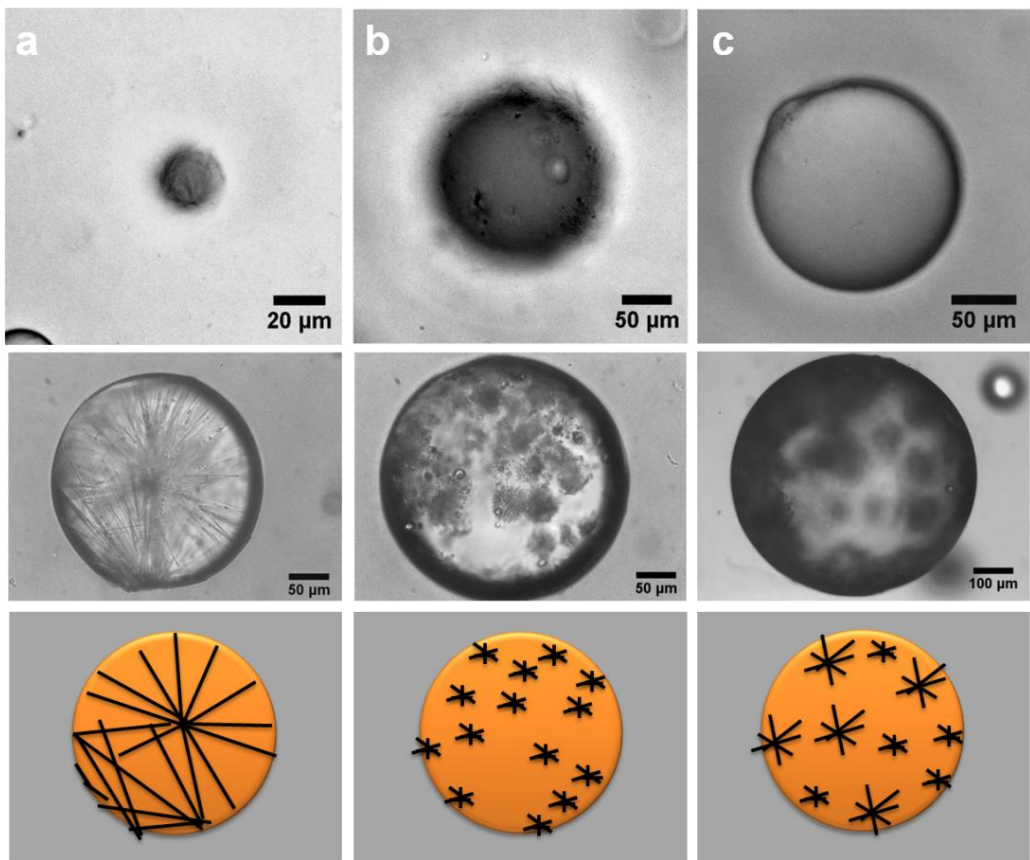


**Figure 55.** Microscopic images and schematic diagrams showing crystals' distribution in a) coconut oil, b) goose fat and c) duck fat droplet, having 20% solids concentration, stored at room temperature for 3 days.

#### 6.3.4. Structure of droplets: dense or hollow

As discussed above, coconut oil crystals are long and needle-like, and being stuck to the interface of droplet from inside the droplets, they provide a narrow opening (almost half the size of capillary) for the oil to be sucked by the capillary. **Figure 57** shows a sequence of images showing removal of oil by suction to see what crystal structure remains. Interestingly, the amount of fluid that can be withdrawn varies significantly within the different fats and is quite distinct from previous results for petrolatum emulsions. The size of the liquid neck pulled out of the droplet is 52 μm (almost half the size of capillary), which indicates that the neck width is determined by the spacing between the network of crystals present just inside the droplet interface. It is also important to note here that the crystals do not move from their position, rather they still retain their structure (as they are too long to reposition again in the droplet) and simply

consolidate when most fluid is removed. However, some smaller crystals reposition themselves as the compression of the network occurs because of suction of oil.

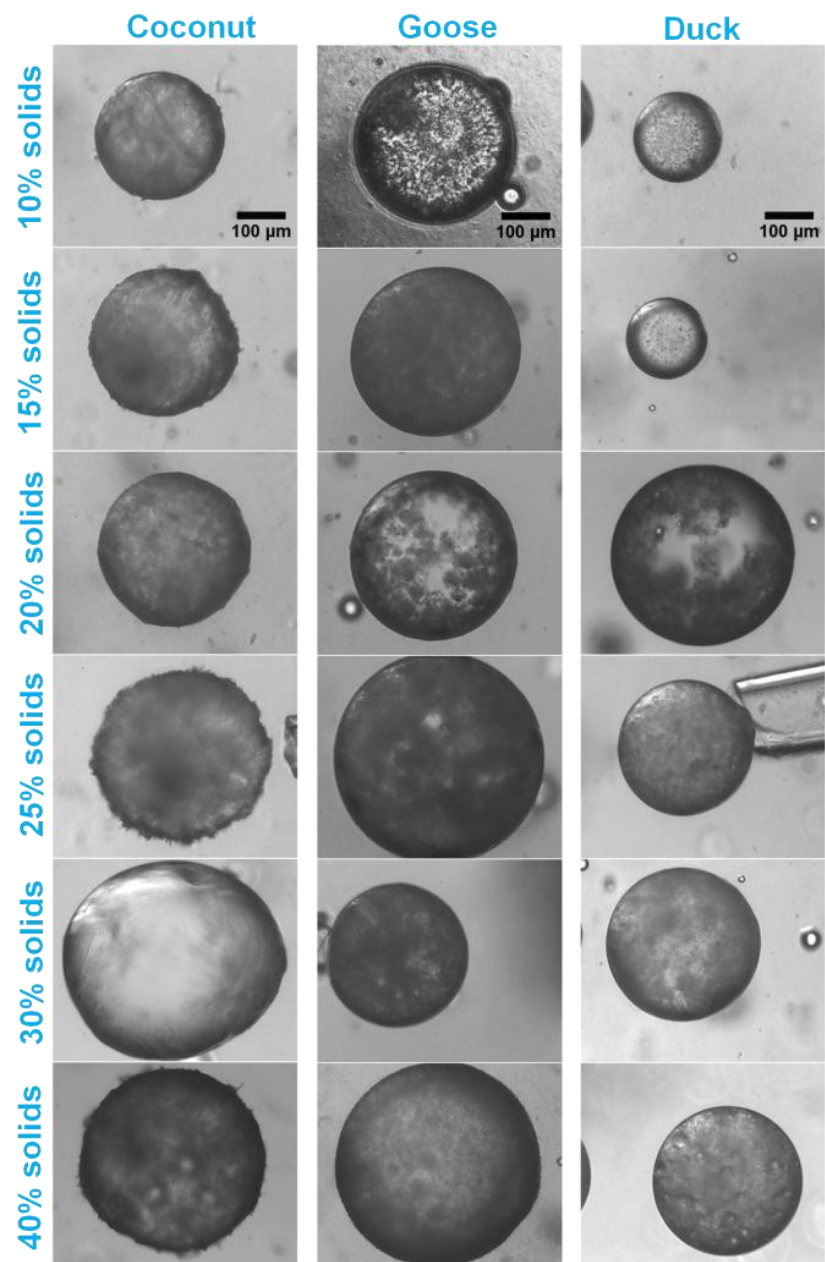


**Figure 56.** Microscopic images showing droplets of coconut oil, goose fat and duck fat, having different solids concentration, stored at room temperature for at least 3 days.

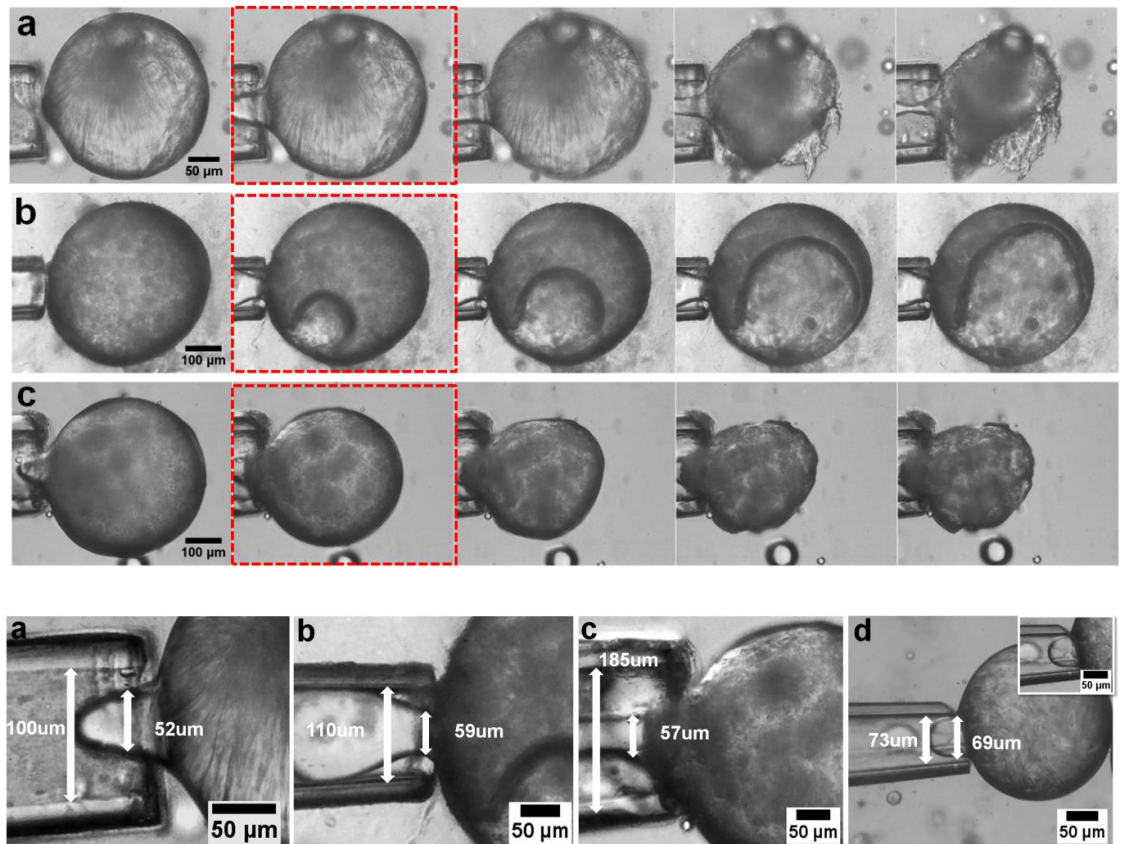


**Figure 57.** Deformation of droplets and the internal crystal network (having 20% solids concentration) during suction of oil: a) coconut oil, b) goose fat and c) duck fat d) vaseline-hexadecane; and size of neck width formed by suction of oil with the help of a pulled capillary.

Goose fat shows a very distinct behaviour. The spherulites tend to move as the oil is sucked out of the droplet, which likely means that the crystals are completely wetted by the liquid oil and they are inside the droplet. As the suction progresses, the droplet structure collapses, indicating a hollow structure. Again here the neck width is almost 54% the size of capillary, which means that even if the crystals are stuck to the interface from the inside, there is a gap between them that determines the volume and rate of fluid flow, which can affect coalescence. Duck fat crystals seem to be at the interface from inside the droplet, because, like coconut oil, the liquid neck width during the oil suction is very narrow. All the above mentioned fats show very different results from previously-studied petrolatum droplets. **Figure 57** shows that the neck of a petrolatum droplet depends only on the size of the capillary rather than on the size or spacing of the crystals.

**Figure 58** shows the direct relation between droplet neck formation during coalescence. The width of the neck formed is similar in each case, which means that there is some resistance to fluid flow through a narrow opening. We assume, it is because of the length of the crystals and their location in the droplets.

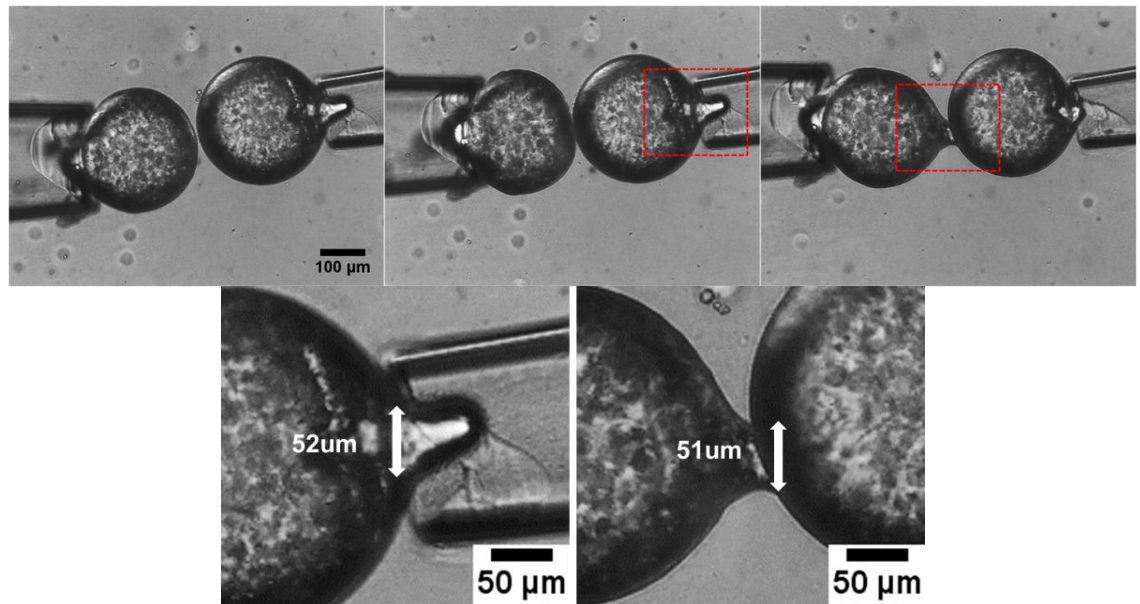


**Figure 58.** Microscopic images showing interparticle spacing between crystals in goose fat.

A narrow neck is weaker than a broader neck because of reduced contact area and stress transmission, increasing the likelihood droplets can move even when arrested. The volume of the fluid available determines the deformation and coalescence in a system but also predicts the final shape of the arrested structure (Dahiya et al., 2016b) as it can affect restructuring or relocation in a network.

### 6.3.5. Wettability of crystals

The wettability of crystals is important to the adhesion properties of edible oil and can influence the behaviour of crystals within a droplet and stabilization of an emulsion (Garti, 2002). Here we compare the affinity of the liquid phase of the fat with its own solid phase by contacting a droplet with a certain solids level with a droplet of oil containing no solid phase. **Figure 59a** shows the three phase, solid/water/oil, contact angle at the oil-water interface for the different droplets. Coconut oil crystals are not significantly wetted by the oil and in some cases have asymmetry, and show two contact angles with the same liquid droplet (image on the very right hand side of **Figure 59a**).

In goose and duck fat, the droplets show complete wettability of the crystals by the liquid oil and hence results in complete coalescence (**Figure 59b** and **59c**). It is also important to note here that the solids concentration has a strong impact on the behaviour of droplets or crystals. For instance, **Figure 59** also shows that the droplets of coconut oil and goose fat with 40% solids have almost the same contact angle as the droplets having 20% solids level.

The droplets of duck fat with 40% solids have a very different wetting state than the lower solids levels, likely because the crystal network has greater cohesion at higher levels but also if surface-active components are present at a higher concentration. Because natural oils contain significant levels of surface active materials like monoglycerides, it is likely that their adsorption causes the complex wetting behaviour we observe. As stated in the thesis, known mixtures of solid and liquid components by physical centrifugal separation of the initial mixtures is prepared. The exact amount of solids present, however, is not known as kinetic effects may reduce the efficiency of crystallization when we form droplets.

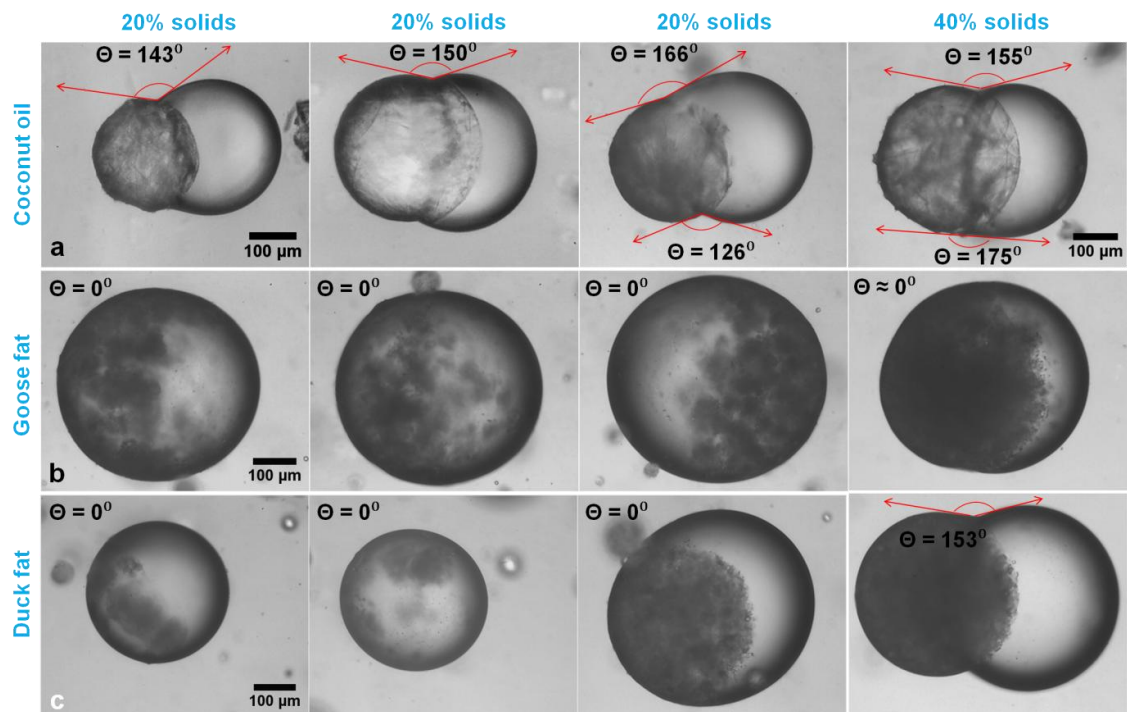


**Figure 59.** Wettability of a) coconut oil, b) goose fat and, c) duck fat crystals: contact angle at oil-water interface when a dispersed droplet (having liquid and solid fraction, left side) is touched to a liquid oil (having liquid fraction only, right side) droplet, having 20% solids concentration, stored for at least 3 days.

### 6.3.6. Heterogeneity in edible fats: distribution of fat crystals

**Figure 60** shows various spatial distributions of crystals in coconut oil droplets, which will also affect coalescence. For instance, in the first and last image, the crystals are long, separated from each other, and spaced a reasonable distance apart, which means fluid will be available to initiate coalescence and stabilize arrest when two droplets are contacted by micromanipulation technique. However, there are some cases where droplets like the second image of **Figure 61**, that have crystals in their upper left region and none in the bottom right. **Figure 61** shows a schematic representation of how such structures could drastically alter coalescence depending on orientation of the droplets when they contact one another.

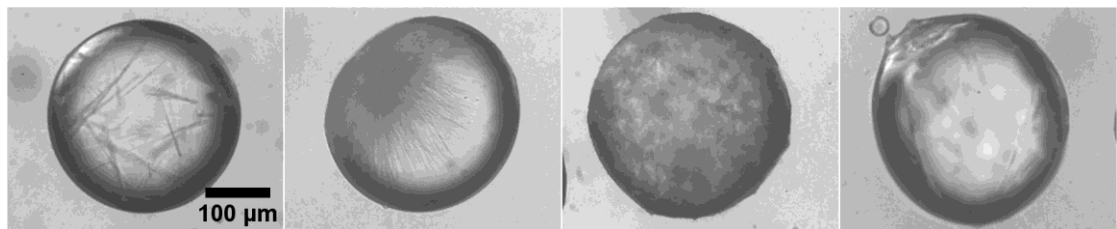


**Figure 60.** Microscopic images showing different distribution of fat crystals in coconut oil (20% solids, prepared and stored at room temperature for 3 days).

Another distinction from petrolatum emulsions (Pawar et al., 2012, Dahiya et al., 2016a), as seen in **Figure 62** for goose fat, is that some droplets require higher pressure to begin their coalescence, which may result from the crystal network behaving as a capsule structure (Berry et al., 2017) which can restrict the droplets from beginning coalescence. Such effects can cause variations in the resulting strain of doublets or can require destruction of the internal network to allow coalescence. **Figure 63** shows heterogeneous structures form as a result of such strong networks, creating different strain values for different doublets. Similar results can be observed in goose fat (**Figure 64**) and duck fat (**Figure 65**). These figures show different strain values for identical solids levels. There is thus a broader distribution of crystals at which the droplets will either coalesce totally or be unable to do so.

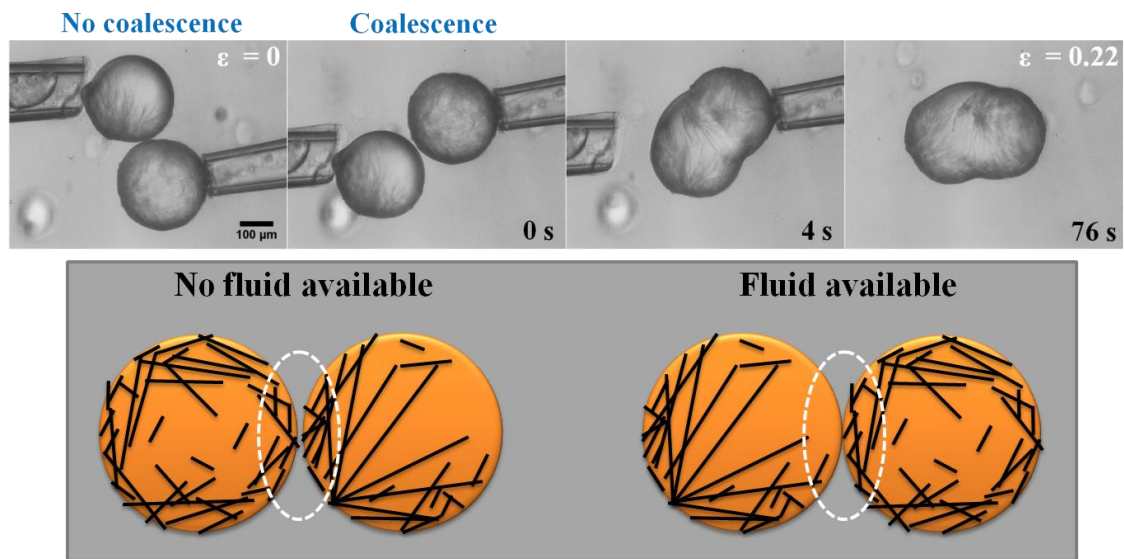


**Figure 61.** Microscopic images and schematic diagram showing effect of availability of liquid oil during coalescence in coconut oil (15% solids)

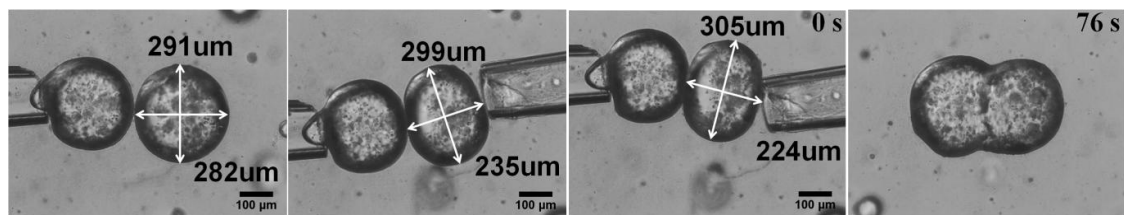


**Figure 62.** Microscopic images showing higher pressure required for breaking the drops' interface to begin coalescence in goose fat (20% solids)

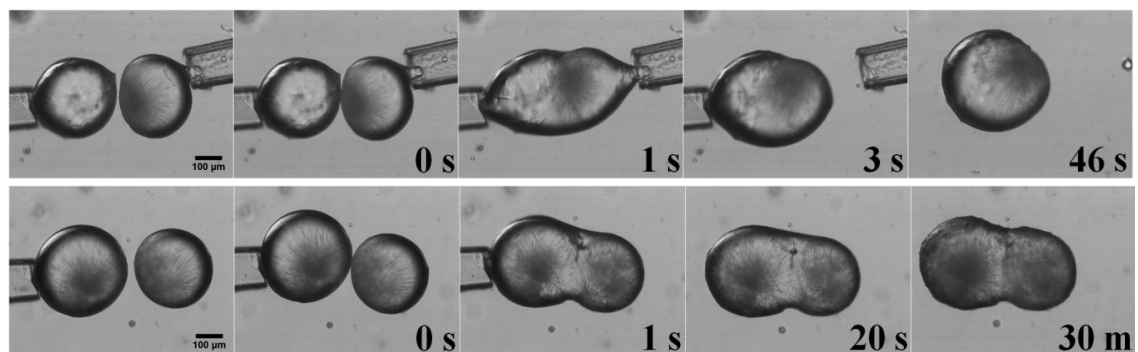


**Figure 63.** Effect of location of crystals on arrested coalescence of coconut oil droplets (20% solids): large and small deformation, respectively.

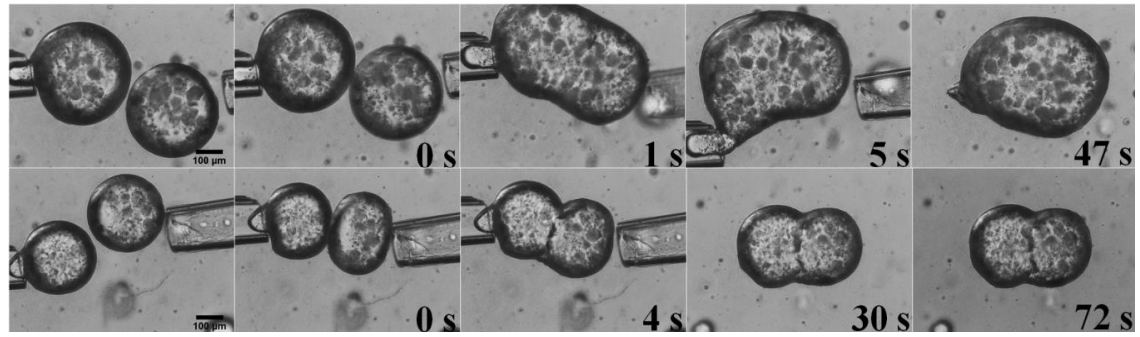


**Figure 64.** Effect of location of crystals on arrested coalescence of goose fat droplets (20% solids): large and small deformation, respectively.

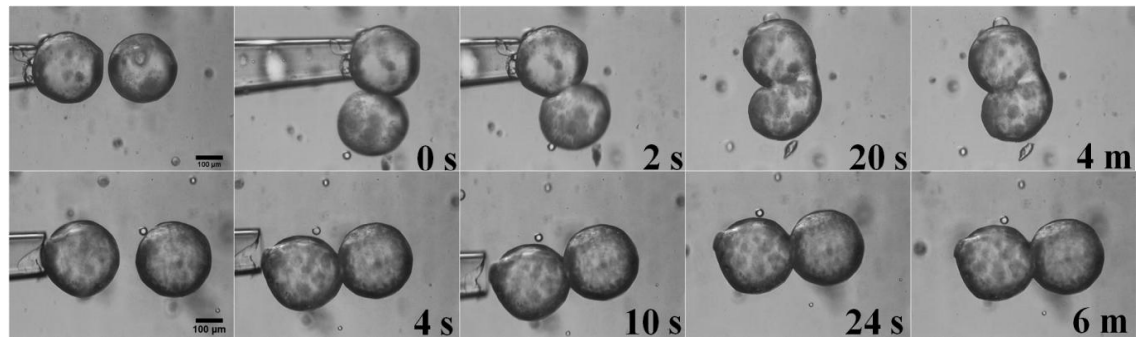


**Figure 65.** Effect of location of crystals on arrested coalescence of duck fat droplets (20% solids): large and small deformation, respectively.

### 6.3.7. Deformation of droplets as a result of coalescence

**Figure 66** illustrates strain for numerous doublets, having different solids levels, of coconut oil. Contrasting with petrolatum results, we see a much more rapid drop in strain for coconut oil that is likely the result of a more cohesive network of crystals. We also observe a much higher variability of the final strain values as a result of the heterogeneous distribution of crystals.

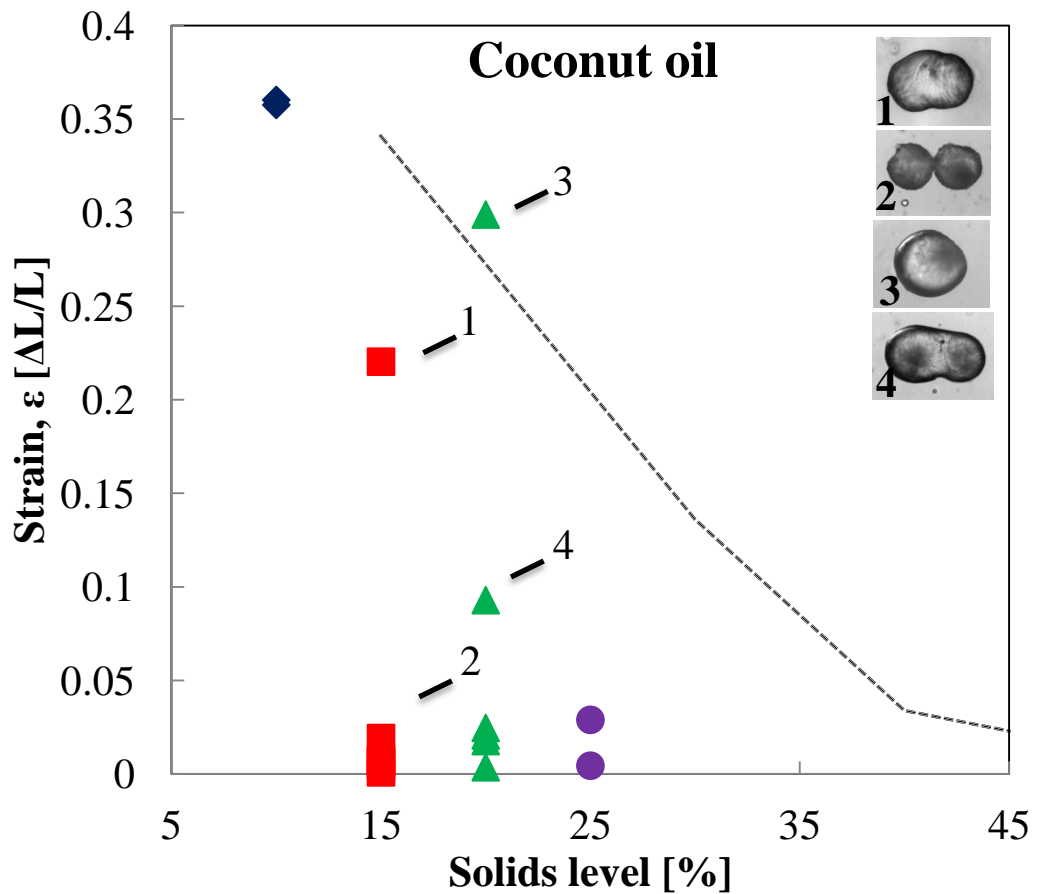


**Figure 66.** Strain of various doublet shapes obtained by coalescence of two droplets in coconut oil (Dotted line represents maximum strain in Vaseline droplets for different solids level).

Similarly, **Figure 67** shows that the strain is inversely proportional to the solid fat content of the droplets in goose fat. Even though the data shows a similar trend to previous studies (Pawar et al., 2012), the values are quite distinct. The current experimental strain (maximum) for 15% solids is around 0.35 whereas earlier it was 0.31, and for 40% solids, the current data shows a maximum strain as high as 0.28 whereas earlier it was 0.04. This variation in the strain of the same solids level doublets is because of heterogeneous crystal structures within droplets.

**Figure 68** shows variation in strain for different solids levels in duck fat. It shows the same trend as observed in previous research (Pawar et al., 2012), but with minor variations occurring in the strain values. And that too is because of complexity of these fat systems, which has different crystallization versus the earlier petrolatum model system. The doublets having 20% and 40% solids have almost same values as shown by earlier work (Pawar et al., 2012, Dahiya et al., 2016a).

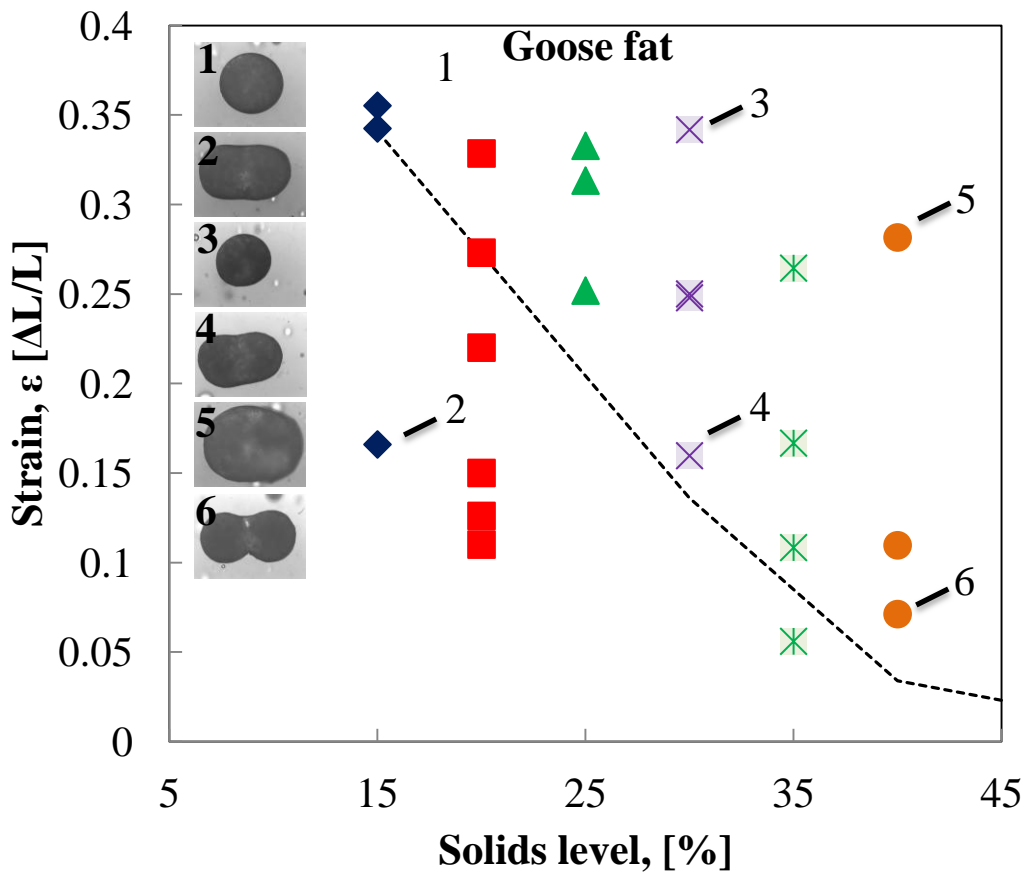


**Figure 67.** Strain of various doublets shapes obtained from coalescence of two droplets in goose fat (Dotted line represents maximum strain in Vaseline droplets for different solids level).

#### 6.4. Conclusion

The effects of different fat crystal partitioning states on arrested coalescence has been investigated for coconut oil, goose fat, and duck fat, for droplets containing 15 - 40% solid fat content (SFC). The results indicate that the deformation, or strain, of the droplets, as a result of arrested coalescence can strongly vary depending on the location and distribution of crystals in an emulsion droplet. Arrested coalescence starts by formation of a liquid oil bridge between droplets but the positioning of fat crystals can lead to significant variations in initiation and stability of subsequent coalescence and its arrest. Arrested coalescence by edible fats is found to follow trends established earlier for model petrochemical emulsions: higher solids content results in earlier arrest so that droplets form less compact shapes. However, edible systems exhibit much greater variability during arrest within an emulsion with otherwise identical conditions.

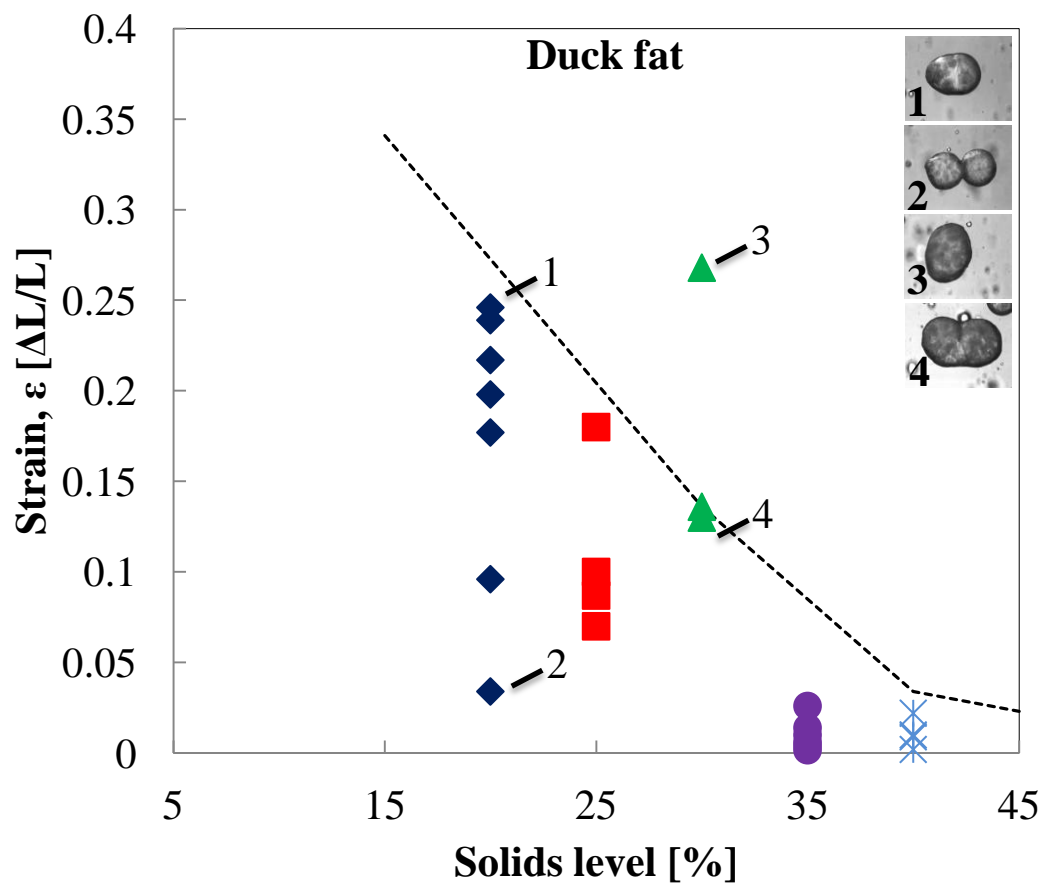


**Figure 68.** Strain of various doublets shapes obtained from coalescence of two droplets in duck fat (Dotted line represents maximum strain in Vaseline droplets for different solids level).

## **CHAPTER 7 Conclusions & Recommendations**

This study was carried out to broaden the knowledge of dynamic arrest of coalescing viscoelastic droplets by exploring varying droplet size and multiple connections, as in a real emulsion, which have not been studied before. Furthermore, this study also examined arrested coalescence behaviour in edible systems to reconcile with past work on model, petroleum-based emulsions. The following section summarize some key conclusions along with recommendations for future research.

Arrested coalescence in emulsions is a complex field, which has a range of relevant variables. The effects of different size of droplets on deformation of droplets was investigated. Arrested doublets made with identical droplets having smaller radii had higher strain as compared to doublets made with identical droplets having larger radii, because of increased interfacial curvature. The polydispersity in a system can also significantly influence the strain in droplets. The doublet formed by two non-identical droplets had lower strains than doublets formed by monodisperse droplets because of less neck surface area.

The project then focused on investigating the stability of aggregates formed by three droplets. Different approach angles were used to study the effect of orientation of third droplet in a system on any meniscus-induced change in the position of droplets. The droplets in triplet shapes were stable when the elasticity dominated the interfacial forces, which preserves the initial arrested shape. However, when interfacial forces dominated the elasticity, the droplets repositioned in the network and moved to a minimal energy state, which resulted into a more compact shape. This restructuring occurred when the two necks in a structure met as a result of overlapping of liquid menisci. The restructuring was not seen in shapes having higher approach angles because the volume of liquid available was not sufficient to overlap.

In the next phase of the project, bulk emulsions were investigated to observe the similarities or differences in the microstructures when compared with doublets and triplets. Larger numbers of droplets and flow were also studied in flowing systems to better represent real emulsions. The strain in the flowing systems' microstructure was higher than for more static systems, but was more variable throughout the structure. Restructuring is quite relevant and becomes more significant when droplets move in a

shear field. As seen before for doublets, droplets having higher solids levels formed less deformed and porous networks. Droplets having lower solids levels formed highly deformed, and more compact structure.

Finally, the later phase of this work probes the microstructure formed in edible emulsions: coconut oil, goose fat and duck fat. Heterogeneity of the edible fats made the arrested phenomena more complex. Where coconut oil formed long, elongated crystals near the oil-water interface; goose fat and duck fat formed spherulites inside and near the droplet surface. The resulting strain in doublets for these three fats seemed to be dependent on the location of crystals in the droplets, which is very different than petrolatum (investigated in earlier parts of this work) which had crystals more uniformly distributed and mobile within the droplets, and was fully wetted by hexadecane. This study also found that the force required to begin coalescence varied for edible system because of the complex structural nature of droplets.

With regards to future research in this area, considerable recommendations can be made. Strain in microstructure is both governed by size and number of droplets. The effect of size of droplets was explained in model systems. More work is needed to quantify the effects of droplets sizes in more edible emulsions. Also, the doublets formed under this study were formed without direct measurement of the pressures initiating coalescence. Future work could therefore evaluate the force needed to begin the coalescence of droplets both in model and edible systems. In this research, structure compactness has been shown to be associated with restructuring, and a more complete model is needed to predict the ultimate structure formation if restructuring happens in a network.

This work has also developed new ways to study arrested emulsion formation in bulk emulsions through controlled removal of continuous phase yield stresses allow controlled droplets flow and coalescence, but larger structures must also be studied to give broader microstructure. Since the mechanisms studied affect the rheological properties of the emulsion, perhaps another study could be conducted on measuring the elasticity of individual droplets and multidroplets formed by both mono- and polydisperse droplets. The future work could also focus on forming 2D multidroplet networks by, for example, incorporating some external energies field like vibration. Finally, the research has shown heterogeneity in edible fats to be a strong factor in

producing distinct results as compared to model systems. However, these investigations in this area are still in the preliminary stage. Much greater research effort is required in order to fully resolve and reclaim the understanding in this area.

## REFERENCES

- ABISMAIL, B., CANSELIER, J. P., WILHELM, A. M., DELMAS, H. & GOURDON, C. 1999. Emulsification by ultrasound: drop size distribution and stability. *Ultrasonics Sonochemistry*, 6, 75-83.
- AHN, K., AGRESTI, J., CHONG, H., MARQUEZ, M. & WEITZ, D. 2006. Electrocoalescence of drops synchronized by size-dependent flow in microfluidic channels. *Applied Physics Letters*, 88, 264105.
- ARKUS, N., MANOHARAN, V. N. & BRENNER, M. P. 2009. Minimal energy clusters of hard spheres with short range attractions. *Physical review letters*, 103, 118303.
- AVEYARD, R., BINKS, B. P. & CLINT, J. H. 2003. Emulsions stabilised solely by colloidal particles. *Advances in Colloid and Interface Science*, 100, 503-546.
- AWAD, T. S. & SATO, K. 2002. Fat Crystallization in O/W Emulsions Controlled by Hydrophobic Emulsifier Additives. *Physical properties of lipids*, 37.
- BARNES, H. A. 1994. Rheology of emulsions—a review. *Colloids and Surfaces A: Physicochemical and Engineering Aspects*, 91, 89-95.
- BARNES, H. A., HUTTON, J. F. & WALTERS, K. 1989. *An Introduction to Rheology*, Elsevier.
- BELL, A., GORDON, M., JIRASUBKUNAKORN, W. & SMITH, K. 2007. Effects of composition on fat rheology and crystallisation. *Food Chemistry*, 101, 799-805.
- BENSON, B. R., STONE, H. A. & PRUD'HOMME, R. K. 2013. An “off-the-shelf” capillary microfluidic device that enables tuning of the droplet breakup regime at constant flow rates. *Lab on a Chip*, 13, 4507-4511.
- BERRY, J. D., METTU, S. & DAGASTINE, R. R. 2017. Precise measurements of capsule mechanical properties using indentation. *Soft Matter*, 13, 1943-1947.
- BIBETTE, J., MASON, T., GANG, H., WEITZ, D. & POULIN, P. 1993. Structure of adhesive emulsions. *Langmuir*, 9, 3352-3356.
- BINKS, B. P., CLINT, J., MACKENZIE, G., SIMCOCK, C. & WHITBY, C. 2005. Naturally occurring spore particles at planar fluid interfaces and in emulsions. *Langmuir*, 21, 8161-8167.
- BINKS, B. P., RODRIGUES, J. A. & FRITH, W. J. 2007. Synergistic interaction in emulsions stabilized by a mixture of silica nanoparticles and cationic surfactant. *Langmuir*, 23, 3626-3636.

- BIRD, J. C., RISTENPART, W. D., BELMONTE, A. & STONE, H. A. 2009. Critical angle for electrically driven coalescence of two conical droplets. *Physical review letters*, 103, 164502.
- BLAKE, A. I. & MARANGONI, A. G. 2014. Structure and physical properties of plant wax crystal networks and their relationship to oil binding capacity. *Journal of the American Oil Chemists' Society*, 91, 885-903.
- BOODE, K., BISPERINK, C. & WALSTRA, P. 1991. Destabilization of O/W emulsions containing fat crystals by temperature cycling. *Colloids and Surfaces*, 61, 55-74.
- BOODE, K. & WALSTRA, P. 1993. Partial coalescence in oil-in-water emulsions 1. Nature of the aggregation. *Colloids and Surfaces A: Physicochemical and Engineering Aspects*, 81, 121-137.
- BOODE, K., WALSTRA, P. & DE GROOT-MOSTERT, A. 1993. Partial coalescence in oil-in-water emulsions 2. Influence of the properties of the fat. *Colloids and Surfaces A: Physicochemical and Engineering Aspects*, 81, 139-151.
- BORÓWKO, M. 2000. *Computational methods in surface and colloid science*, CRC Press.
- BORWANKAR, R. P., LOBO, L. A. & WASAN, D. T. 1992. Emulsion stability—kinetics of flocculation and coalescence. *Colloids and surfaces*, 69, 135-146.
- BRADY, J. E. & SENESE, F. 2008. *Chemistry, Student Study Guide: The Study of Matter and Its Changes*, John Wiley & Sons.
- BRAKKE, K. A. 1992. The surface evolver. *Experimental mathematics*, 1, 141-165.
- BRAZIER-SMITH, P., JENNINGS, S. & LATHAM, J. An investigation of the behaviour of drops and drop-pairs subjected to strong electrical forces. *Proceedings of the Royal Society of London A: Mathematical, Physical and Engineering Sciences*, 1971. The Royal Society, 363-376.
- BROOKER, B. 1993. The stabilisation of air in cake batters—the role of fat. *Food Structure*, 12, 2.
- BROOKER, B. 1996. The role of fat in the stabilisation of gas cells in bread dough. *Journal of Cereal Science*, 24, 187-198.
- BUSHELL, G. 2011. *Primary particle polydispersity in fractal aggregates*, University of New South Wales Library.

- BUTTERY, R. G., GUADAGNI, D. G. & LING, L. C. 1973. Flavor compounds. Volatilities in vegetable oil and oil-water mixtures. Estimation of odor thresholds. *Journal of Agricultural and Food Chemistry*, 21, 198-201.
- CAGGIONI, M., BAYLES, A. V., LENIS, J., FURST, E. M. & SPICER, P. T. 2014. Interfacial stability and shape change of anisotropic endoskeleton droplets. *Soft Matter*, 10, 7647-7652.
- CAGGIONI, M., LENIS, J., BAYLES, A. V., FURST, E. M. & SPICER, P. T. 2015. Temperature-induced collapse, and arrested collapse, of anisotropic endoskeleton droplets. *Langmuir*, 31, 8558-8565.
- CAMPBELL, E., BAKER, N., BANDURRAGA, M., BELCHER, M., HECKEL, C., HODGSON, A., HUGHES, J., INGALA, T., LAMPERT, D., LOUIS, E., MACCASKILL, D., MCNEILL, G., NUGENT, M., PALADINI, E., PRICE, J., REDDY, R., SHARP, J., SMITH, S., STRAYER, D., WAINWRIGHT, B. & WALDINGER, L. 2006. Food Fats and Oils. *Institute of Shortenings and Edible Oils*, Eighth Edition.
- CHANAMAI, R. & MCCLEMENTS, D. J. 2000. Dependence of creaming and rheology of monodisperse oil-in-water emulsions on droplet size and concentration. *Colloids and Surfaces A: Physicochemical and Engineering Aspects*, 172, 79-86.
- CHANG, C., BOGER, D. V. & NGUYEN, Q. D. 1998. The yielding of waxy crude oils. *Industrial & engineering chemistry research*, 37, 1551-1559.
- CHEN, G., TAN, P., CHEN, S., HUANG, J., WEN, W. & XU, L. 2013. Coalescence of pickering emulsion droplets induced by an electric field. *Physical review letters*, 110, 064502.
- CHOW, G. & GONSALVES, K. 1996. Particle synthesis by chemical routes. *Nanomaterials: Synthesis, Properties and Applications*, 55.
- CLARK, M. M. & FLORA, J. R. 1991. Floc restructuring in varied turbulent mixing. *Journal of Colloid and Interface Science*, 147, 407-421.
- COLLINS, R. T., JONES, J. J., HARRIS, M. T. & BASARAN, O. A. 2008. Electrohydrodynamic tip streaming and emission of charged drops from liquid cones. *Nature Physics*, 4, 149-154.
- COSGROVE, T. 2010. *Colloid science: principles, methods and applications*, John Wiley & Sons.

- COUPLAND, J. N. & MCCLEMENTS, D. J. 2001. Droplet size determination in food emulsions: comparison of ultrasonic and light scattering methods. *Journal of Food Engineering*, 50, 117-120.
- COURTHAUDON, J.-L., DICKINSON, E. & DALGLEISH, D. G. 1991. Competitive adsorption of  $\beta$ -casein and nonionic surfactants in oil-in-water emulsions. *Journal of colloid and interface science*, 145, 390-395.
- CRAMP, G. L., DOCKING, A. M., GHOSH, S. & COUPLAND, J. N. 2004. On the stability of oil-in-water emulsions to freezing. *Food Hydrocolloids*, 18, 899-905.
- DAHIYA, P., CAGGIONI, M. & SPICER, P. T. 2016a. Arrested coalescence of viscoelastic droplets: polydisperse doublets. *Phil. Trans. R. Soc. A*, 374, 20150132.
- DAHIYA, P., DEBENEDICTIS, A., ATHERTON, T. J., CAGGIONI, M., PRESCOTT, S. W., HARTEL, R. W. & SPICER, P. T. 2016b. Arrested coalescence of viscoelastic droplets: Triplet shape and restructuring. *arXiv preprint arXiv:1612.06497*.
- DAHMS, G. H. & ZOMBECK, A. 1995. New formulation possibilities offered by silicone copolyols. *Cosmetics and Toiletries-Carol Stream*, 110, 91-101.
- DARLING, D. F. 1982. Recent advances in the destabilization of dairy emulsions. *Journal of Dairy Research*, 49, 695-712.
- DEMAN, J. & BEERS, A. 1987. Fat crystal networks: structure and rheological properties. *Journal of Texture Studies*, 18, 303-318.
- DERJAGUIN, B. & CHURAEV, N. 1989. The current state of the theory of long-range surface forces. *Colloids and surfaces*, 41, 223-237.
- DERJAGUIN, B. V. 1987. Some results from 50 years' research on surface forces. *Surface Forces and Surfactant Systems*, 17-30.
- DICKINSON, E. 1992. *Introduction to food colloids*, Oxford University Press.
- DICKINSON, E. 2009. Hydrocolloids as emulsifiers and emulsion stabilizers. *Food Hydrocolloids*, 23, 1473-1482.
- DICKINSON, E. 2010. Flocculation of protein-stabilized oil-in-water emulsions. *Colloids and Surfaces B: Biointerfaces*, 81, 130-140.
- DICKINSON, E. 2012. Use of nanoparticles and microparticles in the formation and stabilization of food emulsions. *Trends in Food Science & Technology*, 24, 4-12.

- DICKINSON, E. & GOLDING, M. 1998. Influence of calcium ions on creaming and rheology of emulsions containing sodium caseinate. *Colloids and Surfaces A: Physicochemical and Engineering Aspects*, 144, 167-177.
- DICKINSON, E., GOLDING, M. & POVEY, M. J. 1997. Creaming and flocculation of oil-in-water emulsions containing sodium caseinate. *Journal of Colloid and Interface Science*, 185, 515-529.
- DICKINSON, E. & MCCLEMENTS, D. J. 1995. *Advances In Food Colloids*, Springer.
- DICKINSON, E., RITZOULIS, C. & POVEY, M. J. 1999. Stability of emulsions containing both sodium caseinate and Tween 20. *Journal of Colloid and Interface Science*, 212, 466-473.
- DICKINSON, E. & STAINSBY, G. 1982. *Colloids in food*, Applied Science Publishers.
- DICKINSON, E. & STAINSBY, G. 1988. *Advances in food emulsions and foams*, Elsevier Applied Science Publishers Ltd.
- DINSMORE, A., HSU, M. F., NIKOLAIDES, M., MARQUEZ, M., BAUSCH, A. & WEITZ, D. 2002. Colloidosomes: selectively permeable capsules composed of colloidal particles. *Science*, 298, 1006-1009.
- DRELON, N., GRAVIER, E., DAHERON, L., BOISSERIE, L., OMARI, A. & LEAL-CALDERON, F. 2006. Influence of tempering on the mechanical properties of whipped dairy creams. *International dairy journal*, 16, 1454-1463.
- EASTOE, J. & COSGROVE, T. 2005. Colloid Science, principles methods and applications. Blackwell publishing: Cambridge, MA.
- ECCLESTON, G. 1997. Functions of mixed emulsifiers and emulsifying waxes in dermatological lotions and creams. *Colloids and Surfaces A: Physicochemical and Engineering Aspects*, 123, 169-182.
- EDELSTEIN, A. S. & CAMMARATRA, R. 1998. *Nanomaterials: synthesis, properties and applications*, CRC Press.
- EGGERSDORFER, M., KADAU, D., HERRMANN, H. J. & PRATSINIS, S. E. 2010. Fragmentation and restructuring of soft-agglomerates under shear. *Journal of colloid and interface science*, 342, 261-268.
- EGGERSDORFER, M. L., KADAU, D., HERRMANN, H. J. & PRATSINIS, S. E. 2011. Multiparticle sintering dynamics: from fractal-like aggregates to compact structures. *Langmuir: the ACS journal of surfaces and colloids*, 27, 6358.

- EGGERSDORFER, M. L., KADAU, D., HERRMANN, H. J. & PRATSINIS, S. E. 2012. Aggregate morphology evolution by sintering: number and diameter of primary particles. *Journal of aerosol science*, 46, 7-19.
- EGGERSDORFER, M. L. & PRATSINIS, S. E. 2013. Restructuring of aggregates and their primary particle size distribution during sintering. *AICHE Journal*, 59, 1118-1126.
- ELIMELECH, M., GREGORY, J., JIA, X. & WILLIAMS, R. 1997. Particle deposition and aggregation, measurement, modeling and simulation. *Colloids and Surfaces A: Physicochemical and Engineering Aspects*, 1, 93-94.
- EOW, J. S. & GHADIRI, M. 2002. Electrostatic enhancement of coalescence of water droplets in oil: a review of the technology. *Chemical Engineering Journal*, 85, 357-368.
- EOW, J. S., GHADIRI, M., SHARIF, A. O. & WILLIAMS, T. J. 2001. Electrostatic enhancement of coalescence of water droplets in oil: a review of the current understanding. *Chemical engineering journal*, 84, 173-192.
- FAN, H. & STRIOLO, A. 2012. Mechanistic study of droplets coalescence in Pickering emulsions. *Soft Matter*, 8, 9533-9538.
- FANG, H., ZHANG, L., LUO, L., ZHAO, S., AN, J., XU, Z., YU, J., OTTOVA, A. & TIEN, H. T. 2001. A study of thin liquid films as related to the stability of crude oil emulsions. *Journal of colloid and interface science*, 238, 177-182.
- FENNEMA, O. R., DAMODARAN, S. & PARKIN, K. L. 2008. *Fennema's food chemistry*, CRC.
- FISHER, S. M. 1998. *A mathematical model for aggregation in colloidal systems*.
- FORREST, S. & WITTEN JR, T. 1979. Long-range correlations in smoke-particle aggregates. *Journal of Physics A: Mathematical and General*, 12, L109.
- FREDRICK, E., WALSTRA, P. & DEWETTINCK, K. 2010. Factors governing partial coalescence in oil-in-water emulsions. *Advances in Colloid and Interface Science*, 153, 30-42.
- FRIBERG, S., LARSSON, K. & SJOBLOM, J. 2003. *Food Emulsions*, CRC Press.
- FROSTAD, J. M., COLLINS, M. C. & LEAL, L. G. 2014. Direct measurement of the interaction of model food emulsion droplets adhering by arrested coalescence. *Colloids and Surfaces A: Physicochemical and Engineering Aspects*, 441, 459-465.

- GARTI, N. 2002. Food Emulsifiers: Structure–Reactivity Relationships, Design, and Applications. *Physical properties of lipids*, 265.
- GHOSH, S. 2007. *Effect of Dispersed Phase Crystallization on Aroma Release from Oil-in-water Emulsions*. Citeseer.
- GHOSH, S., CRAMP, G. L. & COUPLAND, J. N. 2006. Effect of aqueous composition on the freeze-thaw stability of emulsions. *Colloids and Surfaces A: Physicochemical and Engineering Aspects*, 272, 82-88.
- GIERMANSKA, J., THIVILLIERS, F., BACKOV, R., SCHMITT, V., DRELON, N. & LEAL-CALDERON, F. 2007. Gelling of oil-in-water emulsions comprising crystallized droplets. *Langmuir*, 23, 4792-4799.
- GOFF, H. D. & HARTEL, R. W. 2013. *Ice cream*, Springer Science & Business Media.
- GOODWIN, J. 2009. *Colloids and interfaces with surfactants and polymers*, John Wiley & Sons.
- HARTEL, R. W. & HARTEL, R. W. 2001. *Crystallization in foods*, Aspen Publication.
- HEERTJE, I. 1993. Microstructural studies in fat research. *Food structure*, 12, 10.
- HENDRICKSON, K. J. 2013. *Factors Affecting Microscopic Observations of Arrested Coalescence in Triglyceride Emulsions*.
- HENRY, J. V., FRYER, P. J., FRITH, W. J. & NORTON, I. T. 2009. Emulsification mechanism and storage instabilities of hydrocarbon-in-water sub-micron emulsions stabilised with Tweens (20 and 80), Brij 96v and sucrose monoesters. *Journal of colloid and interface science*, 338, 201-206.
- HIEMENZ, P. C. 1986. *Principles of colloid and surface chemistry*, M. Dekker New York.
- HIMAWAN, C., STAROV, V. & STAPLEY, A. 2006. Thermodynamic and kinetic aspects of fat crystallization. *Advances in colloid and interface science*, 122, 3-33.
- HODGE, S. & ROUSSEAU, D. 2003. Flocculation and coalescence in water-in-oil emulsions stabilized by paraffin wax crystals. *Food Research International*, 36, 695-702.
- HODGE, S. & ROUSSEAU, D. 2005. Continuous-phase fat crystals strongly influence water-in-oil emulsion stability. *Journal of the American Oil Chemists' Society*, 82, 159-164.

- HOLMBERG, K., SHAH, D. O. & SCHWUGER, M. J. 2002. *Handbook of applied surface and colloid chemistry*, John Wiley & Sons.
- HOME, D. S. 1996. Protein-stabilized emulsions. *Current Opinion in Colloid & Interface Science*, 1, 752-758.
- HSIAO, L. C., NEWMAN, R. S., GLOTZER, S. C. & SOLOMON, M. J. 2012. Role of isostaticity and load-bearing microstructure in the elasticity of yielded colloidal gels. *Proceedings of the National Academy of Sciences*, 109, 16029-16034.
- HSU, C.-T., CHANG, C.-H. & LIN, S.-Y. 2000. Study on surfactant adsorption kinetics: effects of interfacial curvature and molecular interaction. *Langmuir*, 16, 1211-1215.
- HUNTER, R. 1986. Foundations of Colloid Science. Clarendon Press, Oxford.
- HUYBRECHTS, J., BRUYLANTS, P., VAES, A. & DE MARRE, A. 2000. Surfactant-free emulsions for waterborne, two-component polyurethane coatings. *Progress in Organic Coatings*, 38, 67-77.
- ITHO, N., KOMATSU, H., HANDA, T. & MIYAJIMA, K. 1995. Emulsion and vesicle formation of retinol and retinyl palmitate with egg yolk phosphatidylcholine. *Journal of colloid and interface science*, 174, 148-155.
- IVANOV, I. B. & KRALCHEVSKY, P. A. 1997. Stability of emulsions under equilibrium and dynamic conditions. *Colloids and Surfaces A: Physicochemical and engineering aspects*, 128, 155-175.
- JANSSEN, P. J. & ANDERSON, P. D. 2011. Modeling film drainage and coalescence of drops in a viscous fluid. *Macromolecular Materials and Engineering*, 296, 238-248.
- JAQUET, B., LAZZARI, S., COLONNA, L., COLOMBO, G., SOOS, M. & MORBIDELLI, M. 2017. Effects of Coalescence on Shear-Induced Gelation of Colloids. *Langmuir*, 33, 1180-1188.
- JOSCELYNE, S. M. & TRÄGÅRDH, G. 2000. Membrane emulsification—a literature review. *Journal of Membrane Science*, 169, 107-117.
- JUNG, M., HUBERT, D. H., VAN VELDHOVEN, E., FREDERIK, P., VAN HERK, A. M. & GERMAN, A. L. 2000. Vesicle— Polymer Hybrid Architectures: A Full Account of the Parachute Architecture. *Langmuir*, 16, 3165-3174.
- JURIAANSE, A. & HEERTJE, I. 1988. Microstructure of shortenings, margarine and butter-a review. *Food Structure*, 7, 8.

- KABALNOV, A. S. & SHCHUKIN, E. D. 1992. Ostwald ripening theory: applications to fluorocarbon emulsion stability. *Advances in colloid and interface science*, 38, 69-97.
- KALNIN, D., GARNAUD, G., AMENITSCH, H. & OLLIVON, M. 2002. Monitoring fat crystallization in aerated food emulsions by combined DSC and time-resolved synchrotron X-ray diffraction. *Food research international*, 35, 927-934.
- KERKER, M. 2013. *The scattering of light and other electromagnetic radiation: physical chemistry: a series of monographs*, Academic press.
- KLIMPEL, R. & HOGG, R. 1986. Effects of flocculation conditions on agglomerate structure. *Journal of Colloid and Interface Science*, 113, 121-131.
- KOOS, E., KANNOADE, W. & WILLENBACHER, N. 2014. Restructuring and aging in a capillary suspension. *Rheologica acta*, 53, 947-957.
- KOZAN, M. 2007. Characterization Of Colloidal Nanoparticle Aggregates Using Light Scattering Techniques.
- KRAFT, D. J., DE FOLTER, J. W., LUIGJES, B., CASTILLO, S. I., SACANNA, S., PHILIPSE, A. P. & KEGEL, W. K. 2010. Conditions for equilibrium solid-stabilized emulsions. *The Journal of Physical Chemistry B*, 114, 10347-10356.
- KRAFT, D. J., VLUG, W. S., VAN KATS, C. M., VAN BLAADEREN, A., IMHOF, A. & KEGEL, W. K. 2009. Self-assembly of colloids with liquid protrusions. *J. Am. Chem. Soc*, 131, 1182-1186.
- LAUGA, E. & BRENNER, M. P. 2004. Evaporation-driven assembly of colloidal particles. *Physical review letters*, 93, 238301.
- LEAL, L. G. 2004. Flow induced coalescence of drops in a viscous fluid. *Physics of fluids*, 16, 1833-1851.
- LEE, D. & WEITZ, D. A. 2008. Double emulsion-templated nanoparticle colloidosomes with selective permeability. *Advanced Materials*, 20, 3498-3503.
- LEE, R. F. 1999. Agents which promote and stabilize water-in-oil emulsions. *Spill Science & Technology Bulletin*, 5, 117-126.
- LEONG, T. G., LESTER, P. A., KOH, T. L., CALL, E. K. & GRACIAS, D. H. 2007. Surface tension-driven self-folding polyhedra. *Langmuir*, 23, 8747-8751.

- LEVINE, S., BOWEN, B. D. & PARTRIDGE, S. J. 1989. Stabilization of emulsions by fine particles I. Partitioning of particles between continuous phase and oil/water interface. *Colloids and Surfaces*, 38, 325-343.
- LONCIN, M. 2012. *Food Engineering: Principles And Selected Applications*, Elsevier.
- LUCASSEN-REYNNDERS, E. & KUIJPERS, K. 1992. The role of interfacial properties in emulsification. *Colloids and surfaces*, 65, 175-184.
- MA, Q., WANG, W., LIU, Y., YANG, J., SHI, B. & GONG, J. 2017. Wax adsorption at paraffin oil–water interface stabilized by Span80. *Colloids and Surfaces A: Physicochemical and Engineering Aspects*.
- MALCOLM, J. 1990. Faraday communications. Ultrasonic monitoring of crystallization in an oil-in-water emulsion. *Journal of the Chemical Society, Faraday Transactions*, 86, 1147-1148.
- MANDELBROT, B. B. & PIGNONI, R. 1983. The fractal geometry of nature.
- MANOHARAN, V. N. 2006. Colloidal spheres confined by liquid droplets: Geometry, physics, and physical chemistry. *Solid state communications*, 139, 557-561.
- MANOHARAN, V. N., ELSESSER, M. T. & PINE, D. J. 2003. Dense packing and symmetry in small clusters of microspheres. *Science*, 301, 483-487.
- MASON, T., KRALL, A., GANG, H., BIBETTE, J. & WEITZ, D. A. 1996. Monodisperse emulsions: properties and uses. *Encyclopedia of emulsion technology*, 4, 299-335.
- MBANGA, B. L., VOORHES, K. K. & ATHERTON, T. J. 2014. Simulating defect textures on relaxing nematic shells. *Physical Review E*, 89, 052504.
- MCCLEMENTS, D. 2005. Food Emulsions: Principles, Practice and Technology. CRC Press: Boca Raton, Florida.
- MCCLEMENTS, D., DUNGAN, S., GERMAN, J. B., SIMONEAU, C. & KINSELLA, J. 1993. Droplet Size and Emulsifier Type Affect Crystallization and Melting of Hydrocarbon-in-Water Emulsions. *Journal of food science*, 58, 1148-1151.
- MCCLEMENTS, D. J. 1998. *Food Emulsions: Principles, Practice, and Techniques*, Taylor & Francis.
- MCCLEMENTS, D. J. 2002. Colloidal basis of emulsion color. *Current opinion in colloid & interface science*, 7, 451-455.
- MCCLEMENTS, D. J. 2004. *Food Emulsions: Principles, Practices, and Techniques, Second Edition*, Taylor & Francis.

- MCCLEMENTS, D. J. 2007a. Critical review of techniques and methodologies for characterization of emulsion stability. *Critical Reviews in Food Science and Nutrition*, 47, 611-649.
- MCCLEMENTS, D. J. 2007b. *Understanding and controlling the microstructure of complex foods*, Elsevier.
- MCCLEMENTS, D. J., DICKINSON, E. & POVEY, M. J. 1990. Crystallization in hydrocarbon-in-water emulsions containing a mixture of solid and liquid droplets. *Chemical physics letters*, 172, 449-452.
- MCKENNA, B. M. 2003. *Texture in Food*, Woodhead Pub.
- MCLEAN, J. D. & KILPATRICK, P. K. 1997. Effects of asphaltene aggregation in model heptane–toluene mixtures on stability of water-in-oil emulsions. *Journal of colloid and interface science*, 196, 23-34.
- MEAKIN, P. & JULLIEN, R. 1988. The effects of restructuring on the geometry of clusters formed by diffusion-limited, ballistic, and reaction-limited cluster–cluster aggregation. *The Journal of chemical physics*, 89, 246-250.
- MÉNDEZ-VELASCO, C. & GOFF, H. D. 2012. Fat structure in ice cream: A study on the types of fat interactions. *Food Hydrocolloids*, 29, 152-159.
- MENG, G., ARKUS, N., BRENNER, M. P. & MANOHARAN, V. N. 2010. The free-energy landscape of clusters of attractive hard spheres. *Science*, 327, 560-563.
- MILLER, D., WIENER, E.-M., TUROWSKI, A., THUNIG, C. & HOFFMANN, H. 1999. O/W emulsions for cosmetics products stabilized by alkyl phosphates—rheology and storage tests. *Colloids and Surfaces A: Physicochemical and Engineering Aspects*, 152, 155-160.
- MILLER, D. J., HENNING, T. & GRÜNBEIN, W. 2001. Phase inversion of W/O emulsions by adding hydrophilic surfactant—a technique for making cosmetics products. *Colloids and Surfaces A: Physicochemical and engineering aspects*, 183, 681-688.
- MOHRAZ, A. 2016. Interfacial routes to colloidal gelation. *Current Opinion in Colloid & Interface Science*, 25, 89-97.
- MUGUET, V., SEILLER, M., BARRATT, G., OZER, O., MARTY, J. & GROSSIORD, J. 2001. Formulation of shear rate sensitive multiple emulsions. *Journal of controlled release*, 70, 37-49.

- MULDER, H. & WALSTRA, P. 1974. *The milk fat globule. Emulsion science as applied to milk products and comparable foods*, Wageningen, Netherlands, Centre for Agricultural Publishing and Documentation.
- MYERS, D. 1988. Surfactants in solution: Micellization and related association phenomena. *Surfactant Science and Technology*, 81-121.
- NADIN, M., ROUSSEAU, D. & GHOSH, S. 2014. Fat crystal-stabilized water-in-oil emulsions as controlled release systems. *LWT-Food Science and Technology*, 56, 248-255.
- NARINE, S. S. & MARANGONI, A. G. 2002. Structure and mechanical properties of fat crystal networks. *Advances in food and nutrition research*, 44, 33-145.
- OBERDISSE, J. 2006. Aggregation of colloidal nanoparticles in polymer matrices. *Soft matter*, 2, 29-36.
- OKOCHI, H. & NAKANO, M. 2000. Preparation and evaluation of w/o/w type emulsions containing vancomycin. *Advanced drug delivery reviews*, 45, 5-26.
- OSTWALD, W. 1919. *A Handbook of Colloid-chemistry: The Recognition of Colloids, the Theory of Colloids and Their General Physico-chemical Properties*, J. & A. Churchill.
- PARK, J.-G., FORSTER, J. D. & DUFRESNE, E. R. 2010. High-yield synthesis of monodisperse dumbbell-shaped polymer nanoparticles. *Journal of the American Chemical Society*, 132, 5960-5961.
- PATEL, A. R., RAJARETHINEM, P. S., GREDOWSKA, A., TURHAN, O., LESAFFER, A., DE VOS, W. H., VAN DE WALLE, D. & DEWETTINCK, K. 2014. Edible applications of shellac oleogels: spreads, chocolate paste and cakes. *Food & function*, 5, 645-652.
- PATIST, A. & BATES, D. 2008. Ultrasonic innovations in the food industry: From the laboratory to commercial production. *Innovative food science & emerging technologies*, 9, 147-154.
- PAWAR, A. B., CAGGIONI, M., ERGUN, R., HARTEL, R. W. & SPICER, P. T. 2011. Arrested coalescence in Pickering emulsions. *Soft Matter*, 7, 7710-7716.
- PAWAR, A. B., CAGGIONI, M., HARTEL, R. W. & SPICER, P. T. 2012. Arrested coalescence of viscoelastic droplets with internal microstructure. *Faraday discussions*, 158, 341-350.

- PAWAR, A. B. & KRETZSCHMAR, I. 2010. Fabrication, assembly, and application of patchy particles. *Macromolecular rapid communications*, 31, 150-168.
- PETRUT, R. F., DANTHINE, S. & BLECKER, C. 2016. Assessment of partial coalescence in whippable oil-in-water food emulsions. *Advances in colloid and interface science*, 229, 25-33.
- PHILIP, J., BONAKDAR, L., POULIN, P., BIBETTE, J. & LEAL-CALDERON, F. 2000. Viscous sintering phenomena in liquid-liquid dispersions. *Physical review letters*, 84, 2018.
- PHILIP, J., POIRIER, J., BIBETTE, J. & LEAL-CALDERON, F. 2001. Gelation and coarsening in dispersions of highly viscous droplets. *Langmuir*, 17, 3545-3552.
- PHILLIPS, G. O. & WILLIAMS, P. A. 2009. *Handbook of hydrocolloids*, Elsevier.
- PICHOT, R. 2010. *Stability and characterisation of emulsions in the presence of colloidal particles and surfactants*. The University of Birmingham.
- PICKERING, S. U. 1907. Cxcvi.—emulsions. *Journal of the Chemical Society, Transactions*, 91, 2001-2021.
- PIORKOWSKI, D. T. & MCCLEMENTS, D. J. 2014. Beverage emulsions: Recent developments in formulation, production, and applications. *Food Hydrocolloids*, 42, 5-41.
- PLACIN, F., FEDER, M. & LEAL-CALDERON, F. 2003. Viscous Sintering Phenomena in Liquid– Liquid Dispersions: Application to the Preparation of Silicone Macroporous Aerogels. *The Journal of Physical Chemistry B*, 107, 9179-9184.
- PRILESZKY, T. A. & FURST, E. M. 2016. Fluid networks assembled from endoskeletal droplets. *Chemistry of Materials*, 28, 3734-3740.
- PRINCEN, H. 1984. Geometry of clusters of strongly coagulated fluid drops and the occurrence of collapsed Plateau borders. *Colloids and surfaces*, 9, 47-66.
- PY, C., REVERDY, P., DOPPLER, L., BICO, J., ROMAN, B. & BAROUD, C. N. 2007. Capillary origami: spontaneous wrapping of a droplet with an elastic sheet. *Physical review letters*, 98, 156103.
- RAMSDEN, W. 1903. Separation of Solids in the Surface-Layers of Solutions and'Suspensions'(Observations on Surface-Membranes, Bubbles, Emulsions, and Mechanical Coagulation).--Preliminary Account. *Proceedings of the royal Society of London*, 72, 156-164.

- RAWLE, A. 2001. Basic principles of particle size analysis. Malvern Instruments. *Malvern, UK.*
- RELIKIN, P., FABRE, M. & GUICHARD, E. 2004. Effect of fat nature and aroma compound hydrophobicity on flavor release from complex food emulsions. *Journal of agricultural and food chemistry*, 52, 6257-6263.
- ROGERS, T. L., OVERHOFF, K. A., SHAH, P., SANTIAGO, P., YACAMAN, M. J., JOHNSTON, K. P. & WILLIAMS, R. O. 2003. Micronized powders of a poorly water soluble drug produced by a spray-freezing into liquid-emulsion process. *European journal of pharmaceutics and biopharmaceutics*, 55, 161-172.
- ROMAN, B. & BICO, J. 2010. Elasto-capillarity: deforming an elastic structure with a liquid droplet. *Journal of Physics: Condensed Matter*, 22, 493101.
- ROUSSEAU, D. 2000. Fat crystals and emulsion stability—a review. *Food Research International*, 33, 3-14.
- SACANNA, S., KEGEL, W. & PHILIPSE, A. 2007. Thermodynamically stable Pickering emulsions. *Physical review letters*, 98, 158301.
- SACANNA, S. & PINE, D. J. 2011. Shape-anisotropic colloids: Building blocks for complex assemblies. *Current Opinion in Colloid & Interface Science*, 16, 96-105.
- SATO, K. 1999. Solidification and phase transformation behaviour of food fats—a review. *Lipid/Fett*, 101, 467-474.
- SATO, K. 2001. Crystallization behaviour of fats and lipids—a review. *Chemical Engineering Science*, 56, 2255-2265.
- SATO, K. & UENO, S. 2011. Crystallization, transformation and microstructures of polymorphic fats in colloidal dispersion states. *Current Opinion in Colloid & Interface Science*, 16, 384-390.
- SCHNEIDER, C. A., RASBAND, W. S. & ELICEIRI, K. W. 2012. NIH Image to ImageJ: 25 years of image analysis. *Nature methods*, 9, 671.
- SCHUSTER, D. 1996. *Encyclopedia of emulsion technology*, CRC Press.
- SELOMULYA, C., BUSHELL, G., AMAL, R. & WAITE, T. D. 2003. Understanding the role of restructuring in flocculation: the application of a population balance model. *Chemical Engineering Science*, 58, 327-338.

- SIMON, S. B., JESTIN, J., PALERMO, T. & BARRÉ, L. C. 2008. Relation between solution and interfacial properties of asphaltene aggregates. *Energy & Fuels*, 23, 306-313.
- SIMOVIC, S., HEARD, P., HUI, H., SONG, Y., PEDDIE, F., DAVEY, A. K., LEWIS, A., RADES, T. & PRESTIDGE, C. A. 2009. Dry hybrid lipid– silica microcapsules engineered from submicron lipid droplets and nanoparticles as a novel delivery system for poorly soluble drugs. *Molecular pharmaceutics*, 6, 861-872.
- SOTTMANN, T. & STREY, R. 2005. Fundamentals of Interface and Colloid Science. Elsevier: Amsterdam.
- SPICER, P. T. & HARTEL, R. W. 2005. Crystal comets: Dewetting during emulsion droplet crystallization. *Australian journal of chemistry*, 58, 655-659.
- STANCIK, E. J., KOUKHAN, M. & FULLER, G. G. 2004. Coalescence of particle-laden fluid interfaces. *Langmuir*, 20, 90-94.
- STONE, H. A., LISTER, J. R. & BRENNER, M. P. Drops with conical ends in electric and magnetic fields. Proceedings of the Royal Society of London A: Mathematical, Physical and Engineering Sciences, 1999. The Royal Society, 329-347.
- STRATFORD, K., ADHIKARI, R., PAGONABARRAGA, I., DESPLAT, J.-C. & CATES, M. E. 2005. Colloidal jamming at interfaces: A route to fluid-bicontinuous gels. *Science*, 309, 2198-2201.
- STUDART, A. R., SHUM, H. C. & WEITZ, D. A. 2009. Arrested coalescence of particle-coated droplets into nonspherical supracolloidal structures. *The Journal of Physical Chemistry B*, 113, 3914-3919.
- SUBRAMANIAM, A. B., ABKARIAN, M., MAHADEVAN, L. & STONE, H. A. 2005. Colloid science: Non-spherical bubbles. *Nature*, 438, 930-930.
- TADROS, T. F. 2011. *Colloids in Agrochemicals, Volume 5: Colloids and Interface Science*, John Wiley & Sons.
- TADROS, T. F. 2013. *Emulsion formation and stability*, John Wiley & Sons.
- TAYLOR, G. Disintegration of water drops in an electric field. Proceedings of the Royal Society of London A: Mathematical, Physical and Engineering Sciences, 1964. The Royal Society, 383-397.

- THANASUKARN, P., PONGSAWATMANIT, R. & MCCLEMENTS, D. 2004a. Influence of emulsifier type on freeze-thaw stability of hydrogenated palm oil-in-water emulsions. *Food Hydrocolloids*, 18, 1033-1043.
- THANASUKARN, P., PONGSAWATMANIT, R. & MCCLEMENTS, D. J. 2004b. Impact of fat and water crystallization on the stability of hydrogenated palm oil-in-water emulsions stabilized by whey protein isolate. *Colloids and Surfaces A: Physicochemical and Engineering Aspects*, 246, 49-59.
- THIEL, A., HARTEL, R., SPICER, P. & HENDRICKSON, K. 2016. Coalescence behavior of pure and natural fat droplets characterized via micromanipulation. *Journal of the American Oil Chemists' Society*, 93, 1467-1477.
- THIVILLIERS-ARVIS, F., LAURICHESSE, E., SCHMITT, V. & LEAL-CALDERON, F. 2010. Shear-induced instabilities in oil-in-water emulsions comprising partially crystallized droplets. *Langmuir*, 26, 16782-16790.
- THIVILLIERS, F., DRELON, N., SCHMITT, V. & LEAL-CALDERON, F. 2006. Bicontinuous emulsion gels induced by partial coalescence: Kinetics and mechanism. *EPL (Europhysics Letters)*, 76, 332.
- THIVILLIERS, F., LAURICHESSE, E., SAADAOUI, H., LEAL-CALDERON, F. & SCHMITT, V. 2008. Thermally induced gelling of oil-in-water emulsions comprising partially crystallized droplets: the impact of interfacial crystals. *Langmuir*, 24, 13364-13375.
- TORZA, S. & MASON, S. 1969. Coalescence of two immiscible liquid drops. *Science*, 163, 813-814.
- TSANTILIS, S. & PRATSINIS, S. E. 2000. Evolution of primary and aggregate particle-size distributions by coagulation and sintering. *AIChe journal*, 46, 407-415.
- VAN AKEN, G. A. 2003. Coalescence mechanisms in protein-stabilized emulsions. *Food emulsions*, 8, 299-325.
- VAN BOEKEL, M. & WALSTRA, P. 1981. Stability of oil-in-water emulsions with crystals in the disperse phase. *Colloids and Surfaces*, 3, 109-118.
- VAN DEN TEMPEL, M. 1979. Rheology of concentrated suspensions. *Journal of Colloid and Interface Science*, 71, 18-20.
- VAN DER KOOIJ, H. M. & SPRAKEL, J. 2015. Watching paint dry; more exciting than it seems. *Soft matter*, 11, 6353-6359.

- VAN RUTH, S. M., KING, C. & GIANNOULI, P. 2002. Influence of lipid fraction, emulsifier fraction, and mean particle diameter of oil-in-water emulsions on the release of 20 aroma compounds. *Journal of agricultural and food chemistry*, 50, 2365-2371.
- VANAPALLI, S. A. & COUPLAND, J. N. 2001. Emulsions under shear—the formation and properties of partially coalesced lipid structures. *Food Hydrocolloids*, 15, 507-512.
- VANAPALLI, S. A., PALANUWECH, J. & COUPLAND, J. N. 2002a. Influence of fat crystallization on the stability of flocculated emulsions. *Journal of agricultural and food chemistry*, 50, 5224-5228.
- VANAPALLI, S. A., PALANUWECH, J. & COUPLAND, J. N. 2002b. Stability of emulsions to dispersed phase crystallization: effect of oil type, dispersed phase volume fraction, and cooling rate. *Colloids and Surfaces A: Physicochemical and Engineering Aspects*, 204, 227-237.
- VELEV, O. D., LENHOFF, A. M. & KALER, E. W. 2000. A class of microstructured particles through colloidal crystallization. *Science*, 287, 2240-2243.
- WALSTRA, P. 1983. Formation of emulsions.
- WALSTRA, P. 2002. *Physical chemistry of foods*, CRC Press.
- WALSTRA, P. 2003a. Changes in dispersity. *Physical chemistry of foods*, 494-565.
- WALSTRA, P. 2003b. Physical chemistry of foods. Marcel Decker. Inc., New York.
- WALSTRA, P. & SMULDERS, P. E. 1998. Emulsion formation. *Modern aspects of emulsion science*.
- WALTHER, A. & MÜLLER, A. H. 2013. Janus particles: synthesis, self-assembly, physical properties, and applications. *Chemical reviews*, 113, 5194-5261.
- WATSON, D. J. & MACKLEY, M. R. 2002. The rheology of aqueous emulsions prepared by direct emulsification and phase inversion from a high viscosity alkyd resin. *Colloids and Surfaces A: Physicochemical and Engineering Aspects*, 196, 121-134.
- WEITZ, D., HUANG, J., LIN, M. & SUNG, J. 1985. Limits of the fractal dimension for irreversible kinetic aggregation of gold colloids. *Physical review letters*, 54, 1416.
- WEITZ, D. & OLIVERIA, M. 1984. Fractal structures formed by kinetic aggregation of aqueous gold colloids. *Physical Review Letters*, 52, 1433.

- WRIGHT, A. & MARANGONI, A. 2006. Crystallization and rheological properties of milk fat. *Advanced Dairy Chemistry Volume 2 Lipids*. Springer.
- WU, T., WANG, H., JING, B., LIU, F., BURNS, P. C. & NA, C. 2015. Multi-body coalescence in Pickering emulsions. *Nature communications*, 6.
- YADHA, V. & HELBLE, J. J. 2004. Modeling the coalescence of heterogenous amorphous particles. *Journal of aerosol science*, 35, 665-681.
- ZHANG, X., BASARAN, O. A. & WHAM, R. M. 1995. Theoretical prediction of electric field-enhanced coalescence of spherical drops. *AICHE Journal*, 41, 1629-1639.
- ZHANG, X., YAO, X., WANG, X., FENG, L., QU, J. & LIU, P. 2014. Robust hybrid raspberry-like hollow particles with complex structures: a facile method of swelling polymerization towards composite spheres. *Soft Matter*, 10, 873-881.